

# ***Postclosure Criticality Analysis Results***

## **Spent Fuel and Waste Disposition**

***Prepared for  
US Department of Energy  
Spent Fuel and Waste Science and Technology  
L. Price, E. Basurto, A. Taconi, P. Jones, A. Barela  
Sandia National Laboratories  
G. Davidson, M. Swinney, N. Kucinski, N. Panicker,  
A. Wysocki  
Oak Ridge National Laboratory  
A. Alsaed and C. Sanders  
EnviroNuclear  
J. Prouty  
Nuclear and Regulatory Support Services***

***November 17, 2023***

***M2SF-23SN010305113***

***M2SF-24SN010305092***

***SAND2023-14328R***

#### DISCLAIMER

This information was prepared as an account of work sponsored by an agency of the U.S. Government. Neither the U.S. Government nor any agency thereof, nor any of their employees, makes any warranty, expressed or implied, or assumes any legal liability or responsibility for the accuracy, completeness, or usefulness, of any information, apparatus, product, or process disclosed, or represents that its use would not infringe privately owned rights. References herein to any specific commercial product, process, or service by trade name, trade mark, manufacturer, or otherwise, does not necessarily constitute or imply its endorsement, recommendation, or favoring by the U.S. Government or any agency thereof. The views and opinions of authors expressed herein do not necessarily state or reflect those of the U.S. Government or any agency thereof.

This is a technical report that does not take into account contractual limitations or obligations under the Standard Contract for Disposal of Spent Nuclear Fuel and/or High-Level Radioactive Waste (Standard Contract) (10 CFR Part 961). To the extent discussions or recommendations in this report conflict with the provisions of the Standard Contract, the Standard Contract governs the obligations of the parties, and this report in no manner supersedes, overrides, or amends the Standard Contract. This report reflects technical work which could support future decision making by DOE. No inferences should be drawn from this report regarding future actions by DOE, which are limited both by the terms of the Standard Contract and Congressional appropriations for the Department to fulfill its obligations under the Nuclear Waste Policy Act including licensing and construction of a spent nuclear fuel repository.

*Prepared by*  
Sandia National Laboratories  
Albuquerque, New Mexico 87185



*Sandia National Laboratories is a multimission laboratory managed and operated by National Technology & Engineering Solutions of Sandia, LLC, a wholly owned subsidiary of Honeywell International Inc., for the U.S. Department of Energy's National Nuclear Security Administration under contract DE-NA0003525. SAND2023-14328R.*



10/7/2019

## APPENDIX E NFCSC DOCUMENT COVER SHEET<sup>1</sup>

Name/Title of Deliverable/Milestone/Revision No. Postclosure Criticality Analysis Results

Work Package Title and Number Probabilistic Post-Closure DPC Criticality Consequence Analyses - SNL SF-23SN01030511

Work Package WBS Number 1.08.01.03.05 Direct Disposal of Dual Purpose Canisters

Responsible Work Package Manager Laura Price *Laura Price*  
(Name/Signature)

Date Submitted November 17, 2023

Quality Rigor Level for Deliverable/Milestone	<input type="checkbox"/> QRL-1 <input type="checkbox"/> Nuclear Data	<input type="checkbox"/> QRL-2	<input checked="" type="checkbox"/> QRL-3	<input type="checkbox"/> QRL-4 Lab QA Program <sup>3</sup>
---	---	--------------------------------	---	---

This deliverable was prepared in accordance with Sandia National Laboratories  
(Participant/National Laboratory Name)

QA program which meets the requirements of  
 DOE Order 414.1     NQA-1     Other

**This Deliverable was subjected to:**

Technical Review

Peer Review

**Technical Review (TR)**

**Peer Review (PR)**

**Review Documentation Provided**

**Review Documentation Provided**

Signed TR Report or,

Signed PR Report or,

Signed TR Concurrence Sheet or,

Signed PR Concurrence Sheet or,

Signature of TR Reviewer(s) below

Signature of PR Reviewer(s) below

**Name and Signature of Reviewers**  
Tara LaForce

*Tara LaForce*

**NOTE 1:** Appendix E should be filled out and submitted with the deliverable. Or, if the PICS:NE system permits, completely enter all applicable information in the PICS:NE Deliverable Form. The requirement is to ensure that all applicable information is entered either in the PICS:NE system or by using the NFCSC Document Cover Sheet.

- In some cases there may be a milestone where an item is being fabricated, maintenance is being performed on a facility, or a document is being issued through a formal document control process where it specifically calls out a formal review of the document. In these cases, documentation (e.g., inspection report, maintenance request, work planning package documentation or the documented review of the issued document through the document control process) of the completion of the activity, along with the Document Cover Sheet, is sufficient to demonstrate achieving the milestone.

**NOTE 2:** If QRL 1, 2, or 3 is not assigned, then the QRL 4 box must be checked, and the work is understood to be performed using laboratory QA requirements. This includes any deliverable developed in conformance with the respective National Laboratory / Participant, DOE or NNSA-approved QA Program.

**NOTE 3:** If the lab has an NQA-1 program and the work to be conducted requires an NQA-1 program, then the QRL-1 box must be checked in the work Package and on the Appendix E cover sheet and the work must be performed in accordance with the Lab's NQA-1 program. The QRL-4 box should not be checked.

This page is intentionally left blank.

## SUMMARY

The United States Department of Energy's (DOE) Office of Nuclear Energy's Spent Fuel and Waste Science and Technology Campaign seeks to better understand the technical basis, risks, and uncertainty associated with the safe and secure disposition of spent nuclear fuel (SNF) and high-level radioactive waste. Commercial nuclear power generation in the United States has resulted in thousands of metric tons of SNF, the disposal of which is the responsibility of DOE (Nuclear Waste Policy Act of 1982, as amended). Any repository licensed to dispose of SNF must meet requirements regarding the long-term performance of that repository. The evaluation of long-term performance of the repository may need to consider the SNF achieving a critical configuration during the postclosure period. Of particular interest is the potential for this situation to occur in dual-purpose canisters (DPCs), which are currently licensed and being used to store and transport SNF but were not designed for permanent geologic disposal. DOE has been considering disposing of SNF in DPCs to avoid the costs and worker dose associated with repackaging the SNF currently stored in DPCs into repository-specific canisters. This report examines the consequences of postclosure criticality to provide technical support to DOE in developing a disposal plan.

**High-Level Purpose of This Work**—A multiyear effort was initiated to examine the potential consequences of criticality with respect to long-term repository performance. In the associated studies, criticality is postulated to occur during the postclosure period in a hypothetical repository containing DPCs. One of the key challenges is the need to create the modeling tools and techniques that may eventually be required to either exclude criticality from or include criticality in a performance assessment as appropriate. To this end, the study team considered features, events, and processes relevant to postclosure criticality and moved forward with the development of tools and techniques to model the potential consequences of postclosure steady-state criticality as well as transient criticality (Price et al. 2021, 2022). The work on modeling steady-state criticality considered multiple canisters in a repository-scale performance assessment while the work on modeling transient criticality focused on a single canister under anticipated repository conditions. This report documents recent advances in developing these analyses.

**Fiscal Year 2023 (FY2023) Accomplishments** - Key areas of progress with respect to steady-state criticality calculations in FY2023 include (1) identifying a computer code that might be an appropriate tool for thermal-hydraulic calculations in simulating boiling in a critical DPC, (2) developing a strategy for modeling thermal-hydraulic-mechanical processes in a critical DPC in which the pressure increase causes the material external to the waste package to fracture, (3) setting up a repository-scale simulation in the hypothetical saturated repository that includes DPCs containing pressurized water reactor SNF and DPCs containing boiling water reactor SNF; changes in transport properties of the backfill and disturbed rock zone as a result of elevated temperatures; a correctly implemented grid spacer degradation model for estimating permanent termination of steady-state criticality; and a variety of criticality start times, durations, and power levels, and (4) providing a possible technical basis for demonstrating that postclosure criticality cannot occur in an unsaturated repository, depending on the specific characteristics of the repository.

With respect to transient criticality calculations, key areas of progress include (1) identifying a computer code that might be an appropriate tool for investigating transient criticality in an unsaturated repository, (2) calculating reactivity insertion rates consistent with anticipated postclosure conditions in a DPC, and (3) demonstrating that transient criticality modeling can be simplified by assuming an initial enrichment of 3 wt%  $^{235}\text{U}$  and local reactivity insertion with partial-length control rods.

**Next Stages of This Work** – The next stages of this work include (1) further investigating and developing the tools identified in FY2023 work, (2) further investigating the technical basis for demonstrating that postclosure criticality cannot occur in an unsaturated repository, and (3) further investigating ways to simplify transient criticality calculations.

## **ACKNOWLEDGEMENTS**

This work was supported by the DOE Office of Nuclear Energy, through the Office of Spent Fuel and Waste Science and Technology.

The authors would like to thank Tara LaForce of Sandia National Laboratories for her technical review and Tim Gunter and Bob Clark from DOE for their suggestions and guidance.

This page is intentionally left blank.

## CONTENTS

ACKNOWLEDGEMENTS .....	vii
1. INTRODUCTION .....	17
1.1 Background .....	17
1.2 Purpose .....	18
1.3 Scope .....	19
1.4 Assumptions .....	19
1.4.1 Assumption 1—Waste packages fail and criticality occurs. ....	19
1.4.2 Assumption 2—Fuel assembly configurations remain intact, but cladding permits radionuclide transport. ....	19
1.4.3 Assumption 3—Credit for basket neutron absorbers is not taken. ....	20
1.4.4 Assumption 4—The steady-state criticality events do not oscillate between being critical and subcritical. ....	20
1.5 Approach .....	20
2. MODELING STEADY-STATE POSTCLOSURE CRITICALITY IN A SATURATED REPOSITORY .....	25
2.1 General Repository Description .....	25
2.2 PFLOTRAN Model Developments .....	32
2.3 Modeling Results .....	36
2.4 Evaluating TH Tools for Boiling Canisters .....	51
2.4.1 Motivation .....	51
2.4.2 FY2022 Full-scale DPC Model .....	51
2.4.3 Full-scale DPC Vertical Pipe Model .....	53
2.4.3.1 StarCCM+ Simulation .....	56
2.4.3.2 STAR-CCM+ Results .....	57
2.4.4 Simple Boiling Test Case .....	58
2.4.5 Two-Dimensional Canister Modeling with TRACE .....	61
2.4.5.1 Two-Dimensional Test Problem .....	61
2.4.5.2 STAR-CCM+ Simulation .....	64
2.4.5.3 Two-Dimensional Test Problem Results .....	65
2.4.6 Planned Verification Work .....	66
2.4.6.1 Single-Phase Water Flow .....	66
2.4.6.2 Two-Phase Boiling .....	67
2.5 DPCs Sealed in a Bentonite Backfill .....	67
2.6 Further Work .....	71
3. MODELING STEADY-STATE POSTCLOSURE CRITICALITY IN AN UNSATURATED REPOSITORY .....	73
3.1 General Repository Description .....	73
3.2 PFLOTRAN Model Developments .....	74
3.3 PFLOTRAN Model .....	75

3.4	Parametric Study of Infiltration, Power Level, and Waste Package Breach Size .....	78
3.5	Modeling Results .....	79
3.6	Further Work.....	87
4.	REACTIVITY INSERTION RATE ANALYSIS FOR TRANSIENT CRITICALITY .....	89
5.	MODELING TRANSIENT CRITICALITY IN A SATURATED REPOSITORY .....	91
5.1	Application of SIMULATE-3K to a DPC .....	91
5.2	Approach for FY2023 .....	92
5.3	Transient Criticality Results.....	92
5.3.1	Simplified DPC Development .....	92
5.3.2	Comparison of Simplified and As-Loaded PWR DPC—Local and Global Reactivity Insertions at a Constant Insertion Rate .....	93
5.3.3	Simplified PWR DPC with Partial-Length Control Rods—Local versus Global Reactivity Insertion .....	95
5.3.4	As-Loaded PWR DPC with Partial-Length Control Rods—Local versus Global Reactivity Insertion .....	96
5.3.5	Varied Starting Temperatures .....	99
5.4	Further Work.....	100
6.	MODELING TRANSIENT CRITICALITY IN AN UNSATURATED REPOSITORY .....	103
6.1	Application of Razorback to a DPC.....	103
6.2	Attempted Continuation with RAZORBACK .....	104
6.3	Further Work.....	105
7.	SUMMARY AND CONCLUSIONS .....	107
8.	REFERENCES .....	111
	Appendix A.....	A-1
A-1.	PFLOTRAN Input File.....	A-3
A-2.	PFLOTRAN Waste Form General File (clips).....	A-35
A-3.	PFLOTRAN Source Sink File (clips).....	A-37

## LIST OF FIGURES

Figure 1-1. Conceptual Drawing of Hypothetical Reference Case for Saturated Shale/Argillite.....	22
Figure 1-2. Conceptual Drawing of Hypothetical Reference Case for Unsaturated Alluvium.....	23
Figure 2-1. Full Model Domain Mesh View with Cutout Showing the Repository Region and Finer Grid Resolution .....	26
Figure 2-2. Transparent Views of the Model Domain Colored by Material for (a) Full Model Domain, (b) Zoom View of Repository, and (c) Zoom View at the Well .....	27
Figure 2-3. Vertical $x-z$ Slice through the Model Domain Colored and Labeled by Material .....	28
Figure 2-4. Horizontal ( $x-y$ ) Slice through the Repository Colored by Material Along with Dimensions and Number of Waste Packages .....	29
Figure 2-5. Horizontal ( $x-y$ ) Slice through the Repository Colored by Material ID .....	30
Figure 2-6. Vertical ( $x-y$ ) Slice through the Centermost Waste Packages in the Repository Colored by Material ID.....	31
Figure 2-7. Decay Heat Source Curves for 32-PWR (MPC-32-162) and 89-BWR (MPC-89- W047) Multipurpose Canisters.....	32
Figure 2-8. Horizontal ( $x-y$ ) Slice through Repository and Isometric View of the Model Domain at 0 Years Showing (a) Slice of Waste Packages, Buffer, DRZ, and Shale Host Rock Colored by Material ID; (b) Slice Colored by Temperature; (c) Isometric View of $^{129}\text{I}$ Plumes Colored by $^{129}\text{I}$ Concentration; and (d) Slice Colored by $^{129}\text{I}$ Concentration.....	39
Figure 2-9. Horizontal ( $x-y$ ) Slice through Repository and Isometric View of the Model Domain at 0.1 Years Showing (a) Slice of Waste Packages, Buffer, DRZ, and Shale Host Rock Colored by Material ID; (b) Slice Colored by Temperature; (c) Isometric View of $^{129}\text{I}$ Plumes Colored by $^{129}\text{I}$ Concentration; and (d) Slice Colored by $^{129}\text{I}$ Concentration.....	40
Figure 2-10. Horizontal ( $x-y$ ) Slice through Repository and Isometric View of the Model Domain at 100 Years Showing (a) Slice of Waste Packages, Buffer, DRZ, and Shale Host Rock Colored by Material ID; (b) Slice Colored by Temperature; (c) Isometric View of $^{129}\text{I}$ Plumes Colored by $^{129}\text{I}$ Concentration; and (d) Slice Colored by $^{129}\text{I}$ Concentration.....	41
Figure 2-11. Horizontal ( $x-y$ ) Slice through Repository and Isometric View of the Model Domain at 200 Years Showing (a) Slice of Waste Packages, Buffer, DRZ, and Shale Host Rock Colored by Material ID; (b) Slice Colored by Temperature; (c) Isometric View of $^{129}\text{I}$ Plumes Colored by $^{129}\text{I}$ Concentration; and (d) Slice Colored by $^{129}\text{I}$ Concentration.....	42
Figure 2-12. Horizontal ( $x-y$ ) Slice through Repository and Isometric View of the Model Domain at 300 Years Showing (a) Slice of Waste Packages, Buffer, DRZ, and Shale Host Rock Colored by Material ID; (b) Slice Colored by Temperature; (c) Isometric View of $^{129}\text{I}$ Plumes Colored by $^{129}\text{I}$ Concentration; and (d) Slice Colored by $^{129}\text{I}$ Concentration.....	43
Figure 2-13. Horizontal ( $x-y$ ) Slice through Repository and Isometric View of the Model Domain at 400 Years Showing (a) Slice of Waste Packages, Buffer, DRZ, and Shale Host Rock Colored by Material ID; (b) Slice Colored by Temperature; (c) Isometric View of $^{129}\text{I}$ Plumes Colored by $^{129}\text{I}$ Concentration; and (d) Slice Colored by $^{129}\text{I}$ Concentration.....	44

Figure 2-14. Horizontal ( $x-y$ ) Slice through Repository and Isometric View of the Model Domain at 504 Years Showing (a) Slice of Waste Packages, Buffer, DRZ, and Shale Host Rock Colored by Material ID; (b) Slice Colored by Temperature; (c) Isometric View of  $^{129}\text{I}$  Plumes Colored by  $^{129}\text{I}$  Concentration; and (d) Slice Colored by  $^{129}\text{I}$  Concentration..... 45

Figure 2-15. Horizontal ( $x-y$ ) Slice through Repository and Isometric View of the Model Domain at 504 Years Showing (a) Slice of Waste Packages, Buffer, DRZ, and Shale Host Rock Colored by Material ID; (b) Slice Colored by Temperature; (c) Isometric View of  $^{129}\text{I}$  Plumes Colored by Total  $^{129}\text{I}$  Concentration; and (d) Slice Colored by Total  $^{129}\text{I}$  Concentration ..... 47

Figure 2-16. Vertical ( $x-z$ ) Slice through Repository at “wp2\_BWR” and “wp0\_PWR” as well as Full  $x-z$  View of Repository at 0 Years Showing (a) Slice of Waste Packages, Buffer, DRZ, and Shale Host Rock Colored by Material ID; (b) Slice Colored by Permeability; (c) Full  $x-z$  View of Repository Colored by Temperature; and (d) Slice Colored by Temperature..... 48

Figure 2-17. Vertical ( $x-z$ ) Slice through Repository at “wp2\_BWR” and “wp0\_PWR” as well as Full  $x-z$  View of Repository at 400 Years Showing (a) Slice of Waste Packages, Buffer, DRZ, and Shale Host Rock Colored by Material ID; (b) Slice Colored by Permeability; (c) Full  $x-z$  View of Repository Colored by Temperature; and (d) Slice Colored by Temperature..... 49

Figure 2-18. Waste Package Spacer Vitality Percentage for Two PWR Waste Packages..... 50

Figure 2-19. Waste Package Temperature for two PWR Waste Packages ..... 50

Figure 2-20. Top View of the Three-Ring Setup Used in the FY2022 RELAP5-3D MPC Model ..... 52

Figure 2-21. Component Diagram for the FY2022 RELAP5-3D MPC Model ..... 53

Figure 2-22. Vertical Pipe Setup Used in RELAP5-3D DPC Model ..... 54

Figure 2-23. Heat Structure Grouping Scheme Used in RELAP5-3D MPC Model..... 54

Figure 2-24. Full-Scale DPC RELAP5-3D Model ..... 55

Figure 2-25. Geometries Considered for CFD Modeling: Previous (left) and Current (right) ..... 56

Figure 2-26. Mesh on a Plane Cutting the Fuel Rods ..... 57

Figure 2-27. Simple Boiling Test Case RELAP5-3D Model..... 59

Figure 2-28. Simple Boiling Test Case RELAP5-3D Model..... 60

Figure 2-29. Volume Fraction of Bubbles on a Cut-Section of the Geometry ..... 60

Figure 2-30. Representation of Test Problem: TRACE (left) and CFD (right) ..... 62

Figure 2-31. Test Problem TRACE Model..... 63

Figure 2-32. Vessel Cell Refinement Schemes Used in TRACE Test Problem ..... 64

Figure 2-33. Temperature Contour Predicted by CFD on a Cut Section ..... 65

Figure 2-34. Natural Circulation Contour Predicted by STAR-CCM+ on a Cut Section..... 65

Figure 2-35. Downscaled Canister Model ..... 67

Figure 2-36. A Depiction Conceptualizing a DPC in a Drift Backfilled with Bentonite..... 68

Figure 2-37. An Example of the Results from the New Workflow Predicting  $k_{eff}$  in a Sealed DPC as a Function of Power ..... 70

Figure 2-38. Pressure Buildup in a Sealed DPC as Predicted with RELAP5-3D at a Power Level of 5 MW..... 71

Figure 3-1. Schematic Cross Section of the Unsaturated Zone Model ..... 74

Figure 3-2. Configuration of the Repository and Natural Barrier System Generated Using Cubit, Simulated in PFLOTRAN, and Visualized in ParaView ..... 76

Figure 3-3.  $x$ - $y$  Slice through the Repository Colored by Material ID..... 77

Figure 3-4. Heat Source Curve for 32-PWR, 110-Year OoR Decay Data..... 77

Figure 3-5. Temperature of Repository at 40,000 Years for the 0.25-Year Time-Step Run ..... 78

Figure 3-6. Liquid Saturation in the Centermost Waste Package over 100,000,000 years for Run 1 ..... 80

Figure 3-7. Liquid Saturation and Temperature for Centermost Waste Package for Run 3 ..... 81

Figure 3-8. Liquid Saturation and Temperature for Centermost Waste Package for Run 4 ..... 81

Figure 3-9. Liquid Saturation and Temperature for Centermost Waste Package for Run 5 ..... 81

Figure 3-10. Liquid Saturation and Temperature for Centermost Waste Package for Run 6 ..... 82

Figure 3-11. Liquid Saturation for Run 3 from 24,000 to 50,000 Years ..... 82

Figure 3-12. Liquid Saturation for Run 4 from 24,000 to 50,000 Years ..... 82

Figure 3-13. Liquid Saturation for Run 5 from 24,000 to 50,000 Years ..... 83

Figure 3-14. Liquid Saturation Compared by Maximum Time-Step Size (Runs 3, 7, 8, and 9) ..... 84

Figure 3-15. Temperature Comparison by Maximum Time Step (Runs 3, 7, 8, and 9) ..... 85

Figure 3-16. ParaView Visual of Centermost Waste Package at 24,630 Years..... 86

Figure 4-1. The Four Basket Cell Locations as the Intact Absorber Plates Fall to the Bottom of the Canister ..... 89

Figure 4-2. Reactivity as a Function of Absorber Vertical Displacement (left) and Time (right)..... 90

Figure 5-1. Transient Peak Power versus Enrichment—Varied Insertion Times ..... 93

Figure 5-2. Transient Time versus Peak System Reactivity—1-Second Reactivity Insertion Time ..... 94

Figure 5-3. Transient Total Energy versus Peak System Reactivity—1-Second Reactivity Insertion Time..... 95

## LIST OF TABLES

Table 2-1. DPC (MPC-89-W047) BWR Waste Package Criticality Duration versus Start for Different Power Levels.....	34
Table 2-2. DPC (MPC-32-162) PWR Waste Package Criticality Duration versus Start for Different Power Levels.....	34
Table 2-3. DPC (MPC-89-W047) Randomly Selected BWR Waste Packages, Specific Criticality Start Time, and Constant Power Applied within Single Deterministic Simulation.....	35
Table 2-4. DPC (MPC-32-162) Randomly Selected PWR Waste Packages, Specific Criticality Start Time, and Constant Power Applied within Single Deterministic Simulation.....	36
Table 2-5. Data for BWR and PWR Waste Packages 504 Years after Disposal with Criticality Initiated at 500 Years.....	46
Table 2-6. Data for Selected Breached Subcritical BWR and PWR Waste Packages 504 Years after Disposal.....	46
Table 2-7. Dimensions and Initial Conditions for an MPC-32 Boiling Case .....	56
Table 2-8. Predicted Fluid Properties for Full-Scale MPC-32.....	58
Table 2-9. Predicted Liquid Mass Loss Comparison for Full-Scale MPC-32 .....	58
Table 2-10. Dimensions and Initial Conditions for Simple Boiling Case.....	59
Table 2-11. Predicted Liquid Mass Loss Comparison for Simple Boiling Case .....	61
Table 2-12. Dimensions and Initial Conditions for TRACE Test Problem .....	63
Table 2-13. Axial Power Profile used in TRACE Test Problem .....	63
Table 2-14. Cell Temperatures in the TRACE Cases and the Star-CCM+ Case for the 2D Problem.....	66
Table 2-15. Wall Heat Loss in the TRACE Cases and the Star-CCM+ Case for the 2D Problem.....	66
Table 2-16. Example Temperature Profile for Sealed DPC (500 kW case) .....	69
Table 3-1. Model Variables with Varying Values .....	79
Table 3-2. Breakdown of Different Value Combinations within 10 Unsaturated Zone Simulation Runs.....	79
Table 3-3. Average Amplitude of Temperature and Liquid Saturation Changes as well as Number of Criticality Events by Time Step .....	87
Table 5-1. Summary PWR Local Reactivity Insertion—As-Loaded DPC at Slow Reactivity Insertion Times.....	96
Table 5-2. Summary PWR Local Reactivity Insertion—As-Loaded DPC at Fast Reactivity Insertion Times.....	97
Table 5-3. Summary PWR Global Reactivity Insertion—As-Loaded DPC at Slow Reactivity Insertion Times.....	98
Table 5-4. Summary PWR Global Reactivity Insertion—As-loaded DPC at Fast Reactivity Insertion Times.....	99
Table 5-5. Summary Simplified DPC at Constant Reactivity Insertion Time at Varied Transient Starting Temperatures.....	100

## ACRONYMS

2D or 3D	two-dimensional or three-dimensional
ACRR	Annular Core Research Reactor
BWR	boiling water reactor
CFD	computational fluid dynamics
CFR	Code of Federal Regulations
DOE	US Department of Energy
DPC	dual-purpose canister
DRZ	disturbed rock zone
EBS	engineered barrier system
FEP	feature, event, and/or process
FR	Federal Register
FY	fiscal year
H/X	hydrogen-to-fissile
ID	identification
LBF	lower basin fill
MCNP	Monte Carlo N-Particle Transport
MPC	multipurpose canister
NA	not applicable
NRC	US Nuclear Regulatory Commission
OoR	out of reactor
PA	performance assessment
perm.	permeability
PWR	pressurized water reactor
RANS	Reynolds-Averaged Navier Stokes
REA	rod ejection accident
S3K	SIMULATE-3K
SNF	spent nuclear fuel
SZ	saturated zone
TAD	transportation, aging, and disposal
TH	thermal-hydraulic
UBF	upper basin fill

---

UNF-ST&DARDS	Used Nuclear Fuel – Storage, Transportation & Disposal Analysis Resource and Data Systems
US	United States
UZ	unsaturated zone
WP or wp	waste package

# SPENT FUEL AND WASTE SCIENCE AND TECHNOLOGY POSTCLOSURE CRITICALITY ANALYSIS RESULTS

## 1. INTRODUCTION

The domestic commercial nuclear power industry has generated thousands of metric tons of spent nuclear fuel (SNF), the disposal of which is the responsibility of the United States (US) Department of Energy (DOE) (Nuclear Waste Policy Act 1982, as amended [42 U.S.C. 10101 et seq.]). Any repository licensed to dispose the SNF must meet requirements regarding the long-term performance of a repository used to dispose of that waste. To that end, DOE's Office of Nuclear Energy's Spent Fuel and Waste Science and Technology Campaign seeks to better understand the technical basis, risks, and uncertainty associated with the safe and secure disposition of SNF and high-level radioactive waste. An evaluation of the long-term performance of a repository used to dispose of SNF and high-level waste may need to consider the SNF achieving a critical configuration. Of particular interest is the potential for this situation to occur in dual-purpose canisters (DPCs), which are currently being used to store and transport SNF but were not designed for permanent geologic disposal. Should DOE choose to pursue a disposal plan that includes disposal of SNF in DPCs, a better understanding of the process of postclosure criticality will be needed.

A multiyear effort was initiated to examine the potential consequences of criticality with respect to long-term repository performance. In the associated studies, criticality is postulated to occur during the postclosure period in a hypothetical repository containing DPCs. In the first phase (a scoping phase), the study team developed an approach to creating the modeling tools and techniques that may eventually be required to either exclude criticality from or include criticality in a performance assessment (PA) as appropriate; this effort is documented in Price et al. (2019a). In the second phase, the study team implemented this modeling approach and identified future work, as documented in Price et al. (2019b). The next step was a repository-scale PA examining the potential consequences of postclosure steady-state criticality, an effort that included the development of information, modeling tools, and techniques to support such a PA (Price et al. 2021, 2022). In addition, work on building the capability to model transient criticality progressed, though the effort focused on modeling a single canister rather than multiple canisters under anticipated repository conditions. This report represents the continuation of work on modeling postclosure steady-state and transient criticality and documents the expansion of the information, modeling tools, and techniques featured in Price et al. (2021, 2022).

This report fulfills the Spent Fuel and Waste Science and Technology Campaign milestones M2SF-23SN010305113 and M2SF-24SN010305092.

### 1.1 Background

In 2008, in an effort to initiate the process of constructing a repository for disposal of SNF and high-level waste, DOE submitted the *Yucca Mountain Repository License Application* (DOE 2008a) to the US Nuclear Regulatory Commission (NRC). An update to the license application was completed later in the same year (DOE 2008b) and resubmitted to the NRC in 2009. The license application included a PA analyzing the long-term performance of the repository consistent with applicable requirements given in the Code of Federal Regulations (CFR): 10 CFR Part 63 and 40 CFR Part 197. In that PA, SNF was assumed to be placed in transportation, aging, and disposal (TAD) canisters specifically designed to

transport fuel from its current storage location to the repository, store it for aging purposes (if needed), and dispose it in the repository. These TAD canisters were designed such that the probability of in-package criticality during the repository postclosure period was sufficiently low to exclude it from consideration in the PA (DOE 2008b, Section 2.1.2.2). That is, the probability of criticality was less than one chance in 10,000 of occurring within 10,000 years after disposal.

However, the repository was not completed, and TADs were never built. Utilities have continued the practice of storing SNF in DPCs designed to meet relevant NRC requirements for the storage and transportation of SNF (10 CFR Part 72 and 10 CFR Part 71, respectively). While DPCs were designed, licensed, and loaded to preclude the possibility of criticality during storage and transport of SNF, they were not designed or loaded to preclude the possibility of criticality during the regulated postclosure period following disposal, which can be up to 1,000,000 years.

A key requirement for assessing the long-term performance of a repository is that all features, events, and processes (FEPs) must be included in the PA unless the probability of occurrence of the FEP is below a specified limit or the consequences of its occurrence "... (however probable) can be demonstrated not to be significant" (73 FR 61256). As noted above, for the license application PA, the probability of in-package criticality in TAD canisters during the postclosure period was, by design, less than one chance in 10,000 in 10,000 years after disposal. Thus, postclosure criticality in TAD canisters was excluded from the PA based on probability. Based on studies investigating the probability of occurrence of in-package criticality in DPCs during the postclosure performance period, it is not clear that in-package criticality in DPCs can be excluded from a PA based on probability for all geologies (Hardin et al. 2015).

Therefore, if direct disposal of SNF in DPCs in a geologic repository is to be considered, the associated PA for the repository may have to include in-package criticality. DOE has developed a methodology for addressing the consequences of in-package criticality during the postclosure period (YMP 2003). If DOE pursues a disposal licensing strategy that excludes in-package criticality in DPCs from the PA based on low consequence rather than low probability, DOE will have to demonstrate that the consequences of in-package criticality are not significant in terms of repository performance. Alternatively, if the consequences of in-package criticality are included in the PA, then DOE must demonstrate that the regulatory performance standards can still be met. Regardless of the approach, DOE will need the ability to model the consequences of postclosure in-package criticality in terms of repository performance.

## 1.2 Purpose

One objective of the work described in this report is to develop the capability to include those FEPs that affect or are affected by postclosure criticality in PA calculations. Another objective is to provide the results of PA-type calculations that include the occurrence of criticality, including as many FEPs as possible in the models. The eventual goal is to develop modeling capabilities that can be used either to exclude criticality from a PA based on consequence or to model the occurrence of criticality in a PA if criticality is to be included. The approach used in this report is consistent with that developed in the past (YMP 2003). The work discussed in this report focuses primarily on the consequences of criticality during the postclosure period. However, the discussion in Section 4 examines a method for determining a reasonable reactivity insertion time in the context of a transient criticality, which is a first step toward addressing the probability of occurrence of criticality, and the analyses presented in Section 3.5 suggest that a low-probability argument might be possible for a deep geologic repository in unsaturated rock. Further limitations on the scope of work are described in Section 1.3.

## 1.3 Scope

The approach implemented in the first two phases (Price et al. 2019a,b) and continued here is consistent with relevant regulations and requirements and uses existing generic models (Mariner et al. 2017, 2018) as much as possible. The study team investigated in-package criticality in DPCs exclusively; that is, criticality external to the waste package, either in the near field or far field, is not within the scope of this study. For this report, the only type of waste form considered is commercial SNF in DPCs.

The approach identifies conceptual models (Section 1.5) featuring two different hypothetical repositories and the occurrence of both steady-state criticality (low power and long duration) and transient criticality (high power and short duration). Consistent with DOE's methodology (YMP 2003), the primary consequence of steady-state criticality is a change in the radionuclide inventory, which could affect repository performance; however, other effects of steady-state criticality such as thermal and chemical effects are considered as well. The same effects can result from a transient criticality. However, for transient criticality the primary consequence is a sudden power pulse, which might damage neighboring waste packages, the engineered barrier system (EBS) in the vicinity of the critical waste package, or the host rock.

## 1.4 Assumptions

The assumptions discussed below are simplifying or bounding in nature and were made to facilitate the analyses described in this report.

### 1.4.1 Assumption 1—Waste packages fail and criticality occurs.

To facilitate criticality calculations, it is assumed that the waste packages fail, water enters the waste packages, and the configuration of water and SNF in the waste packages has an effective neutron multiplication factor ( $k_{eff}$ ) greater than or equal to 1.0. This combination of circumstances forms a conservative assumption for the purposes of this study. The probability that these conditions occur is not calculated, although for the purposes of studying the effects of transient criticality, reasonable bounds on reactivity insertion time are investigated (Section 4).

### 1.4.2 Assumption 2—Fuel assembly configurations remain intact, but cladding permits radionuclide transport.

Conservative, yet seemingly paradoxical, fuel conditions are assumed for performing criticality analyses and repository performance analyses.

For the criticality analyses, it is assumed that the fuel pins and cladding in each DPC remain intact such that the fuel pins are retained in their original assembly lattice configurations. This assumption is conservative because it represents the most reactive credible fuel configuration under disposal conditions. Low enriched fuel (i.e., less than 5 wt%  $^{235}\text{U}$ ) is more reactive in a lumped lattice configuration (i.e., in fuel assemblies) compared to a homogeneous configuration. Additionally, commercial fuel assemblies are designed to be undermoderated (i.e., hydrogen-to-fissile [H/X] atomic ratio less than optimum). Configurations involving reduction in fuel pin pitch (i.e., damage to grid spacers) or degraded fuel (i.e., damaged cladding) are typically of lower reactivity than intact fuel assemblies because they result in a system that is further undermoderated. Mechanisms that could result in configurations with optimum moderation (e.g., relatively uniform pin pitch expansion) or preferentially separate fissile isotopes from neutron absorbers in the fuel are not postulated in the work described in this report.

To examine criticality consequences relative to repository performance, the study team assumed that the cladding has failed, thereby permitting radionuclides to be released into a breached waste package and to be transported into the EBS and beyond.

### 1.4.3 Assumption 3—Credit for basket neutron absorbers is not taken.

Because of the relatively high corrosion rate of aluminum-based materials, it was assumed that borated aluminum-based neutron absorbers in each DPC degrade within tens or hundreds of years once water enters the DPC. Although borated aluminum corrosion products (e.g.,  $B_4C$ ) may remain in the DPCs, the presence of neutron absorber material conservatively was not credited in the  $k_{eff}$  calculations performed for these analyses. The location of neutron absorber material inside the basket is paramount for criticality control, and it is difficult to justify whether the absorber material would maintain its original location after corrosion over tens or hundreds of years in an aqueous environment. As described in Section 4, a preliminary effort to bound reactivity insertion magnitude and rates given a transient criticality event considers highly stylized scenario involving absorber material falling through a DPC.

### 1.4.4 Assumption 4—The steady-state criticality events do not oscillate between being critical and subcritical.

In the uncontrolled environment of a DPC disposed of in a repository, a criticality event in a DPC is likely to oscillate between critical and subcritical as fission and fission heat change the environmental conditions (e.g., Doppler broadening of  $^{238}U$  neutron capture resonances in the SNF; water expands and boils, reducing moderator density; buildup of fission product neutron poisons such as  $^{135}Xe$ ). Modeling this cyclic reactivity in a waste package in a repository-scale model was beyond current modeling capabilities. Therefore, in the model of a hypothetical saturated shale repository discussed in Section 2, it was assumed that the heat generated by the steady-state criticality event in a DPC is exactly balanced by heat loss through convection, conduction, radiation, and evaporation, such that there is no cyclic behavior. In contrast, this assumption was not made in the studies described in Section 3, which considers an unsaturated repository where an insufficient quantity of water in the DPC (i.e., a low liquid saturation) can end a criticality event.

## 1.5 Approach

Two different hypothetical repositories are considered as geologic reference cases in the criticality analyses discussed in this report: a saturated repository in shale and an unsaturated repository in alluvium. The approach to estimating the consequences of steady-state criticality on the performance of the hypothetical saturated repository involves calculating and comparing the doses to a member of the public (1) with the occurrence of steady-state criticality and (2) without the occurrence of any criticality. Preliminary results of a such a calculation for steady-state criticality in this hypothetical saturated shale repository indicate that the occurrence of steady-state criticality does not change the calculated dose to a member of the public compared to the case that does not include the occurrence of criticality (Price et al. 2021). That preliminary work included very few FEPs that had been identified as relevant to repository performance when a criticality occurs, so work in the following year focused on identifying relevant FEPs (Alsaed and Price 2020) and including some of them into the PA models, such as grid spacer degradation (Price et al. 2022) using a quarter-scale waste package. Fiscal year 2023 (FY2023) work returned to the repository-scale calculations.

With respect to steady-state criticality in the hypothetical unsaturated alluvial repository, the work described in this report focused on the relationship between infiltration rate and water level in a waste package, with the objective of building a technical basis for excluding criticality on the basis of probability.

The approach to estimating the consequences of transient criticality on the performance of each hypothetical repository involves calculating the range of predicted power over time produced by the transient criticality and determining whether the pulse of energy could cause mechanical damage to the engineered or natural barrier. This report gives a range of predicted power that might be generated by a transient postclosure criticality; the approach to determining the extent of mechanical damage to barriers is still being developed.

The geologic reference case for a hypothetical repository in saturated shale, or argillite, is illustrated in Figure 1-1. For this reference case, the repository is placed at a depth of 500 m, the emplacement drifts are backfilled with bentonite as a buffer (Mariner et al. 2017), the drift diameter is 4.5 m, and the waste package center-to-center spacing is 20 m (Hardin and Kalinina 2016). It is assumed that the hydrostatic pressure at repository depth is 50 bar; at this pressure, water boils at approximately 264°C (Weast and Astle 1979). Other characteristics of the host rock are given in relevant subsections of this report and in Section 4.2.2 of Mariner et al. (2017).

Figure 1-2 depicts the hypothetical reference case for a repository in unsaturated alluvium. The repository depth is 250 m, and waste drifts are backfilled with crushed alluvium (based on Mariner et al. 2018). The drift diameter is 4.5 m, and the maximum percolation rate, corresponding to very wet conditions, is 10 mm/yr. Hydrologic and thermal parameters are given below in relevant subsections and in Table 5-1 of Mariner et al. (2018).

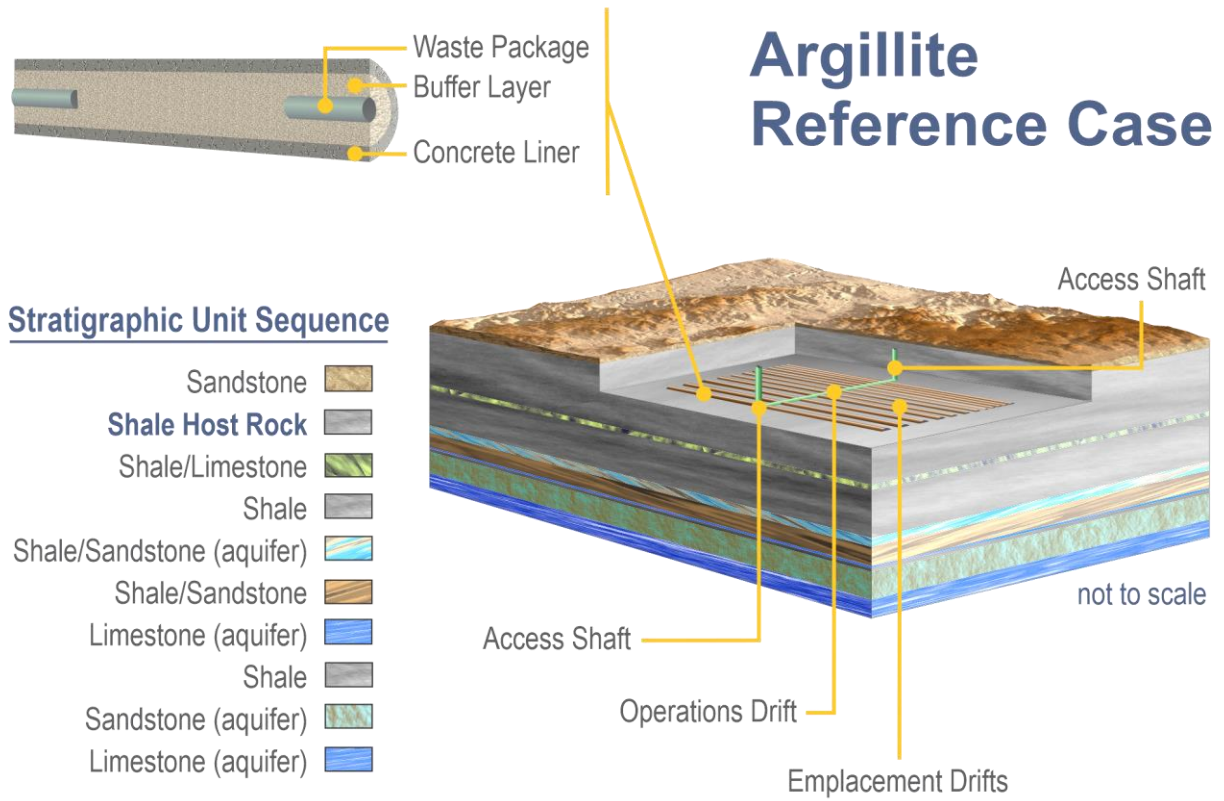


**Figure 1-1. Conceptual Drawing of Hypothetical Reference Case for Saturated Shale/Argillite**

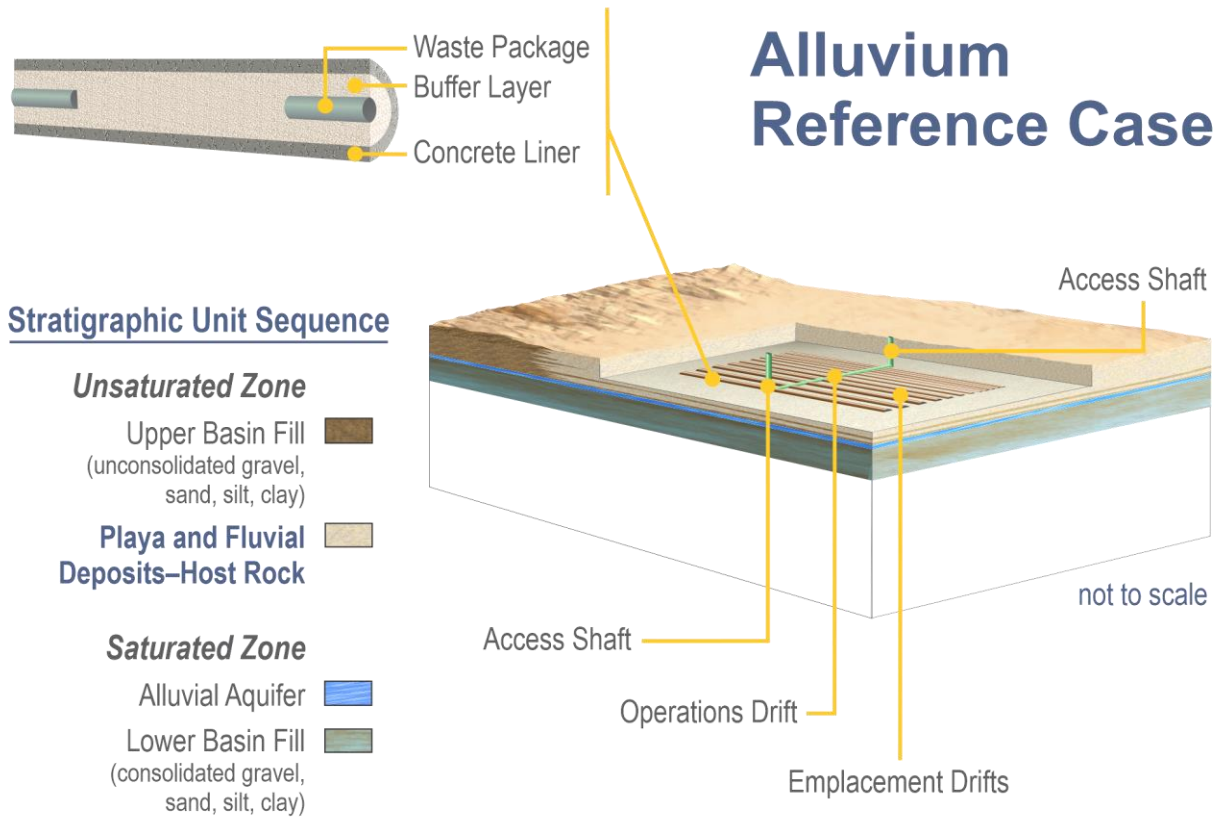


Figure 1-2. Conceptual Drawing of Hypothetical Reference Case for Unsaturated Alluvium

This page is intentionally left blank.

## 2. MODELING STEADY-STATE POSTCLOSURE CRITICALITY IN A SATURATED REPOSITORY

The following sections discuss the model of a steady-state postclosure criticality in a hypothetical saturated repository. Section 2.1 describes the hypothetical reference saturated repository used in these analyses, Section 2.2 outlines the capabilities added to the PFLOTRAN model during FY2023, Section 2.3 presents the results of FY2023 repository-scale PFLOTRAN calculations, Section 2.4 describes an evaluation of tools for modeling thermal-hydraulic (TH) processes in a critical DPC in which boiling occurs, Section 2.5 describes neutronic calculations conducted for a critical DPC in which the pressure build-up could lead to fracturing of the material outside the waste package, , and Section 2.6 identifies further work needed.

### 2.1 General Repository Description

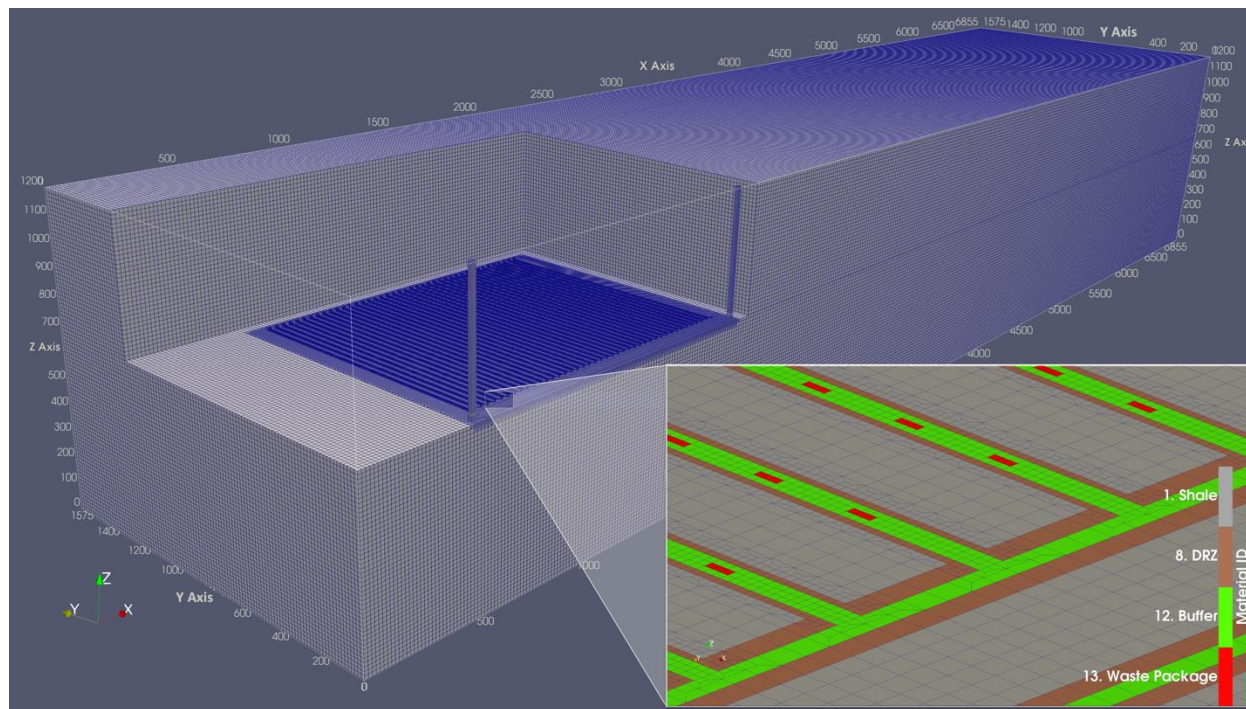
The FY2023 simulations addressing steady-state criticality use a repository-scale model previously used in Price et. al. (2021) that originally was developed in Mariner et al. (2017). Modeling of this hypothetical repository considers the disposal of SNF in DPCs in saturated shale, including near-field components such as the waste package, buffer, disturbed rock zone (DRZ), shale host rock, and other material layers (e.g., overburden, sandstone, siltstone, limestone). Figure 2-1 shows the full model domain mesh with a cutout exposing the repository region with finer grid resolution, along with an inset zoom showing a close-up of the repository region colored by material. The half-symmetry model domain is  $6,855 \times 1,575 \times 1,200$  m. Most of each domain is discretized into cells as large as 15 m on a side and as small as 1.67 m ( $5/3$  m) on a side, the latter being within the emplacement drifts. Transition zones of cells 5 m on a side exist between the finely discretized emplacement zones and the rest of the domain. The mesh of the model consists of 6,925,936 cells, of which about 3,000,000 are smaller cells in the repository area. Figure 2-2 is a transparent view of the model domain colored by material. The repository (brown) is 500 m from the west (left) face of the domain and 515 m below the top face of the domain. The  $x$ -axis is in the east/west direction, the  $y$ -axis is in the north/south direction, and the  $z$ -axis is vertical. The domain is long enough to place a well 5 km down gradient of the repository as shown in the figure and represented by teal box (labeled in Figure 2-2c). Figure 2-3 shows an  $x$ - $z$  (vertical) slice through the repository colored/labeled by material along with an inset zoom at the centermost waste package.

Figure 2-4 shows an  $x$ - $y$  (horizontal) slice through the repository colored by material: shale host rock (gray), DRZ (brown), buffer/backfill (neon green), and waste package (red). The south face of the model domain shown in this figure represents the reflection boundary. Two vertical shafts, one at either end of the southern-most hall, are gridded; they are about 1,280 m long. The half-symmetry model consists of 42 drifts and 50 waste packages per drift (2,100 waste packages).

Figure 2-5 shows an  $x$ - $y$  slice through the repository colored by material and provides a visual of regions where boiling water reactor (BWR) waste packages are located (west 1/3 region of the repository) as well as where pressurized water reactor (PWR) waste packages are located (east 2/3 region of the repository) along with twelve labeled white circles representing observation points of interest. The visual also includes numbering associated with waste packages on the  $y$ -axis and drift number on the  $x$ -axis. The blue-shaded BWR region resides in the first 14 drifts starting on the west side of the repository and consists of 700 waste packages. The dark-gray-shaded PWR region includes drifts 14 through 41 and consists of 1,400 waste packages. Figure 2-6 shows an  $x$ - $z$  (vertical) slice through the centermost waste packages in the repository colored by material, blue-shaded BWR waste package locations, dark-gray-

shaded PWR waste package locations, and 6 additional white spheres representing observation points of interest in the shale material.

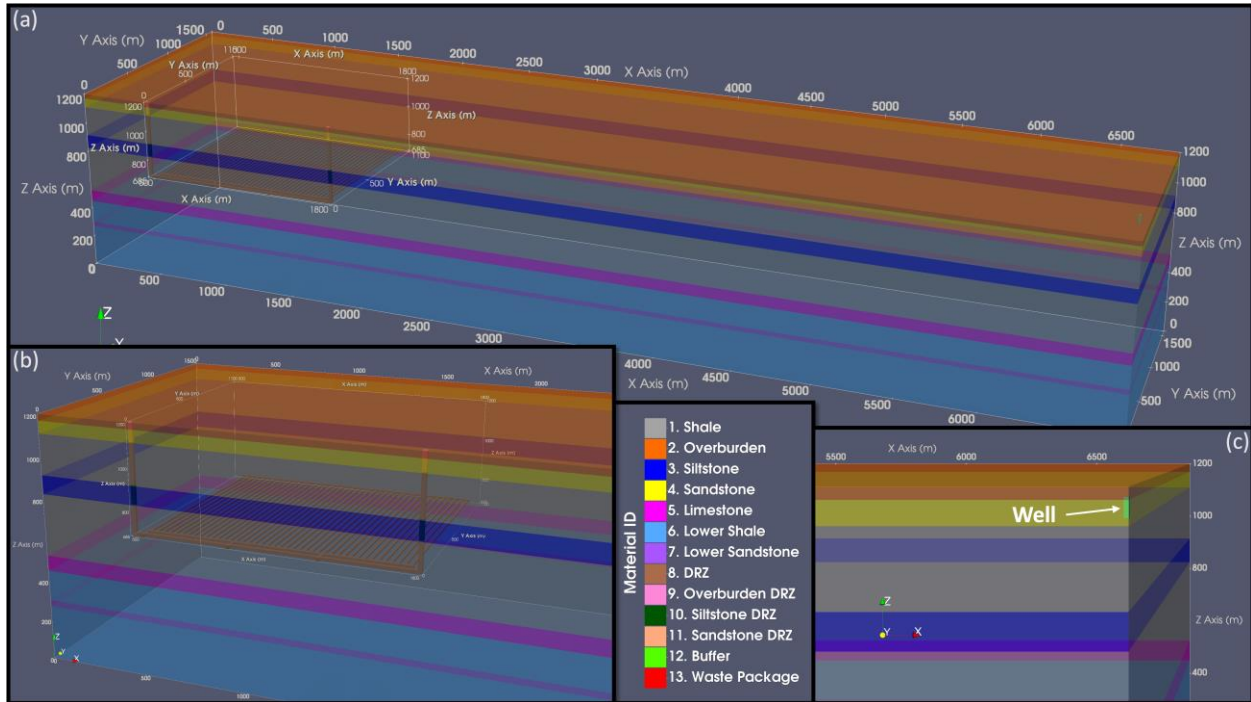
Figure 2-7 plots decay heat curves for  $10^6$  years, rescaled to 110 years out-of-reactor (OoR) from multipurpose canisters (MPCs) using a 32-PWR (MPC-32-162) and 89-BWR (MPC-89-W047). Thermal energy (watts per waste package volume; 4,634.8 W initially for the PWR and 5,449.0 for the BWR for elements representing a single waste package) entering the model domain is updated as a function of time according to values in the lookup table.



NOTE: Inset zoom on bottom right corner shows a close-up of the repository region colored by Material ID along with mesh showing the grid cell size at the waste package level.

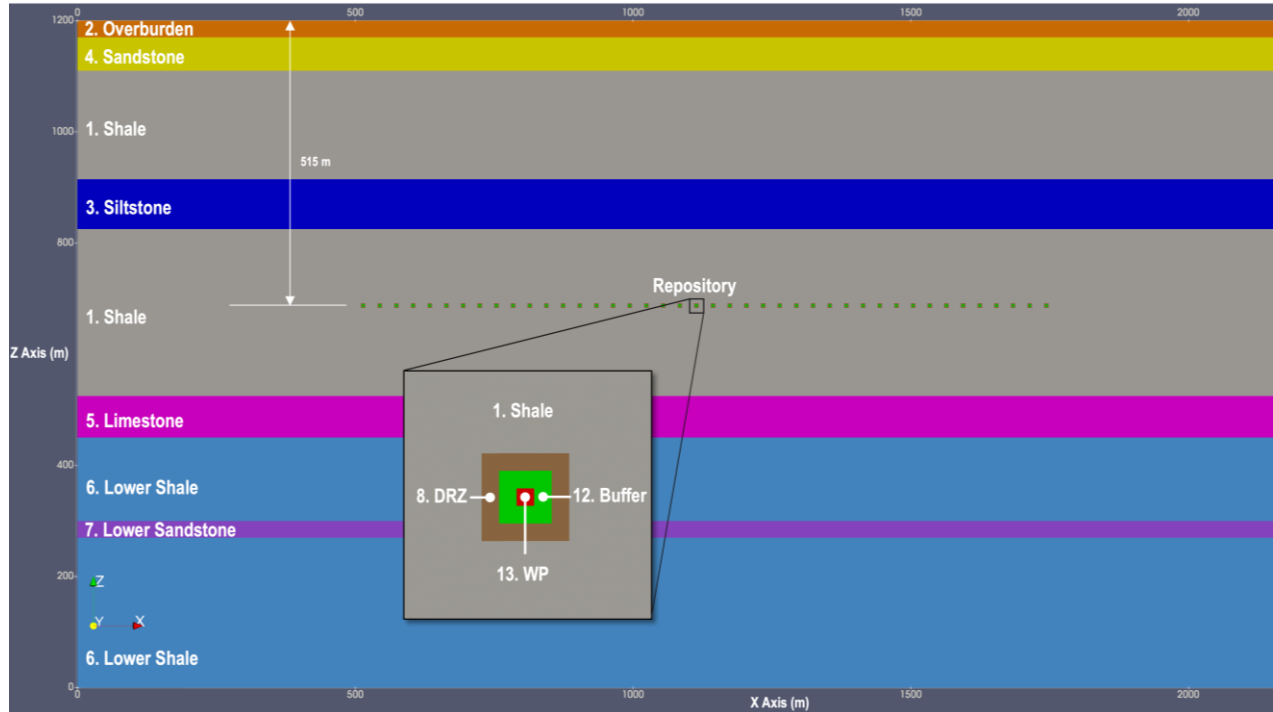
DRZ = disturbed rock zone

**Figure 2-1. Full Model Domain Mesh View with Cutout Showing the Repository Region and Finer Grid Resolution**



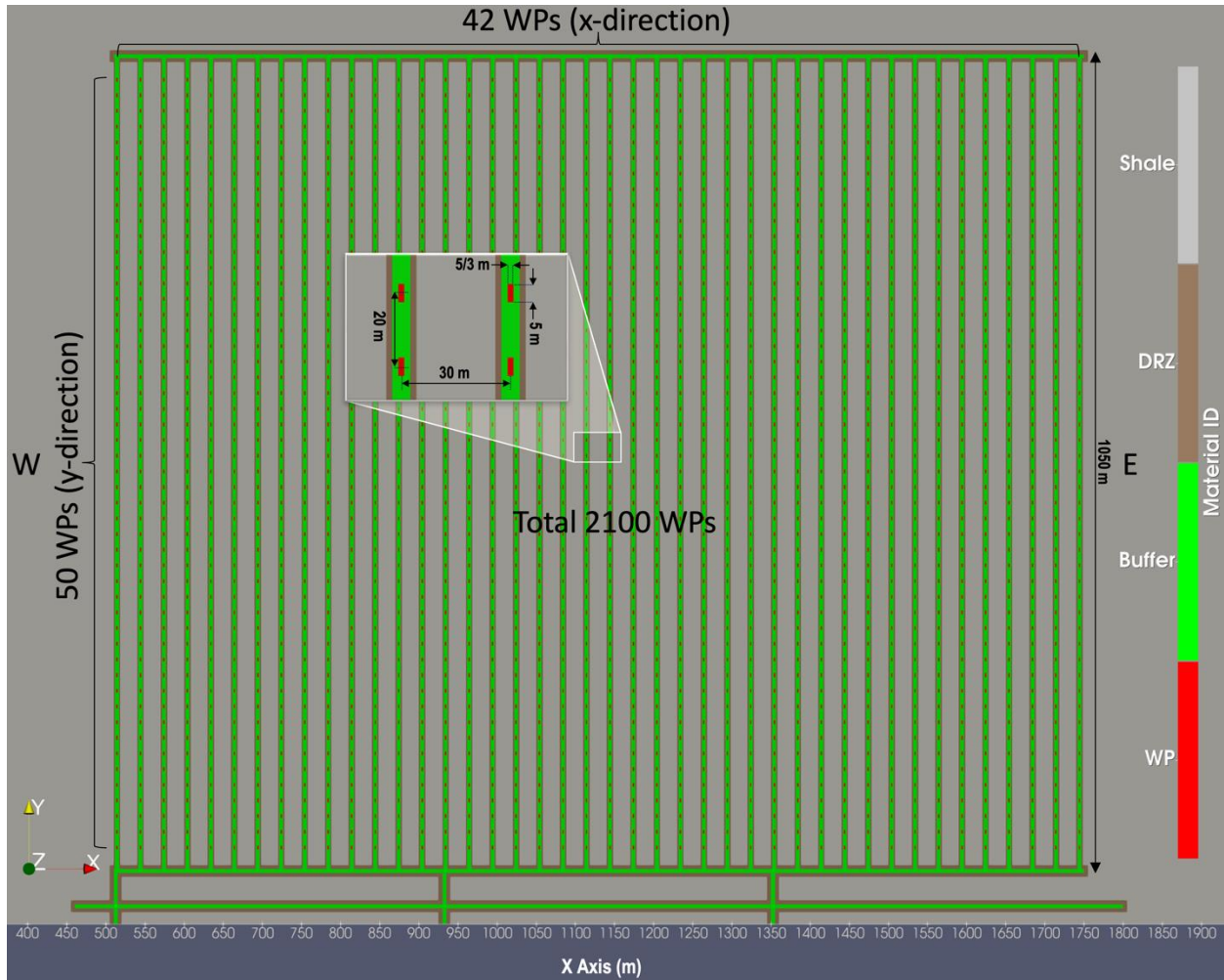
NOTE: The well is represented by the teal box on the right in (a) and (c).  
 DRZ = disturbed rock zone

**Figure 2-2. Transparent Views of the Model Domain Colored by Material for (a) Full Model Domain, (b) Zoom View of Repository, and (c) Zoom View at the Well**



NOTE: Inset zoom on top left corner shows a close-up of the centermost waste package region.  
 DRZ = disturbed rock zone  
 WP = waste package

**Figure 2-3. Vertical x-z Slice through the Model Domain Colored and Labeled by Material**

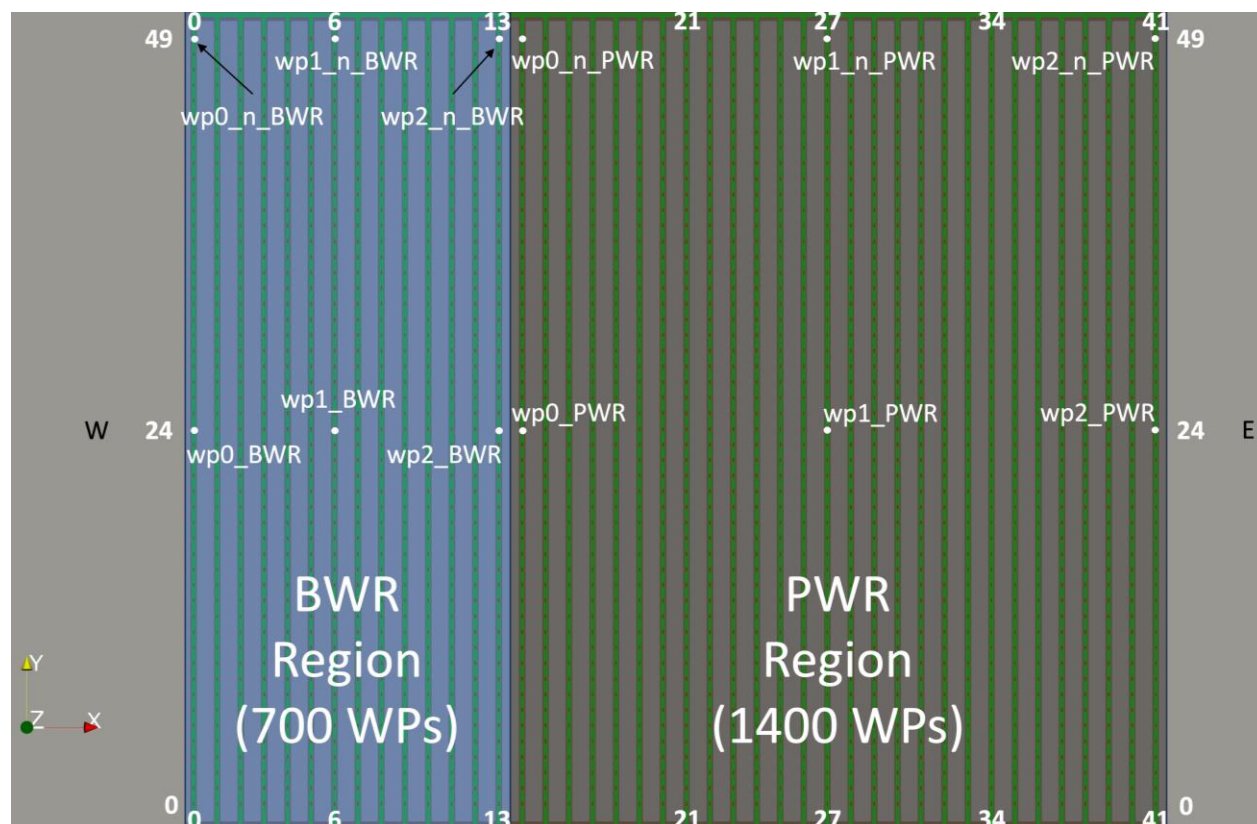


NOTE: Inset zoom showing a close-up of four waste packages with spacing dimensions.

DRZ = disturbed rock zone

WP = waste package

**Figure 2-4. Horizontal (x-y) Slice through the Repository Colored by Material Along with Dimensions and Number of Waste Packages**



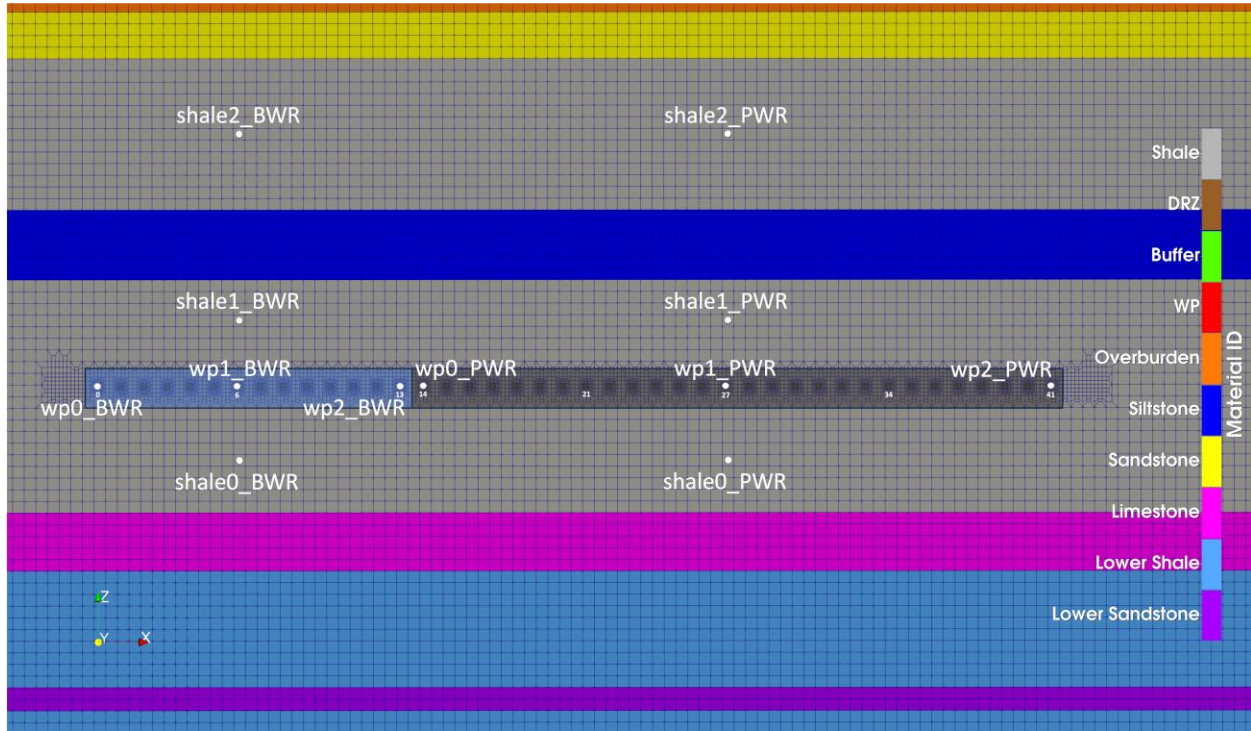
NOTE: The third of the repository region shaded blue corresponds to the location of BWR waste packages, and the two thirds of the region shaded dark gray corresponds to the location of PWR waste packages. There are twelve labeled white circles representing observation points of interest, numbering of drifts in the x direction, and numbering of waste packages in the y direction.

BWR = boiling water reactor

PWR = pressurized water reactor

WP or wp = waste package

**Figure 2-5. Horizontal (x-y) Slice through the Repository Colored by Material ID**



NOTE: The blue-shaded repository region corresponds to the location of BWR waste packages, and the dark-gray-shaded repository region corresponds to the location of PWR waste packages. There are twelve labeled white circles representing observation points of interest: (six for waste package locations and six for locations in the shale material layers). In addition, some drifts under waste package regions are numbered.

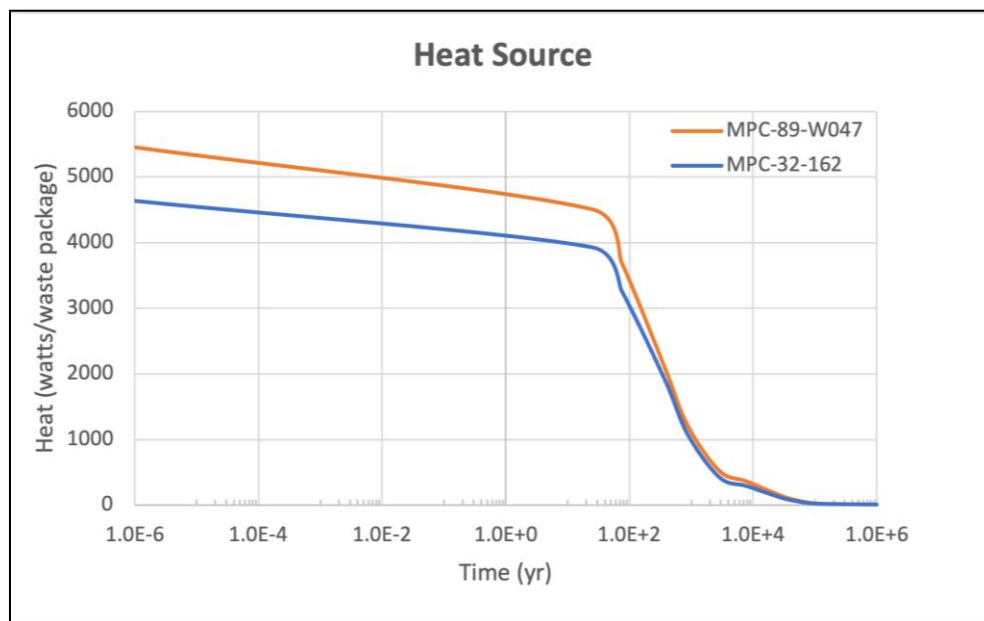
BWR = boiling water reactor

DRZ = disturbed rock zone

PWR = pressurized water reactor

WP or wp = waste package

**Figure 2-6. Vertical (x-y) Slice through the Centermost Waste Packages in the Repository Colored by Material ID**



NOTE: Heat sources represent DPCs that are 110 years OoR.  
MPC = multipurpose canister

**Figure 2-7. Decay Heat Source Curves for 32-PWR (MPC-32-162) and 89-BWR (MPC-89-W047) Multipurpose Canisters**

## 2.2 PFLOTRAN Model Developments

In FY2023, the FY2022 quarter-waste package shale model developments were incorporated into the repository-scale model. This effort included (1) incorporating criticality start times, the constant power associated with these start times, criticality end times associated with fissile depletion, and the updated grid spacer degradation model; (2) resolving criticality start time issue previously seen in FY2022 simulations; and (3) extending the smectite-to-illite transition model beyond the backfill.

One of the goals for FY2023 included incorporating eight criticality start times and three constant powers associated with these critical events that had been developed in the previous year (Price et al. 2022). Table 2-1 and Table 2-2 show start times of criticality, constant powers, and the duration of the criticality event (based on quantity of fissile material) for MPC-89-W047 (89-BWR) and MPC-32-162 (32-PWR), respectively. Eight start times of criticality were selected from these tables (500; 1,000; 5,000; 10,000; 20,000; 50,000; 100,000; and 500,000 years) to be set up in a single deterministic simulation along with all three constant powers (1, 2, 4 kW). For the initial deterministic simulation, 24 BWR waste packages and 24 PWR waste packages were randomly selected, and each was set up with one of the possible configurations based on the 8 start times of criticality and 3 constant powers. Table 2-3 includes the randomly selected waste packages within the BWR region along with the specific combination of criticality start time and the constant power associated with them. Similarly, Table 2-4 includes information for waste packages experiencing a critical event within the PWR region. The “Waste Package Name” column included in these tables are drift/waste package number designators, where the first number after “wp” is drift number and the second is waste package number in the specified drift.

Figure 2-5 includes the numbering of drifts in the  $x$  direction (0 to 41, total of 42 drifts) and the numbering of waste packages in the  $y$  direction (0 to 49, total of 50 waste packages per drift). The input deck set up for these criticality combinations is shown in Appendix A-1 within the WASTE\_FORM\_GENERAL block. A total of 48 waste packages (24 BWR, 24 PWR) are set up to go through a critical event at one of the specified combinations previously mentioned and referenced in the tables above. For all other waste packages (2,052) in the model domain, a decay heat (either BWR or PWR) is applied using SOURCE\_SINK (Appendix A-3), where a FLOW\_CONDITION is specified. WASTE\_FORM blocks (Appendix A-2) are also specified for each waste package region, but noncritical waste packages use a secondary MECHANISM\_CUSTOM block where the inventory is specified and a CANISTER\_DEGRADATION\_MODEL is applied.

The grid spacer degradation model was recently revised in Nole et al. (2023) to provide stronger links to the source literature and more intuitive input parameters. Previously in Price et al. (2022), PFLOTRAN simulations using a quarter-waste package shale model showed criticality events terminating at extremely early times when the degradation model was active in the waste form process model, which meant a fast degradation of the grid spacers. It was found that the cause of the very early termination was a unit error within the SPACER\_DEGRADATION\_MECHANISM block in the input deck used to run the simulation. Regardless, the previous model was revised to conform with implications from the literature not understood previously. The new approach uses scaling based on the thickness of the Zircaloy sheets comprising the grid spacers. Detailed application of the new model is provided in Section 3.6.3 of Nole et al. (2023).

FY2022 simulations using the quarter-waste package shale model failed with an error when the start of a criticality event was set to any time after  $10^{-6}$  years, and as a result all simulations were set up with a CANISTER\_BREACH\_TIME of  $10^{-6}$  years and CRIT\_START of  $10^{-6}$  years (Price et al. 2022). The issue causing simulations to fail with a criticality start time other than  $10^{-6}$  years was investigated and resolved. Previously within the code, the denominator of the instant release molality formula could go to zero, which resulted in an infinite value or NaN causing a simulation failure. This issue was resolved by adding a small value to the denominator of the fractions to avoid having a NaN value. In FY2023, the set up for the shale deterministic simulation involved an initial criticality start time of 500 years, followed by the seven other start times previously mentioned.

Both previous shale simulations (Price et al. 2021, 2022) incorporated a model allowing smectite to be transformed into illite, resulting in an increase in permeability. In previous FY simulations, this smectite-to-illite transition model was implemented solely in the buffer material. FY2023 simulations extended the use of this model to both the buffer material and DRZ.

**Table 2-1. DPC (MPC-89-W047) BWR Waste Package Criticality Duration versus Start for Different Power Levels**

Start of Criticality (years)	Duration of Criticality (years)		
	1 kW	2 kW	4 kW
0	236,087	110,932	59,419
100	237,952	108,350	68,911
500	238,935	119,511	83,131
1,000	238,877	109,265	60,841
5,000	233,763	111,981	66,568
10,000	225,109	113,252	62,760
20,000	218,045	117,753	76,551
50,000	193,707	99,681	67,217
100,000	192,513	107,500	64,593
500,000	200,545	105,360	67,013

**Table 2-2. DPC (MPC-32-162) PWR Waste Package Criticality Duration versus Start for Different Power Levels**

Start of Criticality (years)	Duration of Criticality (years)		
	1 kW	2 kW	4 kW
0	28,344	13,319	5,188
100	28,568	13,009	5,040
500	28,686	12,710	5,151
1,000	28,679	13,119	5,389
5,000	28,065	13,445	6,251
10,000	27,026	14,411	6,906
20,000	26,178	14,138	7,127
50,000	23,256	12,400	6,258
100,000	22,012	11,070	5,467
500,000	24,077	12,650	6,239

**Table 2-3. DPC (MPC-89-W047) Randomly Selected BWR Waste Packages, Specific Criticality Start Time, and Constant Power Applied within Single Deterministic Simulation**

BWR Waste Package No.	Waste Package Name	Criticality Start (years)	Constant Power (kW)
1	wp12_24	500	1
2	wp7_36	1,000	1
3	wp10_27	5,000	1
4	wp5_25	10,000	1
5	wp3_12	20,000	1
6	wp12_47	50,000	1
7	wp10_37	100,000	1
8	wp8_16	500,000	1
9	wp1_34	500	2
10	wp4_18	1,000	2
11	wp13_22	5,000	2
12	wp5_49	10,000	2
13	wp1_17	20,000	2
14	wp8_45	50,000	2
15	wp3_7	100,000	2
16	wp6_0	500,000	2
17	wp11_6	500	4
18	wp13_20	1,000	4
19	wp12_27	5,000	4
20	wp8_31	10,000	4
21	wp10_5	20,000	4
22	wp8_38	50,000	4
23	wp3_14	100,000	4
24	wp1_18	500,000	4

NOTE: BWR = boiling water reactor  
wp = waste package

**Table 2-4. DPC (MPC-32-162) Randomly Selected PWR Waste Packages, Specific Criticality Start Time, and Constant Power Applied within Single Deterministic Simulation**

PWR Waste Package No.	Waste Package Name	Criticality Start (years)	Constant Power (kW)
1	wp28_15	500	1
2	wp26_20	1,000	1
3	wp39_17	5,000	1
4	wp31_32	10,000	1
5	wp39_33	20,000	1
6	wp33_43	50,000	1
7	wp38_18	100,000	1
8	wp26_0	500,000	1
9	wp20_27	500	2
10	wp37_6	1,000	2
11	wp32_18	5,000	2
12	wp19_15	10,000	2
13	wp27_9	20,000	2
14	wp38_30	50,000	2
15	wp24_48	100,000	2
16	wp38_40	500,000	2
17	wp36_36	500	4
18	wp14_8	1,000	4
19	wp20_31	5,000	4
20	wp40_13	10,000	4
21	wp35_23	20,000	4
22	wp23_37	50,000	4
23	wp21_47	100,000	4
24	wp34_14	500,000	4

NOTE: PWR = pressurized water reactor  
wp = waste package

## 2.3 Modeling Results

Many simulations (~50) of varying complexity were set up, tested, and built upon to incorporate (1) the use of BWR and PWR waste packages, (2) a total of 48 criticality events in the same repository (24 for BWR region, 24 for PWR region), (3) 8 different start times of the critical events, and (4) 3 different constant power levels associated with these events. Twenty-four combinations of possible criticality events based on Table 2-1 and Table 2-2 were set up within WASTE\_FORM\_GENERAL, WASTE\_FORM, and CRITICALITY\_MECH blocks.

The first set (Figure 2-8 to Figure 2-14) and second set (Figure 2-16 and Figure 2-17) of results shown below stem from two deterministic simulations. The first simulation differed from the second simulation in that the second simulation included (1) the smectite-to-illite transition model applied to both the buffer/DRZ materials, (2) all waste packages specified only through the WASTE\_FORM blocks, (3) a noncritical CRITICALITY\_MECHANISM block with an applied constant power of 0 kW, and (4) only two waste packages (one BWR and one PWR) going through a 1 kW critical event at 500 years. Simplifications between the first and second simulation were made in an effort to have the run complete. The first listed difference was not a simplification but considered use of both the buffer and DRZ materials with the smectite-to-illite transition model. The second listed difference had the second simulation set up with the WASTE\_FORM block for each noncritical waste package in which canisters were specified to breach at 11,000 years instead of using the CANISTER\_DEGRADATION\_MODEL. The third difference is required because of the use of WASTE\_FORM block for noncritical waste packages instead of SOURCE\_SINK blocks. A 0 kW constant power is applied through the CRITICALITY\_MECHANISM block for all waste packages that remain subcritical and is set to use the inventory/decay-heat for either a BWR or PWR. The fourth difference was a great simplification in that only two waste packages (one BWR, one PWR) were set to have a 1 kW criticality event at 500 years. The first simulation was run using 576 processors (16 nodes) on a high-performance computer; it had a runtime of about 7 hours before it failed, reaching 504 years simulation time in the first hour of the runtime. The second simulation was run using 1,022 processors (~29 nodes); it had a runtime of ~15 hours before it was cancelled because of stalling at 500.4 years simulation time. Neither simulation was able to run to the final time of 1,000,000 years and, as a result, debugging efforts are planned for FY2024. Nevertheless, results obtained from ~500-year simulations are presented here.

Results for the first simulation in Figure 2-8 to Figure 2-14 show four views of the model including a horizontal ( $x$ - $y$ ) slice through the repository and an isometric view of the model domain at seven times (0, 0.1, 100, 200, 300, 400, and 504 years). Each figure is specific to one of the seven times. In each figure, the top left view (a) shows an  $x$ - $y$  slice colored by material ID: waste packages, buffer, DRZ, and shale host rock; the top right view (b) shows the same slice colored by temperature ( $^{\circ}\text{C}$ ) at that same simulation time; the bottom left (c) shows the isometric view of the model showing  $^{129}\text{I}$  plumes colored by  $^{129}\text{I}$  concentration; and lastly the bottom right view (d) shows the  $x$ - $y$  slice colored by  $^{129}\text{I}$  concentration.

At 0 years (Figure 2-8), no decay heat is currently being applied, thus initial repository temperature is  $28^{\circ}\text{C}$  and the concentration of  $^{129}\text{I}$  (the only radionuclide being tracked) is zero, which is indicated by a concentration of  $1.0 \times 10^{-20}$  M. At time 0.1 years (Figure 2-9), the decay heat emitted by all BWR and PWR waste packages can be seen in the top right visual and there is no difference in  $^{129}\text{I}$  concentration.

At 100 years (Figure 2-10), a clear difference in repository temperatures due to the BWR (west 1/3 of repository) and PWR (east 2/3 of repository) regions can be seen in the top right visual (b), where the BWR region is noticeably warmer. At 200 years (Figure 2-11), temperatures continue to rise in both regions, and again the BWR region is the higher temperature region. By 300 years (Figure 2-12), temperatures in the repository region continue to rise, but by this time 9 noncritical waste packages have breached (2 BWRs, 7 PWRs) because of the CANISTER\_DEGRADATION\_MODEL applied within these waste packages. The isometric view at 300 years shows  $^{129}\text{I}$  plumes, and the  $x$ - $y$  slice shows  $^{129}\text{I}$  concentrations around  $1.9 \times 10^{-4}$  M at the breached waste packages.

At 400 years (Figure 2-13), temperatures in the repository have not changed much, and 7 more waste packages have breached (3 BWRs, 4 PWRs). By 504 years (Figure 2-14), 16 additional waste packages (6 BWRs, 10 PWRs) have breached, but 6 of them (3 BWRs, 3 PWRs) were deliberately specified to

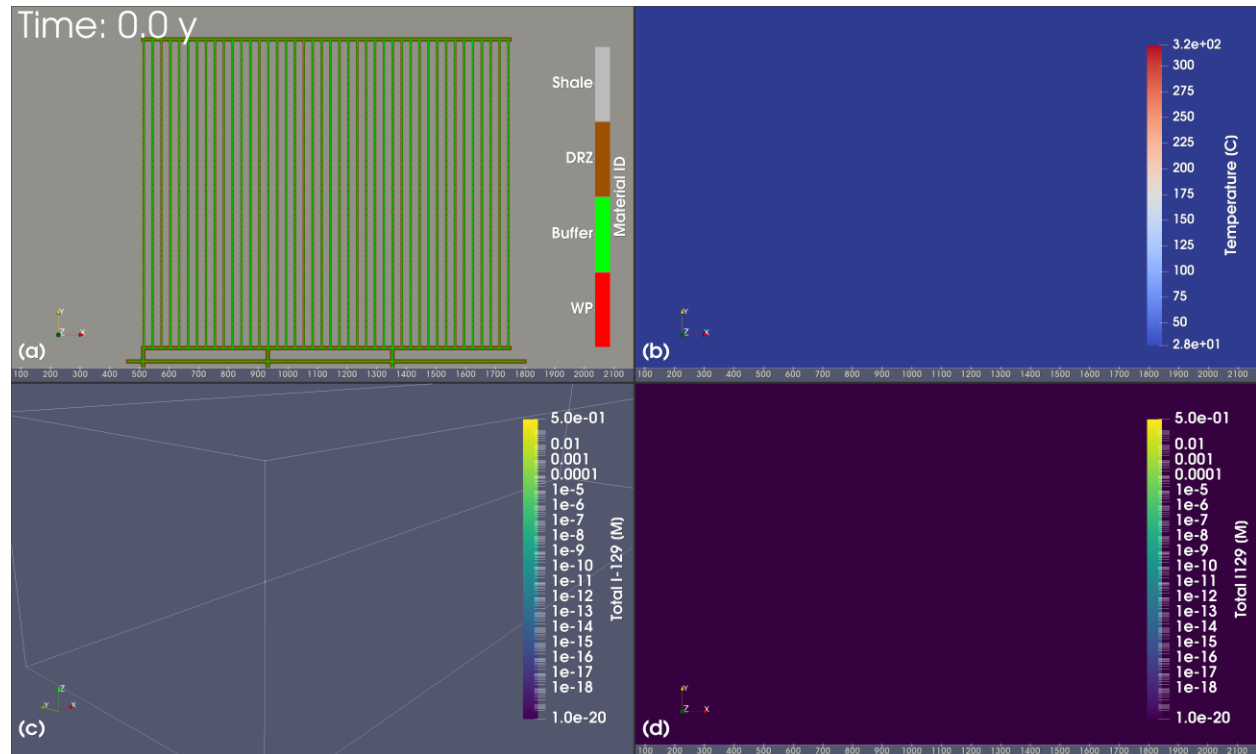
breach at 499 years and have an applied constant power of either 1, 2, or 4 kW (refer to Table 2-3 and Table 2-4). Waste packages going through a critical event at 500 years are circled and labeled. Temperature ( $^{\circ}\text{C}$ ) and  $^{129}\text{I}$  concentration data at 504 years simulation time are presented in Table 2-5 for the BWR and PWR waste packages going through a critical event at 500 years. Waste packages with a 4 kW constant power applied (“wp11\_6” and “wp36\_36”) due to the criticality event experienced higher temperatures and a higher  $^{129}\text{I}$  concentration, as would be expected, when compared to other waste packages with a lower constant power being applied. Both temperature ( $^{\circ}\text{C}$ ) and  $^{129}\text{I}$  concentration data differ when comparing results for various waste packages that have breached by 504 years. This comparison includes both subcritical waste packages that have breached by 504 years (most have breached by 400 years). Lower  $^{129}\text{I}$  concentrations are seen at 504 years for subcritical waste packages when compared to critical waste packages because of earlier breach times that have allowed for concentrations to move out of the waste package region. Temperature differences between waste packages are shown to be as high as about  $100^{\circ}\text{C}$ . These differences can be seen when comparing waste packages with a 4 kW applied constant power to waste packages in the same BWR or PWR region located towards the repository edge where temperatures are generally lower. The opposite can be said when comparing between waste packages located towards the center of either the BWR or PWR regions, where repository temperatures are higher. Figure 2-15 shows the location and name of all waste packages referenced in Table 2-5 and Table 2-6.

Results for the second simulation focus on the incorporation of the illite-to-smectite transition model within the buffer and DRZ material. Figure 2-16 and Figure 2-17 show a vertical ( $x-z$ ) slice through the repository at observation points “wp2\_BWR” and “wp0\_PWR” and a full  $x-z$  view of the repository at 0- and 400-years simulation time, respectively. Initially at the time of 0 years, the permeability is set to be  $1 \times 10^{-20} \text{ m}^2$  and  $1 \times 10^{-18} \text{ m}^2$  for the buffer and DRZ, respectively. By 400 years, the permeability has transformed since the applied model is time and temperature dependent. Within these visuals, the impact on permeability changes can be seen when comparing temperature differences between the BWR and PWR waste packages. For the BWR waste package, the buffer permeability at 400 years is  $4.874 \times 10^{-18} \text{ m}^2$  (initially  $1 \times 10^{-20} \text{ m}^2$ ) and  $1.413 \times 10^{-16} \text{ m}^2$  (initially  $1 \times 10^{-18} \text{ m}^2$ ) for the DRZ. Similarly, for the PWR waste package, the buffer permeability at 400 years is  $3.262 \times 10^{-18} \text{ m}^2$  (initially  $1 \times 10^{-20} \text{ m}^2$ ) and  $8.911 \times 10^{-17} \text{ m}^2$  (initially  $1 \times 10^{-18} \text{ m}^2$ ) for the DRZ. These visuals show the temperature effects on the permeability of the buffer and DRZ materials; future simulations will apply the illite-to-smectite transition model to the shale host rock.

Figure 2-18 and Figure 2-19 present the results for a third simulation, in which the repository contains only PWR waste packages. For this simulation, the focus was on gathering results from implementing the updated grid spacer degradation model. Figure 2-18 shows two PWR waste packages, “wp6\_24” and “wp21\_24”, plotted over the 1,000,000-year simulation. Waste package “wp6\_24” in this simulation was set up to have a criticality event at 500 years with a constant power of 1 kW. Data show that, after the waste package breaches, the spacer vitality degradation rate average (1/yr) is  $1.98 \times 10^{-14} \text{ 1/yr}$ , and the spacer vitality percentage reaches nearly zero by 841 years, indicating that the grid spacers have failed and the criticality event has ceased.

Differing results are seen for “wp21\_24”, which is set up to have a criticality event at 10,000 years with a constant power of 1 kW. After this particular waste package fails, the spacer vitality degradation rate average between 10,000 and 1,000,000 years is  $9.83 \times 10^{-18} \text{ 1/yr}$ , and spacer vitality falls to 0.864 but never reaches zero, meaning that the grid spacers did not fail and the criticality event did not cease as a result of grid spacer failure. That said, the criticality event would have ceased as a result of loss of fissile material (Table 2-2). Temperature plays a key role in explaining the why grid spacers failed in “wp6\_24”

and why they did not fail in “wp21\_24.” Grid spacer failure is a function of the general corrosion rate of the grid spacer material and is highly dependent on the temperature (e.g., Arrhenius equation) (Price et al. 2021). Figure 2-19 shows temperatures for the two waste packages, including a sudden temperature spike due to the occurrence of the criticality event set for both waste packages. For “wp6\_24”, the maximum temperature of 275°C is reached because of the 1 kW critical event set to occur at 500 years (near the time of the peak temperature due to decay heat). This combination of circumstances is the reason grid spacers failed in a few hundred years. For “wp21\_24”, the maximum temperature reached due to the criticality event was 166°C, over 100°C lower than the maximum temperature for waste package “wp6\_24”.

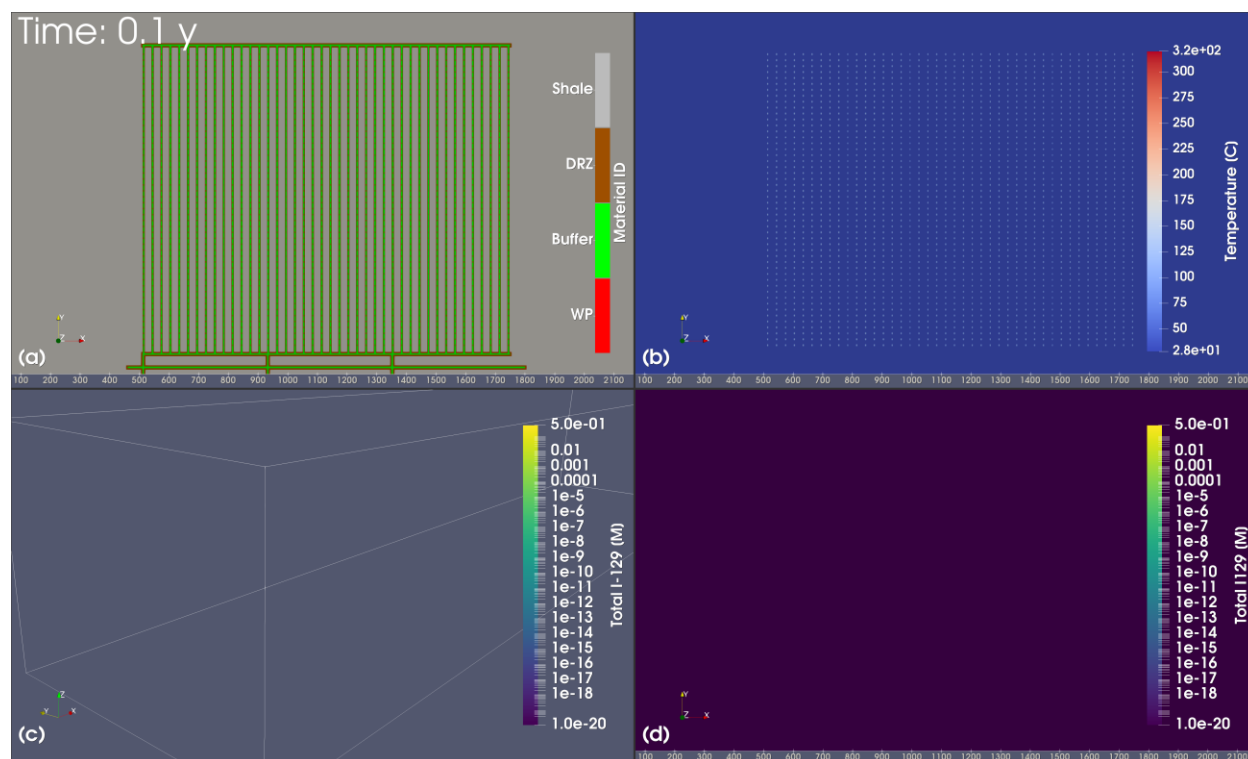


NOTE: Temperature (°C) and <sup>129</sup>I concentration ranges have been rescaled over all time steps.

DRZ = disturbed rock zone

WP = waste package

**Figure 2-8. Horizontal (x–y) Slice through Repository and Isometric View of the Model Domain at 0 Years Showing (a) Slice of Waste Packages, Buffer, DRZ, and Shale Host Rock Colored by Material ID; (b) Slice Colored by Temperature; (c) Isometric View of <sup>129</sup>I Plumes Colored by <sup>129</sup>I Concentration; and (d) Slice Colored by <sup>129</sup>I Concentration**

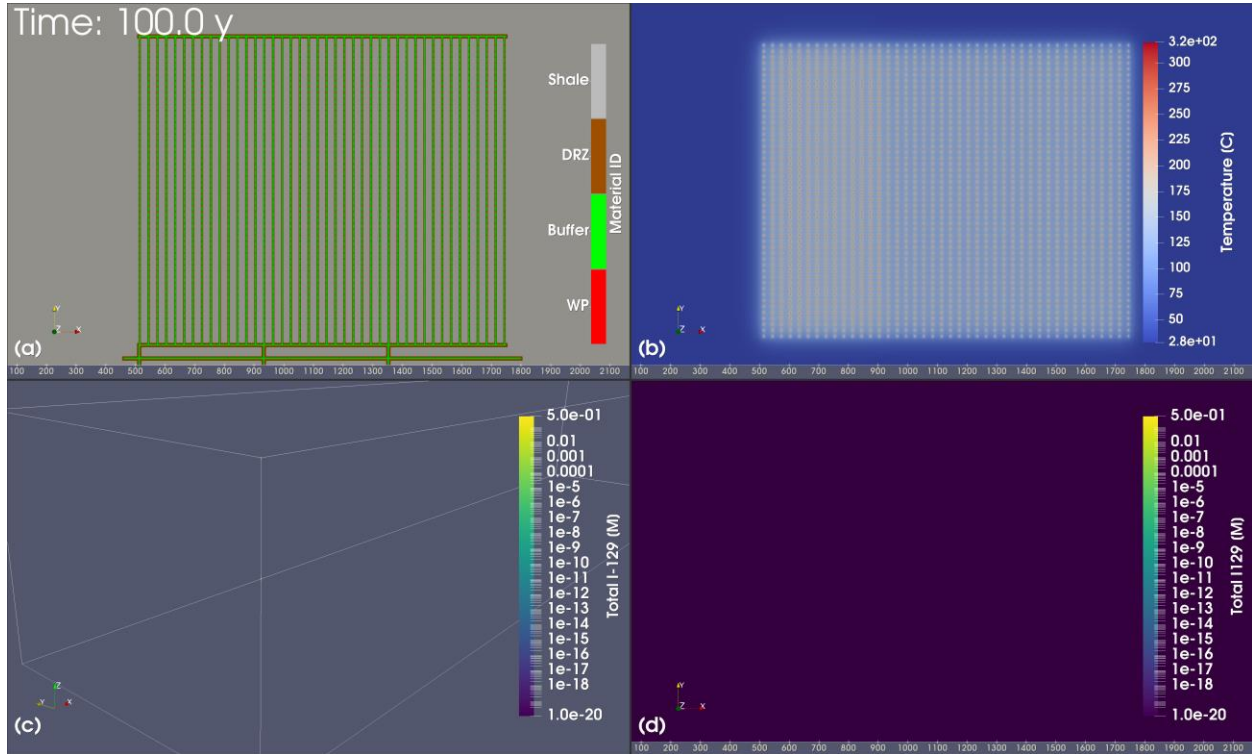


NOTE: Temperature (°C) and  $^{129}\text{I}$  concentration ranges have been rescaled over all time steps.

DRZ = disturbed rock zone

WP = waste package

**Figure 2-9. Horizontal (x-y) Slice through Repository and Isometric View of the Model Domain at 0.1 Years Showing (a) Slice of Waste Packages, Buffer, DRZ, and Shale Host Rock Colored by Material ID; (b) Slice Colored by Temperature; (c) Isometric View of  $^{129}\text{I}$  Plumes Colored by  $^{129}\text{I}$  Concentration; and (d) Slice Colored by  $^{129}\text{I}$  Concentration**

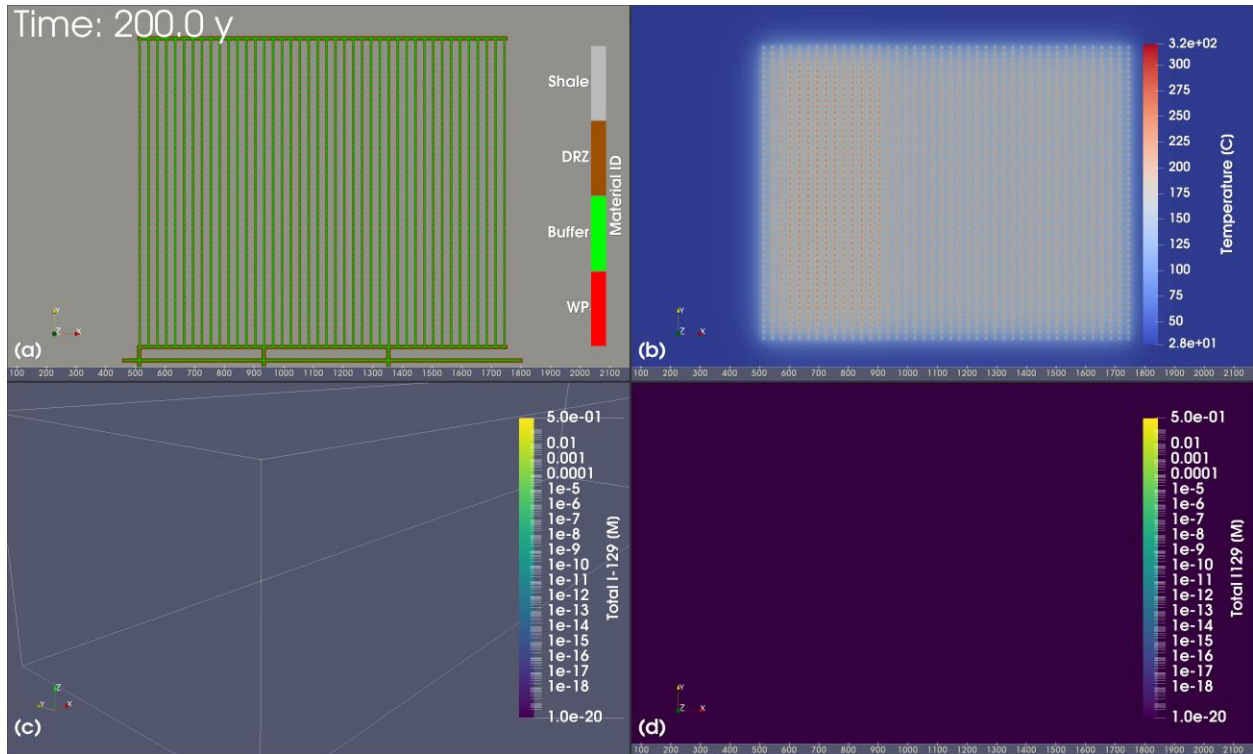


NOTE: Temperature (°C) and <sup>129</sup>I concentration ranges have been rescaled over all time steps.

DRZ = disturbed rock zone

WP = waste package

**Figure 2-10. Horizontal (x-y) Slice through Repository and Isometric View of the Model Domain at 100 Years Showing (a) Slice of Waste Packages, Buffer, DRZ, and Shale Host Rock Colored by Material ID; (b) Slice Colored by Temperature; (c) Isometric View of <sup>129</sup>I Plumes Colored by <sup>129</sup>I Concentration; and (d) Slice Colored by <sup>129</sup>I Concentration**

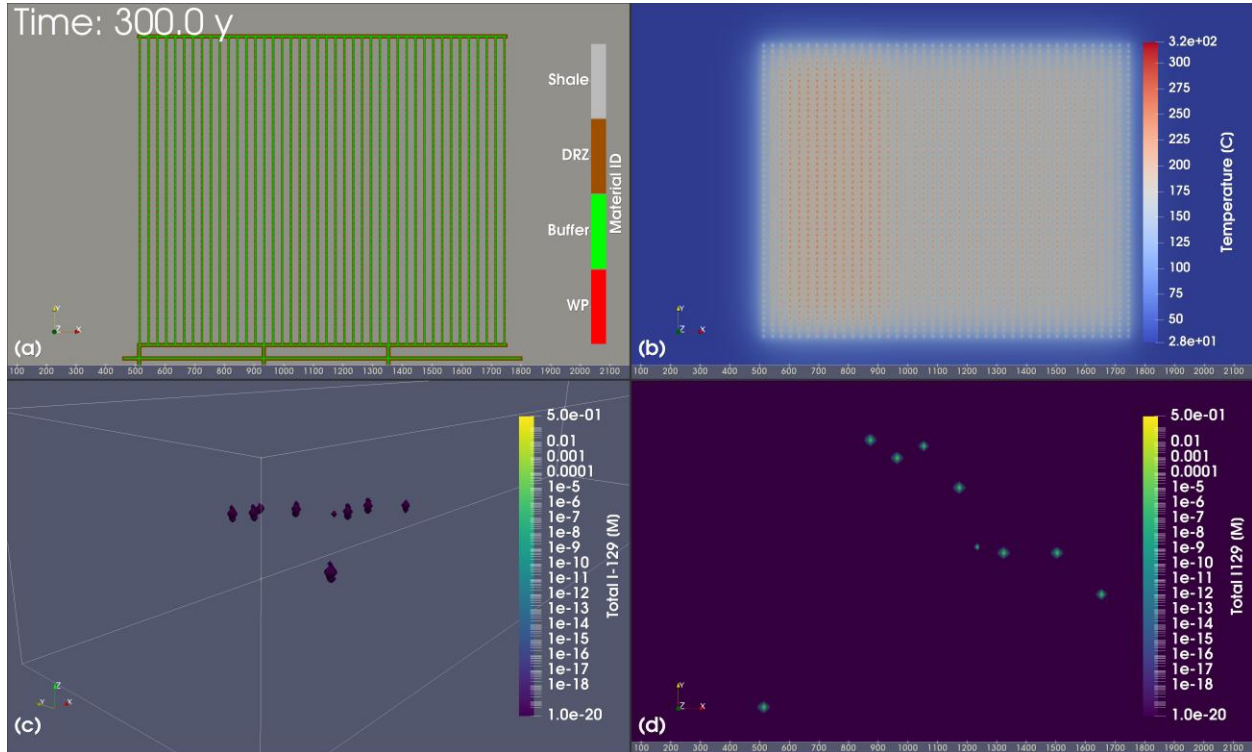


NOTE: Temperature (°C) and  $^{129}\text{I}$  concentration ranges have been rescaled over all time steps.

DRZ = disturbed rock zone

WP = waste package

**Figure 2-11. Horizontal (x–y) Slice through Repository and Isometric View of the Model Domain at 200 Years Showing (a) Slice of Waste Packages, Buffer, DRZ, and Shale Host Rock Colored by Material ID; (b) Slice Colored by Temperature; (c) Isometric View of  $^{129}\text{I}$  Plumes Colored by  $^{129}\text{I}$  Concentration; and (d) Slice Colored by  $^{129}\text{I}$  Concentration**

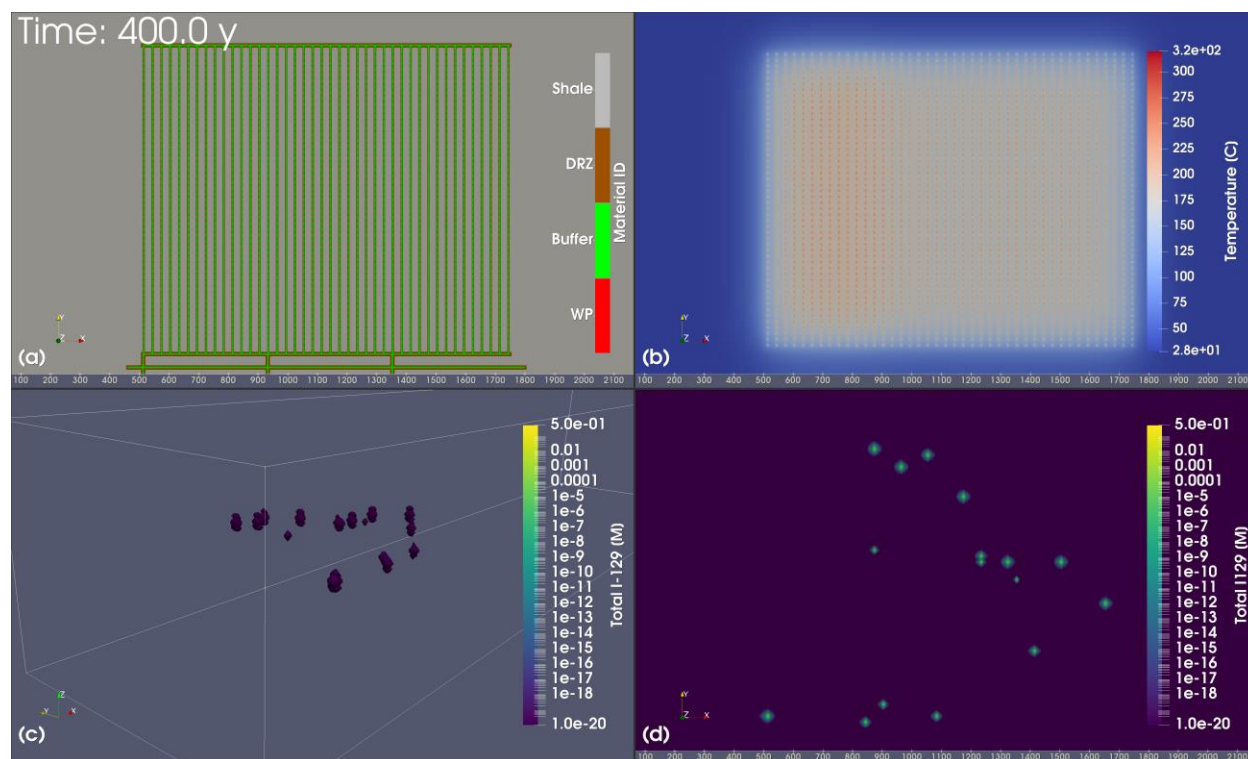


NOTE: Temperature (°C) and <sup>129</sup>I concentration ranges have been rescaled over all time steps.

DRZ = disturbed rock zone

WP = waste package

**Figure 2-12. Horizontal (x-y) Slice through Repository and Isometric View of the Model Domain at 300 Years Showing (a) Slice of Waste Packages, Buffer, DRZ, and Shale Host Rock Colored by Material ID; (b) Slice Colored by Temperature; (c) Isometric View of <sup>129</sup>I Plumes Colored by <sup>129</sup>I Concentration; and (d) Slice Colored by <sup>129</sup>I Concentration**

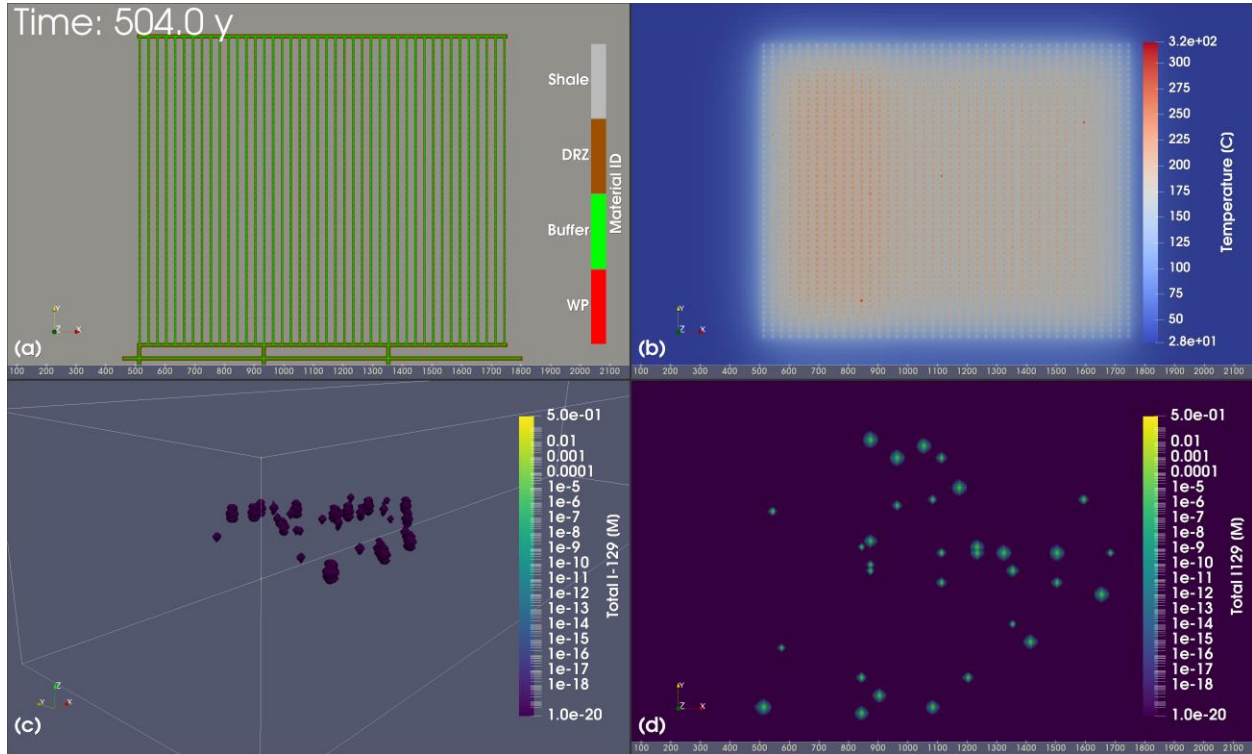


NOTE: Temperature (°C) and total <sup>129</sup>I concentration ranges have been rescaled over all time steps.

DRZ = disturbed rock zone

WP = waste package

**Figure 2-13. Horizontal (x-y) Slice through Repository and Isometric View of the Model Domain at 400 Years Showing (a) Slice of Waste Packages, Buffer, DRZ, and Shale Host Rock Colored by Material ID; (b) Slice Colored by Temperature; (c) Isometric View of <sup>129</sup>I Plumes Colored by <sup>129</sup>I Concentration; and (d) Slice Colored by <sup>129</sup>I Concentration**



NOTE: Temperature (°C) and total <sup>129</sup>I concentration ranges have been rescaled over all time steps.

DRZ = disturbed rock zone

WP = waste package

**Figure 2-14. Horizontal (x-y) Slice through Repository and Isometric View of the Model Domain at 504 Years Showing (a) Slice of Waste Packages, Buffer, DRZ, and Shale Host Rock Colored by Material ID; (b) Slice Colored by Temperature; (c) Isometric View of <sup>129</sup>I Plumes Colored by <sup>129</sup>I Concentration; and (d) Slice Colored by <sup>129</sup>I Concentration**

**Table 2-5. Data for BWR and PWR Waste Packages 504 Years after Disposal with Criticality Initiated at 500 Years**

BWR or PWR	Waste Package Name	Constant Power (kW)	Temperature (°C) at 504 years	Total <sup>129</sup> I (M) at 504 years
BWR	wp12_24	1	289	7.5e-03
BWR	wp1_34	2	292	1.3e-02
BWR	wp11_6	4	320	5.0e-01
PWR	wp28_15	1	274	3.5e-04
PWR	wp20_27	2	300	1.2e-02
PWR	wp36_36	4	315	2.2e-02

NOTE: <sup>129</sup>I concentration is at the specified waste package within the repository, not in the water well.

BWR = boiling water reactor

PWR = pressurized water reactor

wp = waste package

**Table 2-6. Data for Selected Breached Subcritical BWR and PWR Waste Packages 504 Years after Disposal**

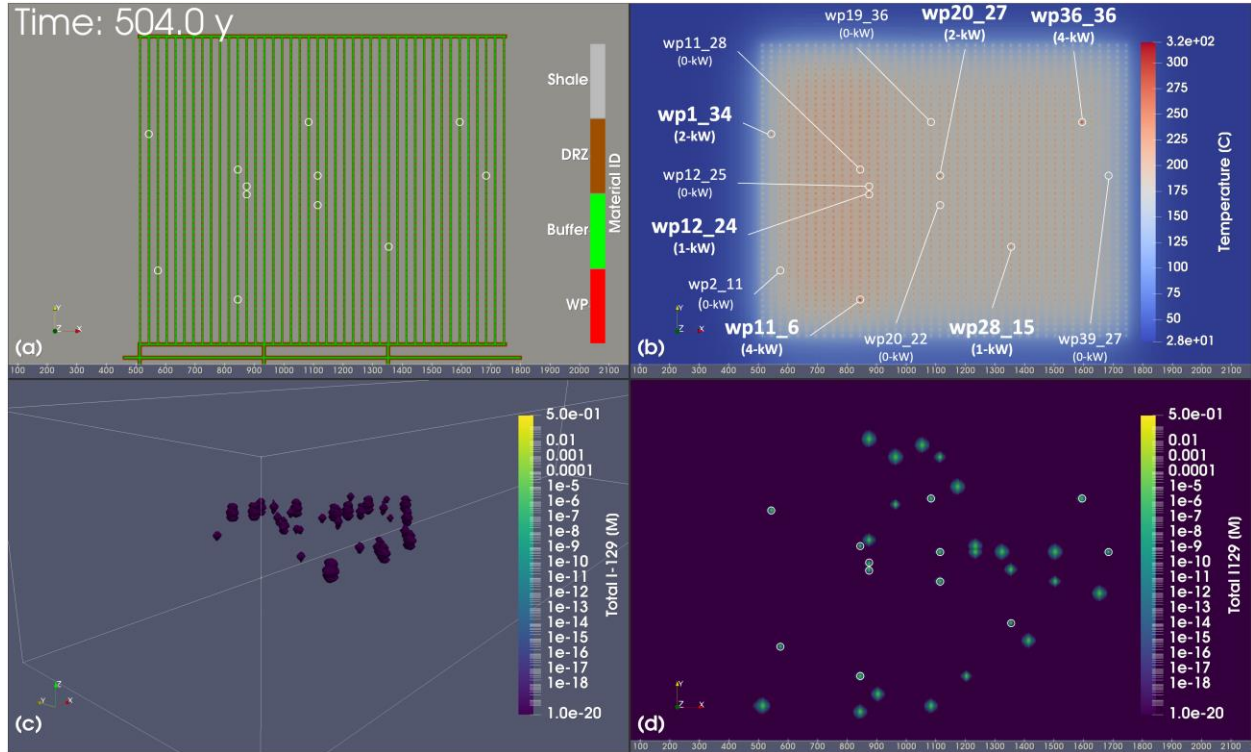
BWR or PWR	Waste Package Name	Constant Power (kW)	Temperature (°C) at 504 years	Total <sup>129</sup> I (M) at 504 years
BWR	wp2_11	0	235	4.0e-04
BWR	wp12_25	0	255	3.6e-04
BWR	wp11_28	0	256	4.1e-04
PWR	wp19_36	0	236	2.7e-04
PWR	wp20_22	0	236	2.2e-04
PWR	wp39_27	0	215	3.2e-04

NOTE: <sup>129</sup>I concentration is at the specified waste package within the repository, not in the water well.

BWR = boiling water reactor

PWR = pressurized water reactor

wp = waste package

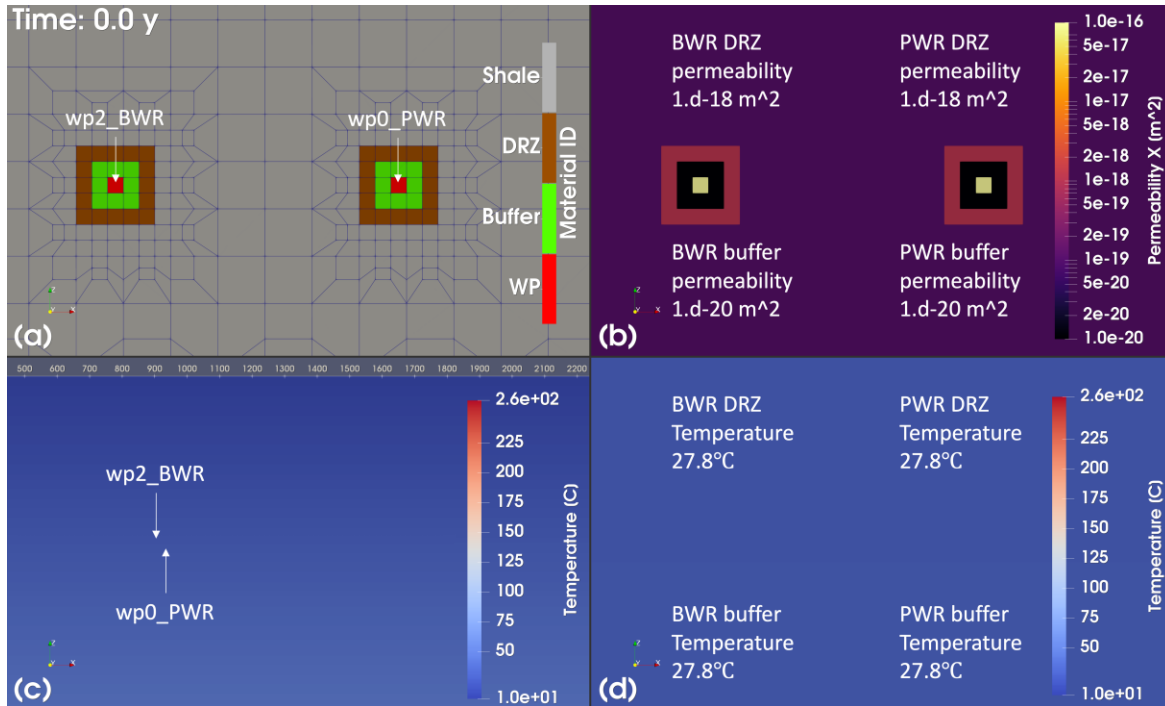


NOTE: Waste packages identified in Table 2-5 and Table 2-6 are circled the x-y slices (a), (b), and (d). Labels are provided in (b).

DRZ = disturbed rock zone

WP or wp = waste package

**Figure 2-15. Horizontal (x-y) Slice through Repository and Isometric View of the Model Domain at 504 Years Showing (a) Slice of Waste Packages, Buffer, DRZ, and Shale Host Rock Colored by Material ID; (b) Slice Colored by Temperature; (c) Isometric View of <sup>129</sup>I Plumes Colored by Total <sup>129</sup>I Concentration; and (d) Slice Colored by Total <sup>129</sup>I Concentration**



NOTE: Observation points of interest are labeled in vertical (x-z) slice in (a) and full x-z view of the repository in (c).

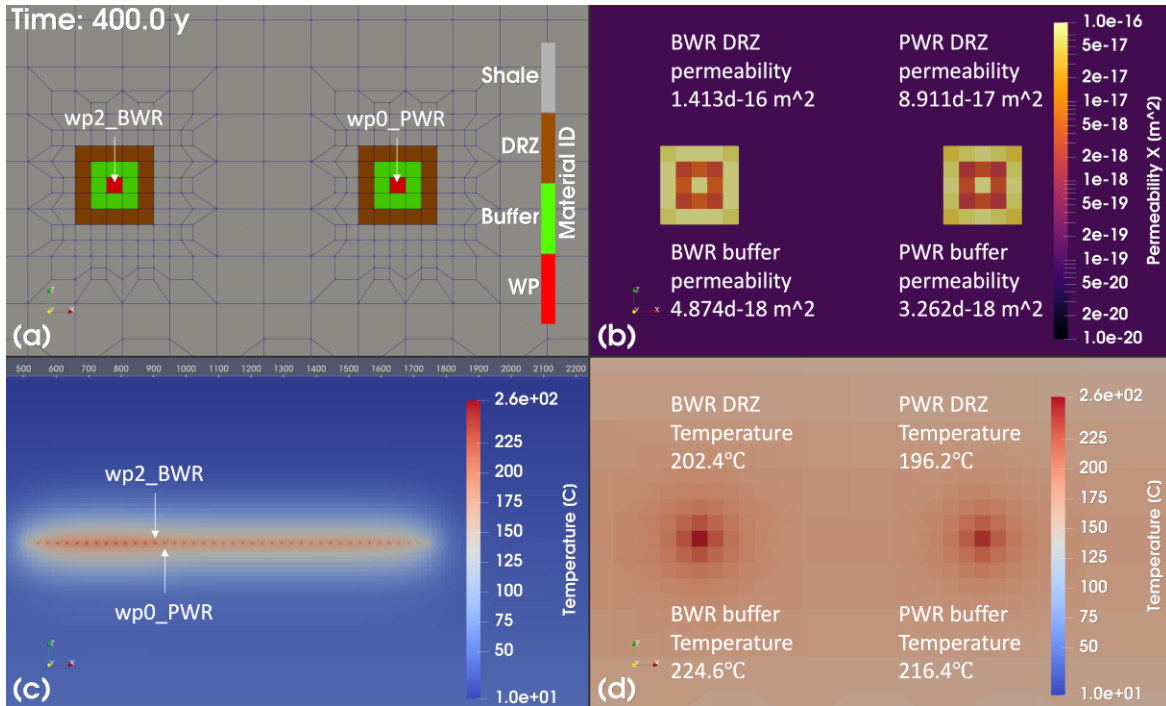
BWR = boiling water reactor

DRZ = disturbed rock zone

PWR = pressurized water reactor

WP or wp = waste package

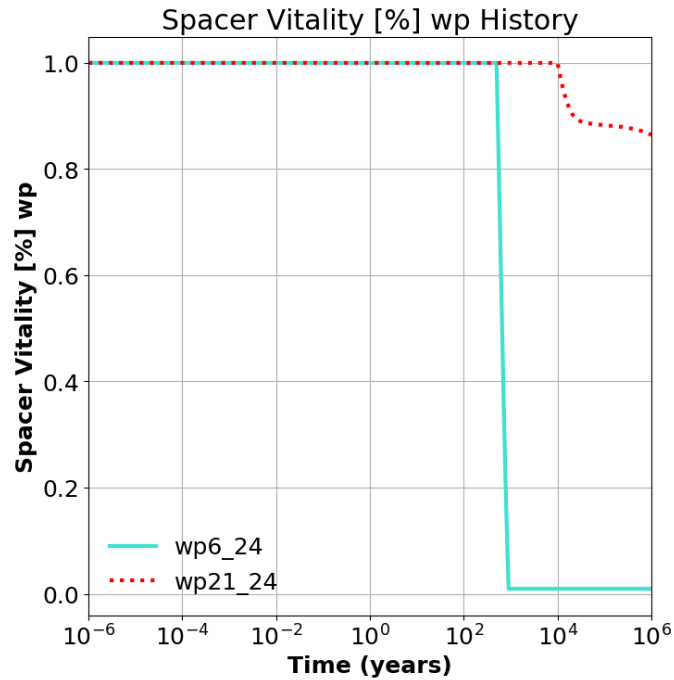
**Figure 2-16. Vertical (x-z) Slice through Repository at “wp2\_BWR” and “wp0\_PWR” as well as Full x-z View of Repository at 0 Years Showing (a) Slice of Waste Packages, Buffer, DRZ, and Shale Host Rock Colored by Material ID; (b) Slice Colored by Permeability; (c) Full x-z View of Repository Colored by Temperature; and (d) Slice Colored by Temperature**



NOTE: Observation points of interest are labeled in vertical (x-z) slice in (a) and full x-z view of the repository in (c).

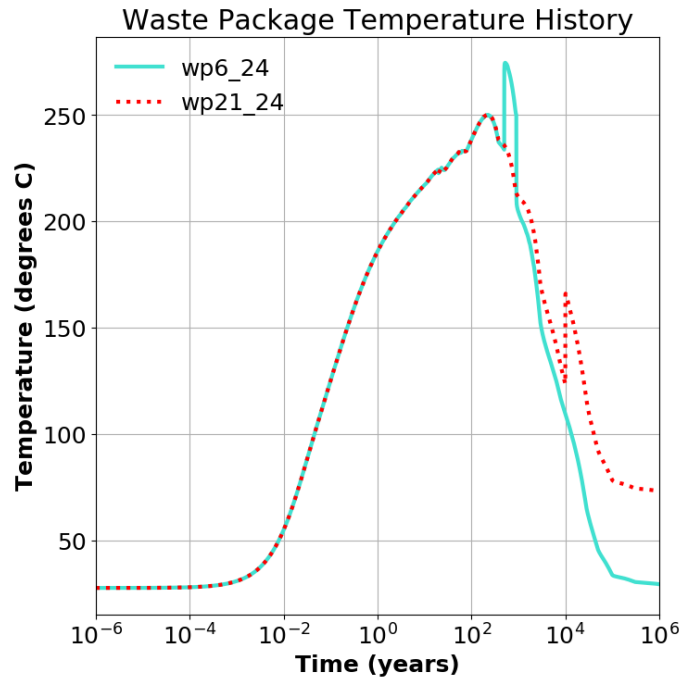
- BWR = boiling water reactor
- DRZ = disturbed rock zone
- PWR = pressurized water reactor
- WP or wp = waste package

**Figure 2-17. Vertical (x-z) Slice through Repository at “wp2\_BWR” and “wp0\_PWR” as well as Full x-z View of Repository at 400 Years Showing (a) Slice of Waste Packages, Buffer, DRZ, and Shale Host Rock Colored by Material ID; (b) Slice Colored by Permeability; (c) Full x-z View of Repository Colored by Temperature; and (d) Slice Colored by Temperature**



NOTE: A 1 kW criticality event is set to occur at 500 years for waste package wp6\_24 and 10,000 years for wp21\_24.  
wp = waste package

**Figure 2-18. Waste Package Spacer Vitality Percentage for Two PWR Waste Packages**



NOTE: A 1 kW criticality event is set to occur at 500 years for waste package wp6\_24 and 10,000 years for wp21\_24.  
wp = waste package

**Figure 2-19. Waste Package Temperature for two PWR Waste Packages**

## 2.4 Evaluating TH Tools for Boiling Canisters

This section and the next section (Section 2.5) focus on processes occurring within a waste package, rather than on processes occurring on a repository scale.

### 2.4.1 Motivation

Accurately modeling the behavior of a waste package undergoing a criticality event requires simulations of neutron radiation transport (neutronics), isotopic depletion and activation in the fuel, and TH processes of the infiltrated groundwater within the canister, as well as potentially other physics depending upon the details of the scenario being modeled. Of these, the TH processes have proved the most challenging. A key objective of the TH analysis is to accurately calculate fuel temperatures and moderator densities for feedback to the neutronic calculation. Calculating these quantities is especially difficult under two-phase fluid conditions, requiring accurate representation of the following physical phenomena:

- Liquid-vapor interface (water level) elevation
- Local nucleate boiling in subcooled liquid at the fuel rod surface
- Vapor superheating
- Two-phase boiling heat transfer between the solid structures (fuel rods, basket walls, canister walls) and the coolant
- Impact of local coolant density/void fraction on local fuel rod heat generation rate

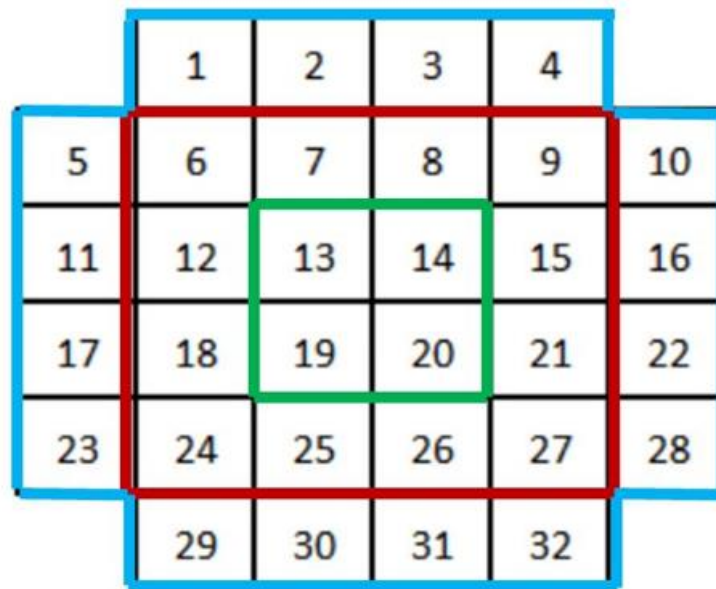
Liquid water is far denser than vapor: 1,600 times denser at atmospheric pressure and 30 times denser at 5 MPa, which is the hydrostatic pressure imposed on a DPC buried 500 m in a saturated repository. Water in its liquid phase is an efficient moderator of neutrons, thus supporting fission reactions. Additionally, the liquid phase is also far more effective at removing heat from the fuel rods than the vapor phase, which impacts fuel temperatures. These factors result in moderator reactivity feedback, which impacts not only the spatial heat generation distribution but also the overall canister criticality. Therefore, accurate calculation of the overall boiling rate as well as the liquid and vapor spatial distributions throughout the canister is of high importance.

A primary objective of FY2023 modeling efforts was to determine RELAP5-3D's (The RELAP5-3D Code Development Team 2018) suitability for predicting the two-phase phenomena listed above. In FY2022, RELAP5-3D was found to provide acceptably accurate predictions under single-phase liquid conditions within the canister, as compared with Star-CCM+ (Benavides et al. 2020). However, after assessing RELAP5-3D's capabilities and performance under two-phase conditions in the FY2023, the study team found that RELAP5-3D does not provide the necessary modeling capabilities for predicting the water level's spatial location and its impact on canister performance given the geometric configuration of this system. A review of the capabilities of a variety of TH codes determined that the NRC's TRACE code (Jones et al. 2021) provides modeling features more suitable for resolving these phenomena in DPCs. A detailed discussion and supporting results are presented in the remainder of this section.

### 2.4.2 FY2022 Full-scale DPC Model

In Swinney et al. (2022), the liquid temperatures (liquid subcooling) over time inside a horizontal quarter-scale DPC canister were calculated using both RELAP5-3D and the STAR-CCM+ code. This comparison shows relatively good agreement, indicating that heat transfer was modeled reasonably well in RELAP5-3D under single-phase conditions. However, additional investigation suggested that it was necessary to more closely evaluate the applicability of RELAP5-3D in simulating this model when extending to two-phase flow.

Figure 2-20 shows a top view of the geometric setup of the assemblies in the FY2022 RELAP5-3D model, while Figure 2-21 shows the component layout of the entire RELAP5-3D model. The 32 assemblies in the basket were grouped into 3 concentric “rings” based on proximity to the radial center of the DPC. A fourth fluid region was modeled outside the basket, representing the flow region between the outermost basket walls and the DPC cylindrical wall. This grouping of assemblies and flow regions was a logical choice in terms of representing the radial convection and conduction of heat from the more central assemblies of the DPC outward toward the outer assemblies and outer structures of the DPC. This grouping scheme resulted in the highest temperature being predicted in the central assemblies with decreasing temperatures predicted towards the outer radius of the canister, which is the expected impact of radial conduction and convection.



NOTE: The green, red, and blue lines show the 3 concentric rings used to group the 32 assemblies in the basket.

**Figure 2-20. Top View of the Three-Ring Setup Used in the FY2022 RELAP5-3D MPC Model**

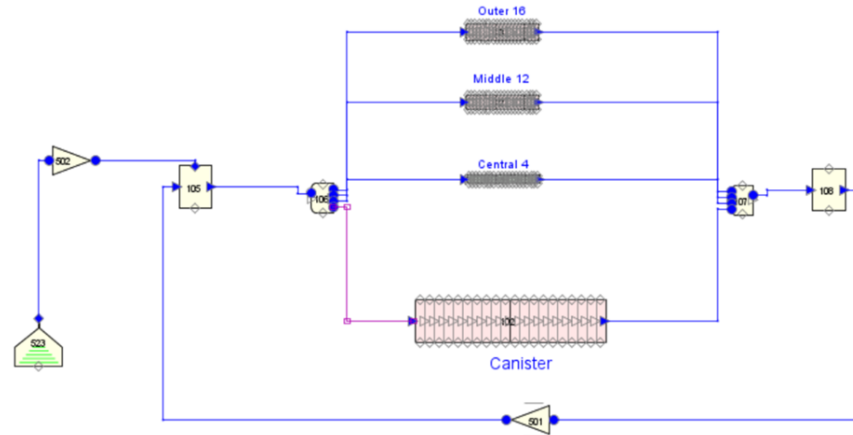


Figure 2-21. Component Diagram for the FY2022 RELAP5-3D MPC Model

However, the FY2022 model had a significant shortcoming in that it did not realistically represent a vertical flow distribution within each flow region, nor the resulting impact of the flow and heat transfer due to bulk natural circulation throughout the canister. In the RELAP5-3D component layout shown in Figure 2-21, the four flow channels (“Outer 16”, “Middle 12”, “Central 4”, and “Canister”) are all modeled as having a single vertical position and connected at common plena on the left and right. Natural circulation is driven by differences in fluid densities at different vertical positions; therefore, the lack of axial dependence in the FY2022 RELAP5-3D model prevents the representation of natural circulation throughout the canister.

Natural circulation/convection is a potentially significant heat transfer contributor that impacts the predicted canister thermal behavior. The FY2022 RELAP5-3D and STAR-CCM+ results showed reasonable agreement between the codes for single-phase conditions; however, as discussed in the previous section, two-phase conditions introduce significant additional modeling challenges, which can lead to far larger discrepancies in results than would be seen under single-phase conditions. Importantly, the FY2022 RELAP5-3D model provides no means of predicting the vertical gas/water interface level within the canister and therefore does not account for the potentially large vertical gradients in temperature and fluid conditions due to a two-phase mixture.

### 2.4.3 Full-scale DPC Vertical Pipe Model

The three-ring core treatment in the FY2022 RELAP5-3D model was replaced with a vertical pipe configuration to realistically model the vertical differences among the assemblies. Although under expected disposal conditions the canister configuration would be horizontal, it was modeled in RELAP5-3D using a “vertical pipe” component. The vertical pipe was made up of eight cells. Each “row” of assemblies (i.e., assemblies 1–4, 5–10, 11–16, etc. shown in Figure 2-22) were grouped as a separate heat structure and were connected to a separate cell of the pipe, with the two remaining cells representing the canister volume above and below the assembly basket. The setup of the vertical pipe representing the canister is detailed in Figure 2-22, and the heat structure grouping is detailed in Figure 2-23.

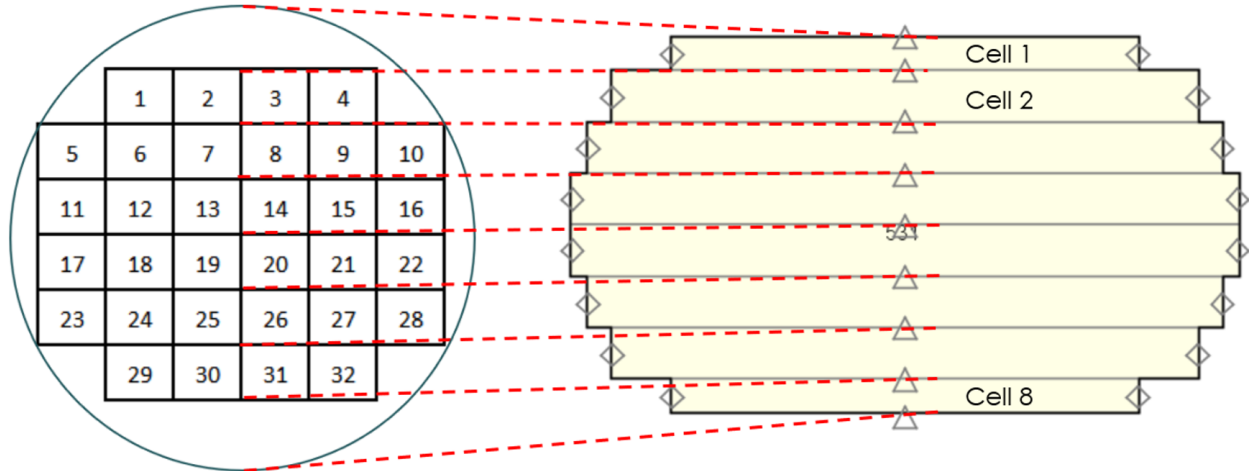


Figure 2-22. Vertical Pipe Setup Used in RELAP5-3D DPC Model

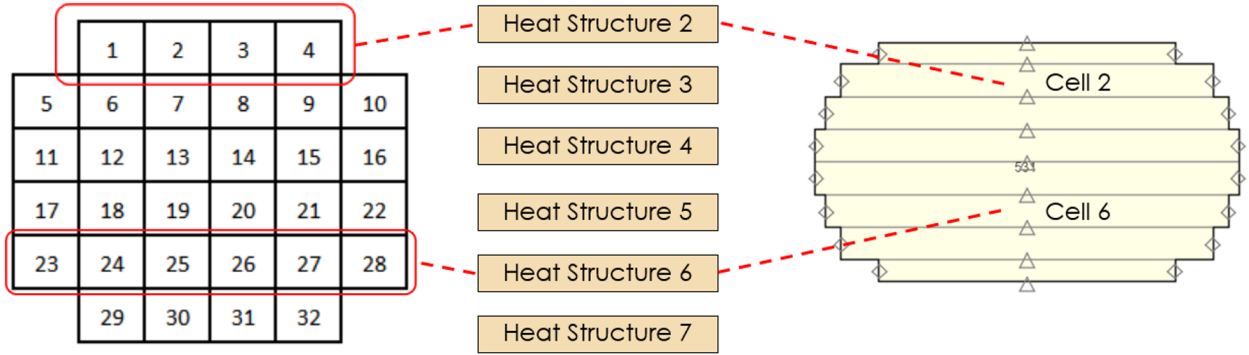


Figure 2-23. Heat Structure Grouping Scheme Used in RELAP5-3D MPC Model

Under two-phase conditions, the vertical pipe modeling scheme allows RELAP5-3D to calculate the water level, either at the boundaries between vertical cells or some fraction of the way along a cell. This representation provides a realistic vertical distribution of void fraction and mixture water density that allows RELAP5-3D to accurately determine the local wall-to-fluid heat transfer coefficient, buoyancy terms, frictional terms, and other parameters for the fluid solution. It also allows RELAP5-3D to provide realistic, vertically dependent, local fluid mixture densities to the neutronics calculation.

Another advantage of modeling the horizontal canister using a vertical pipe is the ability to connect the void fraction of the canister to the power level of each assembly row. For example, in reality, the top row of assemblies (cells 1–4 in Figure 2-23) will produce full power when the pipe cell connected to this row is full of water, and it will produce zero power when the water in the pipe cell has boiled off. While the model and power tables in RELAP5-3D were set up to follow this behavior, the power level in all assemblies was ultimately kept constant to more closely match the setup used in STAR-CCM+.

A primary drawback of the vertical pipe approach is that it neglects temperature and fluid variations in the axial direction (i.e., horizontal direction along the length of the fuel rods). The FY2022 model did account for axial variation, an important effect in the DPC due to the axial power distribution, which is highly skewed toward one end of the fuel. An approach for modeling axial and vertical variation simultaneously is discussed in later sections. However, the vertical pipe approach is presented here as the best available option in RELAP5-3D, at least in terms of modeling two-phase conditions.

A small hole on the side (i.e., the top in this horizontal configuration) of the canister was modeled in RELAP5-3D using a check valve. This valve was intended to allow steam to exit the system while preventing liquid water from entering the system. The model boundary was assumed to be adiabatic with no heat being exchanged with the environment outside of the canister wall. This condition was accomplished in RELAP5-3D by modeling the canister as a pipe without any connection to any heat structures representing the canister wall or surrounding rock. A diagram of the RELAP5-3D model is provided in Figure 2-24.

Relevant dimensions and initial conditions for the full-scale DPC are provided in Table 2-7.

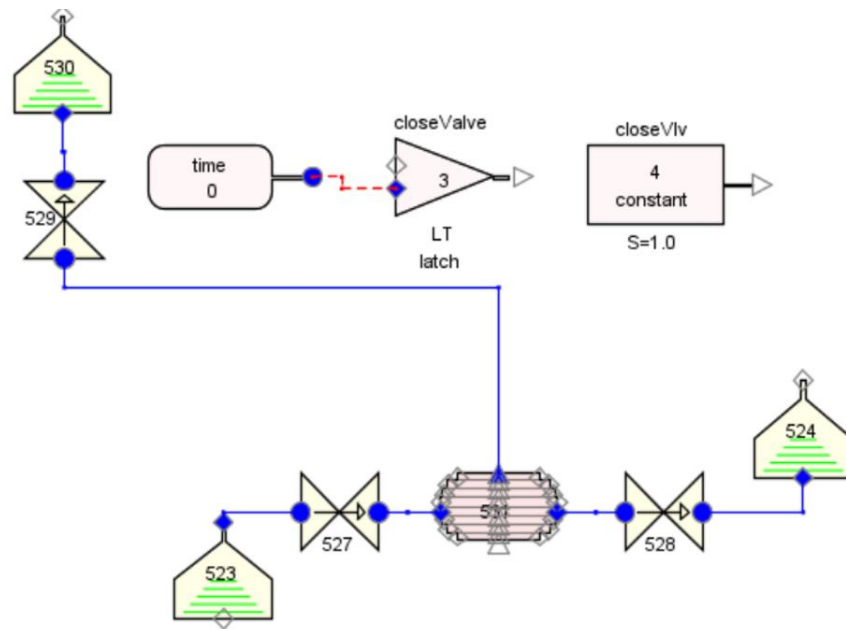


Figure 2-24. Full-Scale DPC RELAP5-3D Model

**Table 2-7. Dimensions and Initial Conditions for an MPC-32 Boiling Case**

Parameter	Value
Canister Volume (m <sup>3</sup> )	7.96
Initial Liquid Volume (m <sup>3</sup> )	7.20
Initial Liquid Volume Fraction (%)	90.5
Pressure (Pa)	4.5 x 10 <sup>6</sup>
Initial Fluid/Gas Temperature (K)	531
Canister Power (kW)	100
Simulation Time (second)	365

### 2.4.3.1 StarCCM+ Simulation

In this subsection, the setup used for verification simulations of boiling in a representative canister using STAR-CCM+ is discussed.

**Geometry**—In FY2022, a quarter portion of the MPC-32 canister, as shown in Figure 2-25 (left) was used for computational fluid dynamics (CFD) modeling and comparison with RELAP5-3D, under the assumption of flow symmetry, to save excessive computational cost. However, such an assumption is valid only for vertically placed, fully flooded canisters in a repository. The original placement of the canister is nearly horizontal, with its major axis nearly parallel to the ground, hence the flow is not expected to be strictly repeatable for each quarter of the canister. Therefore, the previous geometry was replaced with the geometry shown in Figure 2-25 (right). The symmetries of flow are still leveraged to save computational cost; however, this study assumes two vertical planes of symmetry: one plane whose normal is perpendicular to the major axis of the canister and another plane whose normal is parallel to the major axis. The final geometry seen in Figure 2-25 (right) was selected for this study based on the best trade-off between physically realizable representation of canister placed in a repository and CFD calculation expense.



NOTE: The tan rectangle at the back face of the schematic for the current geometry (right) is a visual aid indicating the orientation of one of the vertical planes of symmetry.

**Figure 2-25. Geometries Considered for CFD Modeling: Previous (left) and Current (right)**

**Mesh**—Polyhedral mesh elements were used to discretize the geometry (Figure 2-26) because of their ability to easily resolve the complex spacings (inter-rods, basket-to-rod, etc.) and conform to the complex curvilinear boundaries of the canister geometry with a smaller mesh count. They are also known to have faster solution convergence compared to hexahedral mesh elements. Two cells were inserted between the rods to capture the boiling bubble evolution; however, two cells may not be sufficient to resolve inter-rod TH processes accurately. Even with just two cells, the total mesh count for the canister geometry approached 126 million cells; hence, insertion of more cells in the inter-rod spacings was not attempted. It was decided to proceed with this mesh for the simulation.

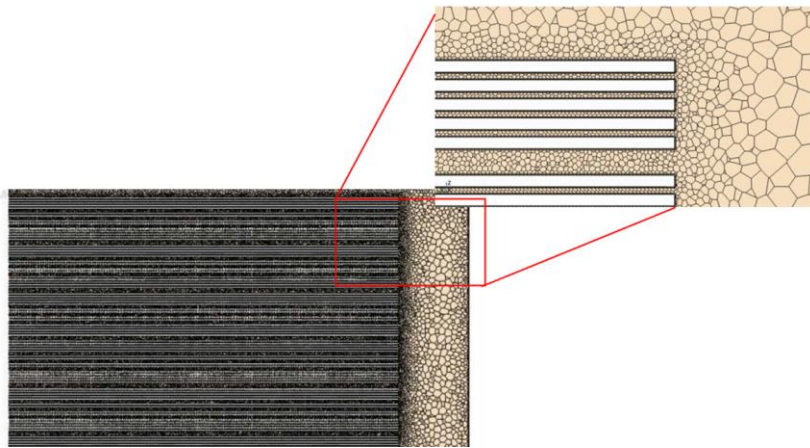


**Figure 2-26. Mesh on a Plane Cutting the Fuel Rods**

**Setup and Postprocessing**—A total of 256 cores on the Ridge compute cluster operated and maintained by the CADES at Oak Ridge National Laboratory were used to conduct the boiling simulations. Because of the excessive computational cost involved in conducting a transient simulation of such a large system, a variable time step was adopted. Initially a very low time step of  $10^{-4}$  seconds was used and was progressively increased to 0.01 seconds. Despite this strategy, the simulation runtime remained approximately 5 days, and a data file of 140 GB was generated in the process. The liquid mass loss due to boiling over time was chosen as the parameter of interest in this comparison. As the liquid level over time is not easily calculated in RELAP5-3D, the liquid mass loss was intended to serve as an analog to the liquid level over time. Ultimately, the change in the liquid level, which can be calculated from the liquid mass loss, will be the input to the neutronics calculations.

#### **2.4.3.2 STAR-CCM+ Results**

The liquid volume fraction, fluid temperature, and vapor temperature in each pipe cell calculated using RELAP5-3D at 365 seconds are provided in Table 2-8.

The liquid mass loss predicted by each code was compared at an arbitrary simulation time. An analytic calculation was also performed as a point of comparison; the results for each code and the analytic calculation are provided in Table 2-9. The liquid mass loss calculated by RELAP5-3D generally matched the value from the analytic solution, but RELAP5-3D value was approximately 4 times smaller than the value predicted by STAR-CCM+. The overprediction of liquid mass loss by StarCCM+ compared to analytic solution and RELAP is still under investigation. The excessive computational cost involved in

performing these simulations prohibited the multiple simulation trials necessary to effectively troubleshoot the problem. Therefore, Section 2.4.4 presents a verification study on a simplified small-scale geometry designed to conveniently isolate the root cause of the problem, seek a quick solution to the problem, and compare predictions for both codes effectively. Then, a return to the real-scale canister model could be performed during the final phases of the verification plan.

**Table 2-8. Predicted Fluid Properties for Full-Scale MPC-32**

Cell	Liquid Volume Fraction	Fluid Temperature (K)	Vapor Temperature (K)
1	0	530.56	531.05
2	0.67	530.69	531.22
3	0.99	530.66	530.59
4	0.99	530.69	530.61
5	0.99	530.73	530.64
6	0.99	530.78	530.66
7	0.99	530.81	530.69
8	1	530.59	530.71

**Table 2-9. Predicted Liquid Mass Loss Comparison for Full-Scale MPC-32**

RELAP5-3D	RELAP5-3D	Star-CCM+	Analytic
Power (kW)	100	100 (25 × 4)	100
Initial liquid mass (kg)	5,673	5,673 (1418 × 4)	5,673
Final liquid mass (kg)	5,649	5,536 (1384 × 4)	5,651
Liquid mass loss (kg)	23.6	137	21.8

#### 2.4.4 Simple Boiling Test Case

Because of the lack of agreement in the liquid mass loss between the full-scale DPC as modeled in RELAP5-3D and STAR-CCM+, a simple test case involving the boiling of water was devised. This simple boiling test case was intended to remove as much complexity from the model as possible to focus on the boiling physics in both codes. For this case, a vertical cylinder of water was modeled using a single cell in RELAP5-3D. The cylinder of water was heated by a heating element and the liquid mass lost due to boiling over time was monitored.

The RELAP5-3D model consisted of three main components: a single-celled pipe representing the cylinder, a valve representing the open face of the cylinder, and a time-dependent volume representing the surrounding environment. Heat was supplied to the cylinder through a powered heat structure. A diagram of the RELAP5-3D model is provided in Figure 2-27.

Relevant dimensions and initial conditions for the simple boiling case are provided in Table 2-10.

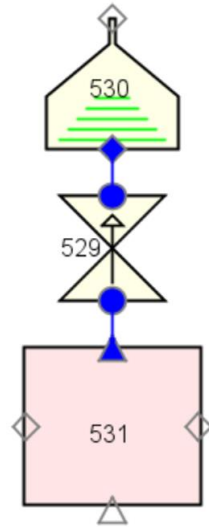


Figure 2-27. Simple Boiling Test Case RELAP5-3D Model

Table 2-10. Dimensions and Initial Conditions for Simple Boiling Case

Parameter	Value
Volume (m <sup>3</sup> )	0.021
Initial Liquid Volume (m <sup>3</sup> )	0.014
Initial Liquid Volume Fraction (%)	65.4
Rod Height (m)	0.18
Rod Radius (m)	0.2
Pressure (Pa)	$4.5 \times 10^6$
Initial Fluid/Gas Temperature (K)	530.6

**StarCCM+ Simulation Setup**—The boiling model, meshing strategy, and quantity compared for both codes were retained from Section 2.4.3 for this comparison study. The geometry considered for the STAR-CCM+ study is provided in Figure 2-28. The dimensions of the geometry and the initial conditions used for simulation are given in Table 2-10. Figure 2-29 shows the evolution of bubbles generated on the rod surface moving in the upward direction due to buoyancy through the water phase. The amount of vapor generated is tracked and deducted from the liquid mass to calculate the liquid mass loss required for comparison.



**Figure 2-28. Simple Boiling Test Case RELAP5-3D Model**

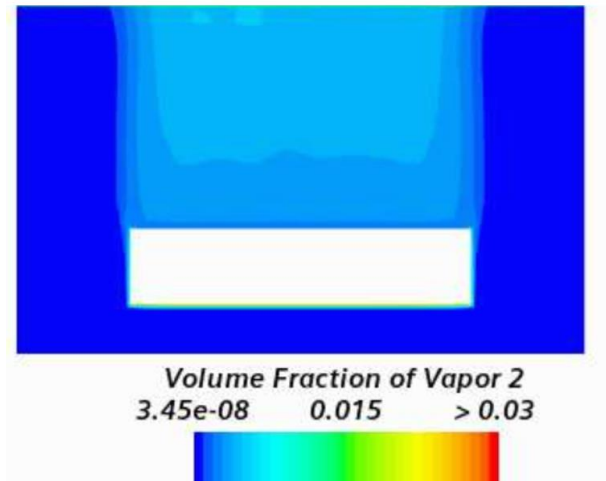


**Figure 2-29. Volume Fraction of Bubbles on a Cut-Section of the Geometry**

The liquid mass loss predicted by each code was compared at an arbitrary simulation time. An analytic calculation was also performed as a point of comparison. The liquid mass loss predicted by each code and by the analytic calculation are provided in Table 2-11. The liquid mass loss predicted by RELAP5-3D matched the value from the analytic calculation, while the liquid mass loss predicted by STAR-CCM+ was higher than the analytic calculation value in both the simple boiling case and the full-scale MPC-32 reported in Section 2.4.3.2 and Table 2-9. The possible causes of overprediction could be the larger time step adopted or the variation of heat of vaporization with pressure, which is held constant for the StarCCM+ simulation. These possible causes for overprediction will be explored in the future work and resolved. Field functions will be generated to account for the variation of heat of vaporization with pressure and will be used to conduct high-fidelity simulations of more complex test problems for boiling to verify the systems code (RELAP5-3D or TRACE), given that analytical solutions are not feasible.

**Table 2-11. Predicted Liquid Mass Loss Comparison for Simple Boiling Case**

Parameters	Simple Boiling Case (submerged rod)		
	RELAP5-3D	STAR-CCM+	Analytic
Power (W)	904		
Simulation time (second)	386		
Initial liquid mass (kg)	10.92	10.92	10.92
Final liquid mass (kg)	10.72	10.63	10.73
Liquid mass loss (kg)	0.20	0.285	0.19

### 2.4.5 Two-Dimensional Canister Modeling with TRACE

Because of ongoing uncertainty about the applicability of RELAP5-3D for simulating critical DPCs, TRACE was chosen for investigation as a potential thermal analysis code capable of modeling a horizontal DPC with liquid loss due to boiling. The “three-dimensional (3D) vessel” component in TRACE is capable of discretization using a Cartesian coordinate system and is capable of blocking flow between selected adjacent cells. Therefore, TRACE is better suited to capture the physics of a horizontal system with channel walls preventing flow in the vertical direction. This capability allows accurate representation of both the vertical direction (i.e., accurate representation of the two-phase water level and local two-phase effects) and axial direction (i.e., accurate representation of the axially dependent power profile) in the DPC canister simultaneously.

Note that RELAP5-3D has a 3D vessel capability, but it is restricted to cylindrical  $(r,z,\theta)$  geometry. For the DPC, the  $z$ -coordinate would be along the horizontal axial length of the fuel assemblies, and the polar  $(r,\theta)$  coordinates would be lateral circular cross section of the canister. For the case of a horizontal cask such as a DPC, the polar geometry makes it impossible to accurately track the two-phase water level because the radial and azimuthal sectors do not align with a given horizontal plane (i.e., cannot accurately resolve the water level elevation). The Cartesian vessel in TRACE can resolve this elevation accurately, whether the water level elevation is at the boundary between two vertical cells or some fraction of elevation within a given cell.

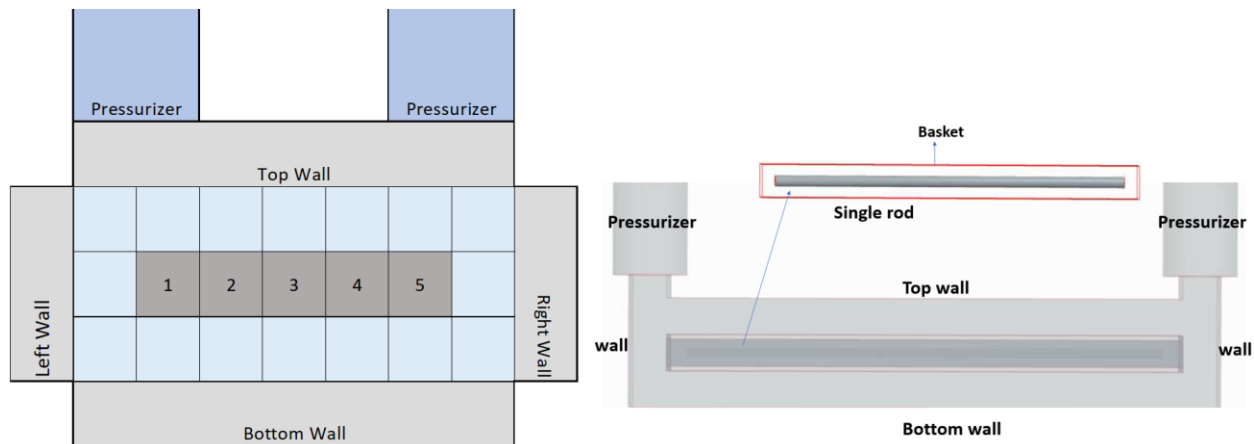
#### 2.4.5.1 Two-Dimensional Test Problem

A simplified, two-dimensional (2D) test problem similar to a horizontal DPC was devised to investigate the potential applicability of TRACE. Initially, the test problem consisted of a simple rectangular prism full of water with a single submerged heat source (similar to the simple boiling modeled in RELAP5-3D [Section 2.4.4]). For various reasons, the following features were also added to the model:

- Steel channel walls were added around the rod, creating a central fluid channel. These channel walls were added to prevent flow between specific cells in the vertical direction.
- Steel walls were added to the faces of the vessel in both the vertical and horizontal directions. A 300 K boundary temperature was established on these walls. The other two vessel faces were kept as adiabatic. These walls were added to improve the heat removal rate from the fluid vessel; furthermore, the heat removed through each wall could be compared between each code.

- Two “pressurizers,” modeled as vertical pipes filled with vapor at the same pressure as the main vessel, were placed above the vessel and connected to the uppermost face. The purpose of these pressurizers was to prevent any large pressure increase in the vessel fluid.
- An axial power profile was applied to the heated rod to intentionally create a flow pattern and a fluid temperature distribution that would theoretically be similar in both codes. Before switching to the axial power profile, TRACE showed a “hysteresis” effect in which the fluid would arbitrarily start flowing in one direction even though the power profile was initially entirely symmetric. The axial power profile used for this test problem was adapted from an 18-cell power profile used in DPC neutronics calculations (Swinney et al. 2021).

A visual representation of this test problem for TRACE and StarCCM+ is provided in Figure 2-30; this figure shows the four walls through which heat losses were compared; it also indicates the five fluid cells in which temperature changes were compared.



NOTE: Not to scale.

**Figure 2-30. Representation of Test Problem: TRACE (left) and CFD (right)**

The test problem as modeled in TRACE is shown in Figure 2-31. The TRACE model consisted of a vessel component connected by single junctions to two pipes representing the pressurizers. A cylindrical heat structure was used to model the heated rod. Planar heat structures were used to model the walls surrounding the central channel and the walls surrounding the main vessel.

Relevant dimensions and initial conditions for the TRACE test problem are provided in Table 2-12. The axial power profile is provided in Table 2-13.

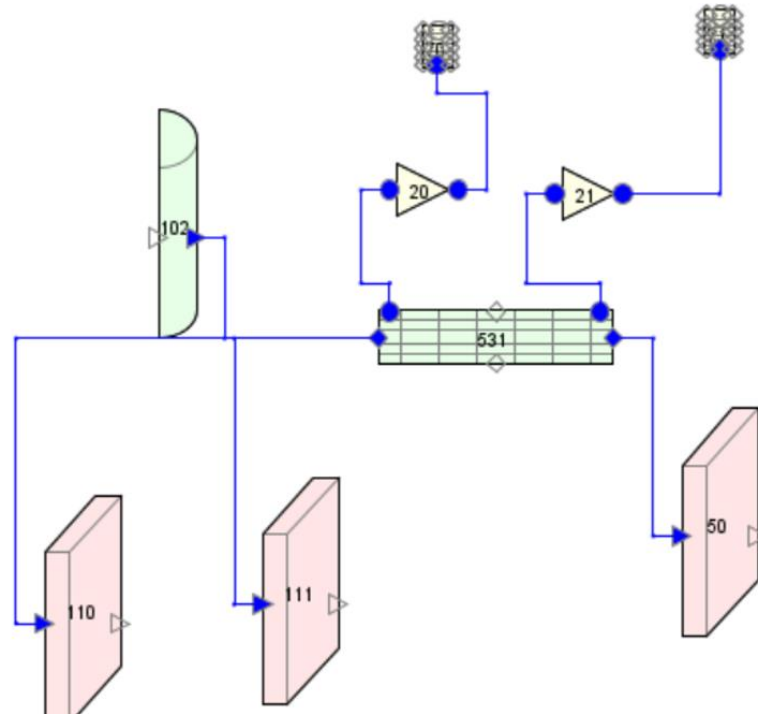


Figure 2-31. Test Problem TRACE Model

Table 2-12. Dimensions and Initial Conditions for TRACE Test Problem

Parameter	Value
Vessel Volume (m <sup>3</sup> )	$3.24 \times 10^{-3}$
Pressurizer Volume (m <sup>3</sup> )	$5.0 \times 10^{-4}$
Channel and Outer Wall Thickness (m)	0.01
Pressure (Pa)	$1.01325 \times 10^5$
Initial Fluid Temperature (K)	300
Initial Vapor Temperature (K)	530.6
Total Power (W)	500
Simulation Time (second)	$2 \times 10^4$

Table 2-13. Axial Power Profile used in TRACE Test Problem

Fluid Cell	Power Fraction (%)	Cell Power (W)
1	89.44	447.2
2	10.09	50.44
3	0.450	2.250
4	0.025	0.124
5	0.001	0.007

Once base case results were obtained, the TRACE “grid mesh” was further refined by increasing the number of cells in the vessel. Cells were added to various specific areas of the vessel to investigate the impact of the refined mesh on heat loss through each wall as well as the fluid temperature in the central channel. A total of eight cell refinement schemes were compared; each refinement scheme is shown in Figure 2-32. For any case in which the central row of cells was split in the vertical direction, the heat structure representing the heated rod in TRACE was split to match the vessel cells because TRACE is unable to connect heat structures to more than one fluid cell simultaneously.

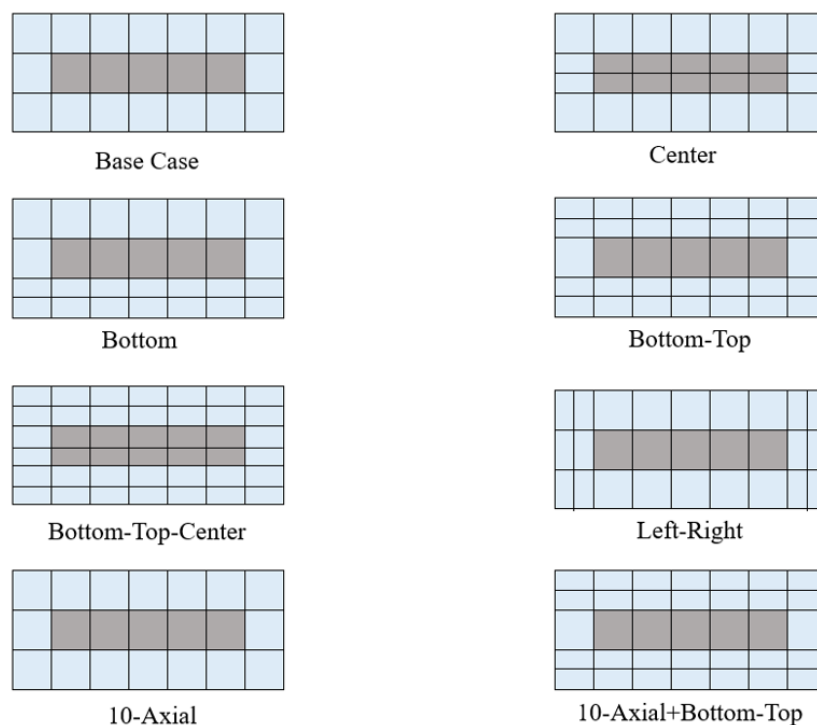


Figure 2-32. Vessel Cell Refinement Schemes Used in TRACE Test Problem

#### 2.4.5.2 STAR-CCM+ Simulation

The geometry used for the STAR-CCM+ simulation is given in Figure 2-30. A two-phase volume of fluid method with a Reynolds-Averaged Navier Stokes (RANS) simulation model was used to predict the natural circulation and associated heat transfer inside the system. The initial liquid level in the bottom of the tank was initialized using a field function for the volume fraction of the liquid. The variation of water density with respect to the temperature was accounted for using steam tables from The International Association for the Properties of Water and Steam (Cooper and Dooley 2007). An asymmetric power profile as given in Table 2-13 was applied to the rod. The simulation was run until the net accumulation of heat reached zero, meaning that the total power produced by the rods was balanced by the total power dissipated through the walls of the system. The temperatures predicted at steady state were volume averaged on five boxes arranged axially along the rod for comparison with TRACE. Figure 2-33 shows the temperature map inside the system. The highest temperatures are observed at the left end because of the peaking of the power. Local temperatures on the surface of the rod on the left end reached the boiling

point because of the high concentration of power in that region. Figure 2-34 shows the natural circulation pattern predicted by the simulation. Natural circulation is dominant in the upper section, and therefore the heat transfer rate through the upper wall is the highest there compared to values at the other walls, as reported in the heat transfer budget presented in Table 2-15.

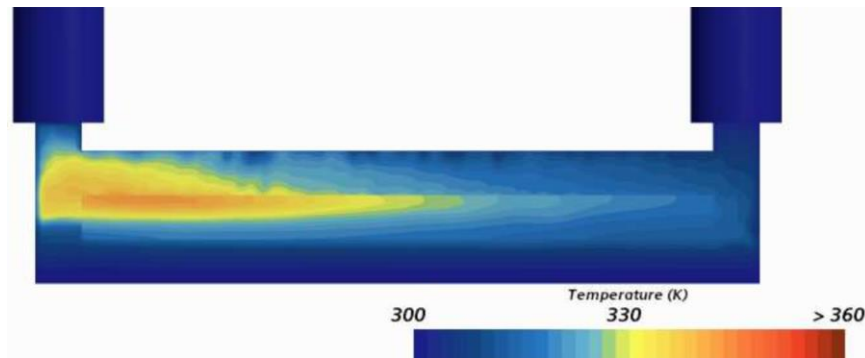


Figure 2-33. Temperature Contour Predicted by CFD on a Cut Section

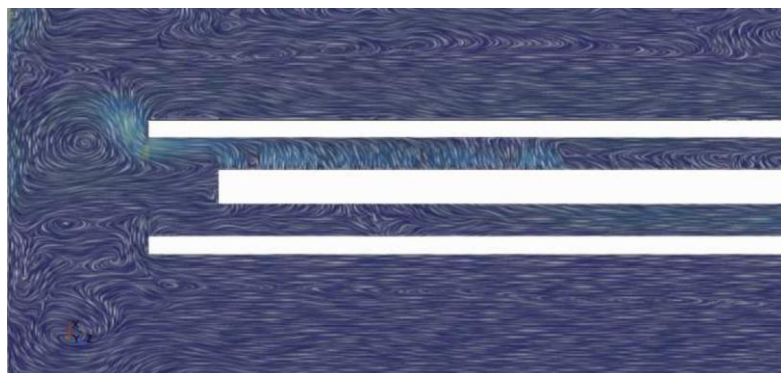


Figure 2-34. Natural Circulation Contour Predicted by STAR-CCM+ on a Cut Section

### 2.4.5.3 Two-Dimensional Test Problem Results

Cell-averaged fluid temperatures in the five central cells were calculated using both TRACE and STAR-CCM+. The results for the TRACE cases and STAR-CCM+ are provided in Table 2-14. The heat loss through each of the four walls surrounding the main vessel was also calculated using both codes, with the results being presented in Table 2-15. The fluid temperatures in the base case show a profile generally similar to that predicted by STAR-CCM+, but with lower temperatures throughout and a larger temperature descent from cells 1 to 2. This observation implies that too much heat was being removed from cell 1 because of the relatively coarse cell mesh in the horizontal direction. The results also indicate that the base case TRACE model rejected too much heat through the bottom wall because of the relatively small number of fluid cells in this region; adding cells near the bottom of the vessel resulted in fluid temperatures and wall heat losses that more closely matched the values predicted by STAR-CCM+. As part of future work, further investigation to minimize error in the predictions will be conducted.

**Table 2-14. Cell Temperatures in the TRACE Cases and the Star-CCM+ Case for the 2D Problem**

	Cell-Average Fluid Temperature (K)				
	1	2	3	4	5
<b>Base Case</b>	321.85	313.42	312.51	312.52	312.58
<b>Center</b>	314.84	315.14	315.12	315.08	315.05
<b>Bottom</b>	324.05	314.97	313.88	313.81	313.79
<b>Bottom-Top</b>	324.25	315.58	314.53	314.43	314.38
<b>Bottom-Top-Center</b>	315.06	313.81	313.87	313.57	313.52
<b>Left-Right</b>	318.33	318.92	318.77	318.58	318.40
<b>10-Axial</b>	319.62	321.70	321.44	321.08	320.73
<b>10-Axial+Top-Bottom</b>	324.13	315.70	314.86	314.85	314.91
<b>STAR-CCM+</b>	330.93	327.53	323.08	319.50	316.94

**Table 2-15. Wall Heat Loss in the TRACE Cases and the Star-CCM+ Case for the 2D Problem**

	Wall Heat Loss (W)				
	Top	Bottom	Left	Right	Total
<b>Base Case</b>	301.88	91.36	59.39	46.17	498.79
<b>Center</b>	225.19	180.10	47.13	46.76	499.17
<b>Bottom</b>	338.19	39.42	68.32	52.77	498.70
<b>Bottom-Top</b>	338.43	31.89	73.11	55.16	498.59
<b>Bottom-Top-Center</b>	356.62	20.41	70.29	51.39	498.72
<b>Left-Right</b>	191.54	212.81	40.28	54.57	499.19
<b>10-Axial</b>	293.94	103.21	44.26	57.36	498.77
<b>10-Axial+Top-Bottom</b>	322.53	40.26	76.57	59.08	498.44
<b>STAR-CCM+</b>	350.77	1.92	112.4	31.50	496.59

### 2.4.6 Planned Verification Work

Significant additional work is required to verify whether TRACE is an acceptable tool for TH calculations in simulating boiling in a critical DPC. The following subsections briefly describe the verification work planned for next year.

#### 2.4.6.1 Single-Phase Water Flow

Additional simulations to investigate TRACE’s water flow predictions are necessary to ensure that the natural circulation calculations in TRACE are accurate. Future verification problems include the following:

1. **Refined Axial Power Profile**—An axial power profile was included in the TRACE test problem developed for this report, but the power profile only contained five cells. A power profile with 18 axial cells should be investigated to match the axial segmentation used in the neutronics models.

2. **Multiple Channels in the  $y$  and  $z$  Directions**—Currently, only a single assembly channel was modeled. Modeling multiple channels in the  $z$ -direction (along which gravity acts) with fluid plena on the left/right of the model will potentially demonstrate the natural circulation loop where fluid exits some channels and enters others.
3. **Multiple Fuel Rods inside One Channel**—Multiple rods inside one channel may be modeled in the  $z$ -direction to investigate the effect of the physical placement of the rods on the overall liquid temperature.
4. **Downscaled Canister**—A downscaled canister with multiple assemblies, plena on both ends, and an outlet on the side of the canister, as shown in Figure 2-35, would combine the features of all previous cases and would represent all the essential features of a full-scale DPC model on a reduced scale.

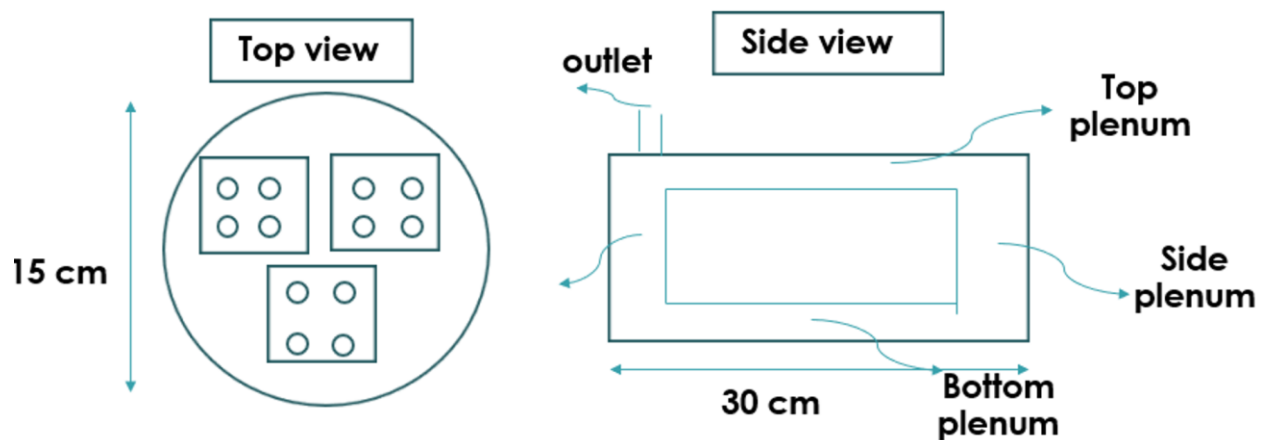


Figure 2-35. Downscaled Canister Model

#### 2.4.6.2 Two-Phase Boiling

Once the natural circulation problems listed above have been verified, the two-phase boiling physics must also be verified. The verification plan is to repeat the single-phase test cases above at a power level sufficient to cause boiling. The goal of these simulations is to verify that TRACE can accurately calculate the canister fluid level over time as the liquid boils. For the case with multiple fuel rods inside one channel, while the full number of rods in the  $z$ -direction (i.e., 18) likely does not need to be modeled, multiple cases may be necessary to determine the minimum number of rods needed to calculate the liquid loss with sufficient accuracy to serve as input to the neutronics model.

## 2.5 DPCs Sealed in a Bentonite Backfill

The scenario hypothesized in this subsection represents the least understood possibility of what could occur in the event of a DPC achieving criticality in a saturated geological repository. It involves a working theory that saturated bentonite clay could seal a DPC and prevent water or steam from escaping.

Figure 2-36 depicts a cartoon version of a drift, where a canister is in a saturated clay backfill within a saturated rock formation. The basic assumptions for this scenario are as follows:

- Saturated bentonite has a very low permeability ( $10^{-18}$  to  $10^{-20}$  m<sup>2</sup>).
- Water could infiltrate the canister slowly over centuries or millenia, but it would not be able to escape on the time scale of a criticality event.
- Sufficient overpressure may result in a fracture or “breakthrough”, allowing the escape of steam or water.
- This scenario could potentially result in higher powers than can be achieved in a permeable backfill.

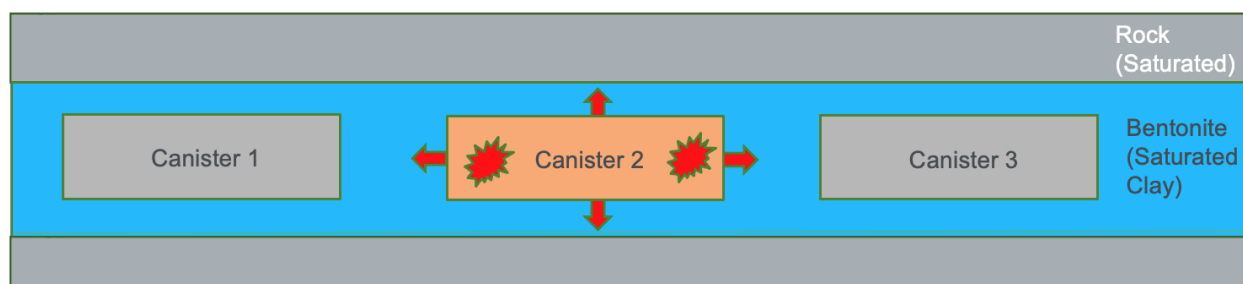


**Figure 2-36. A Depiction Conceptualizing a DPC in a Drift Backfilled with Bentonite**

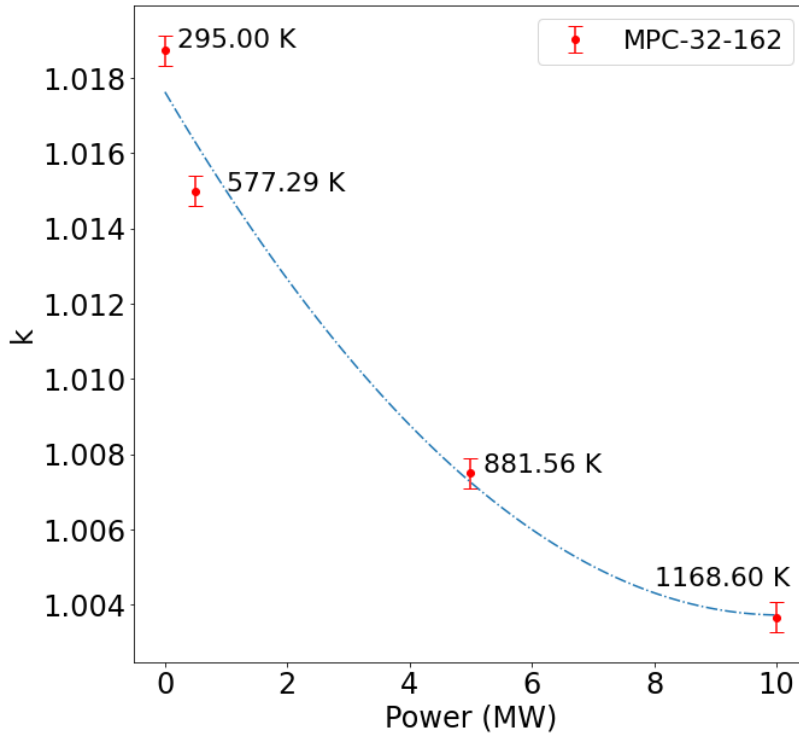
This postulated circumstance is fundamentally different from previous scenarios because the moderator cannot expand to limit criticality. The primary feedback mechanism in this case is Doppler broadening within the fuel itself. In previous scenarios, temperatures were relatively low, and this effect was negligible; however, in this scenario the fuel temperature increases rapidly until Doppler broadening provides sufficient negative feedback to achieve a  $k_{\text{eff}}$  near unity. Therefore, to model this scenario accurately, a radiation transport model with a temperature profile is necessary. However, the models generated with Used Nuclear Fuel – Storage, Transportation & Disposal Analysis Resource and Data Systems (UNF-ST&DARDS) (Clarity et al. 2017) have a homogeneous temperature throughout the model, and there is no existing mechanism for applying a varying temperature to the model.

To pursue analysis of this scenario, a new capability was developed. A new python-based parser tool reads a custom formatted temperature profile describing the fuel, clad, and water temperatures throughout the DPC. The tool modifies the temperatures for the corresponding materials within a standard radiation transport model created with UNF-ST&DARDS. An example of the data used for an MPC-32 is shown in Table 2-16. These data are based off the simplified three-ring RELAP5-3D model illustrated in Figure 2-20, so there are only three radial profiles. Once the higher fidelity TRACE-based TH model is developed, profiles for all 32 assemblies could theoretically be used to perform the analysis for this scenario in the future.

Table 2-16. Example Temperature Profile for Sealed DPC (500 kW case)

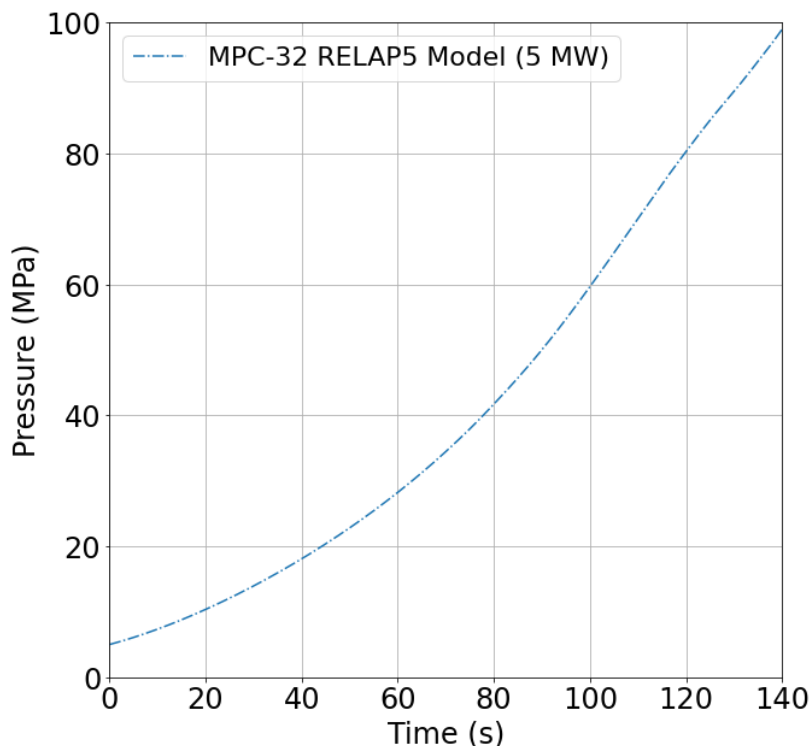
Axial Cell	201 Fuel Center Temperature (K)	201 Clad Outer Temperature (K)	Central Fluid Temperature (K)
1	577.3	538.0	537.0
2	575.7	538.0	537.1
3	557.2	537.8	537.
4	545.7	537.5	537.1
5	540.6	537.3	537.1
6	538.5	537.2	537.1
7	536.5	536.0	535.7
8	533.4	533.2	533.1
9	524.4	524.3	524.2
10	468.3	468.3	468.2
11	422.3	422.3	422.3
12	390.8	390.8	390.8
13	369.1	369.1	369.1
14	353.9	353.9	353.9
15	343.2	343.1	343.1
16	335.5	335.5	335.5
17	330.0	330.0	330.0
18	326.1	326.1	326.1

The initial workflow for analyzing the so-called “sealed” DPC began by providing the power distribution from the Shift model as an input to RELAP5-3D (Pandya et al. 2016). A power level is assumed, and RELAP5-3D generates the associated temperatures for the fuel and other components in the format shown in Table 2-16. The new parser script modifies the original UNF-ST&DARDS model to apply the new temperatures. Then, Shift is used to calculate the new multiplication factor of the system. This process is repeated until the Shift model predicts a  $k_{eff}$  near unity, thus identifying the power level required to provide sufficient Doppler broadening feedback within the fuel to limit criticality within the DPC. An example of this new workflow is given in Figure 2-37. As shown in Figure 2-38, even at 5 MW the pressure builds up rapidly within the canister. If these models are accurate, it would seem that some sort of fracture or “breakthrough” in the backfill, DRZ, and host rock would occur at these pressures, allowing for the water to boil. The Oak Ridge National Laboratory research team is currently collaborating with the geosciences division at Lawrence Berkeley National Laboratory to perform geomechanics simulations to investigate this hypothesis. These calculations are being done with the TOUGH code (Pruess 2004), which is designed for multiphase fluid flow and heat transport in porous media coupled with a geomechanics simulator.



NOTE: The temperatures listed on the plot represent the peak fuel temperatures in the model.  
MPC = multipurpose canister

**Figure 2-37. An Example of the Results from the New Workflow Predicting  $k_{eff}$  in a Sealed DPC as a Function of Power**



NOTE: MPC = multipurpose canister

**Figure 2-38. Pressure Buildup in a Sealed DPC as Predicted with RELAP5-3D at a Power Level of 5 MW**

## 2.6 Further Work

With respect to DPC-scale multiphysics simulation analysis, further work includes (1) verifying whether TRACE is an adequate tool for TH calculations simulating boiling in a critical DPC and (2) continuing the collaboration with geoscience experts to investigate fracturing of the material outside the waste package, should pressures inside the waste package reach levels making that outcome possible.

Future work involving the shale simulations includes debugging efforts that will allow for the current deterministic simulation with multiple criticality events at different times and of different durations to run to completion (1 million years) and allow for further development of this case study. Further development also includes extending the smectite-to-illite transition model to the shale host rock and a further look into the values specified within the material transform model that would be applicable to the shale and DRZ materials.

In addition, for these repository-scale simulations, transport of a second radionuclide,  $^{79}\text{Se}$ , will be examined. Also, in the results of the repository-scale simulations described above, temperatures at the waste package from decay heat would most likely exceed temperature limits for a clay/shale repository. These high temperatures affect some of the FEPs included in the repository model (e.g., grid spacer

degradation, illitization); future work will examine ways to reduce temperatures in the repository (e.g., waste package spacing, drift spacing, etc.).

Finally, the FEPs that were identified as affecting criticality, being affected by criticality, or both (Alsaed and Price 2020) will be reviewed to determine which FEP or FEPs would be good candidates for inclusion in the criticality consequence model.

### 3. MODELING STEADY-STATE POSTCLOSURE CRITICALITY IN AN UNSATURATED REPOSITORY

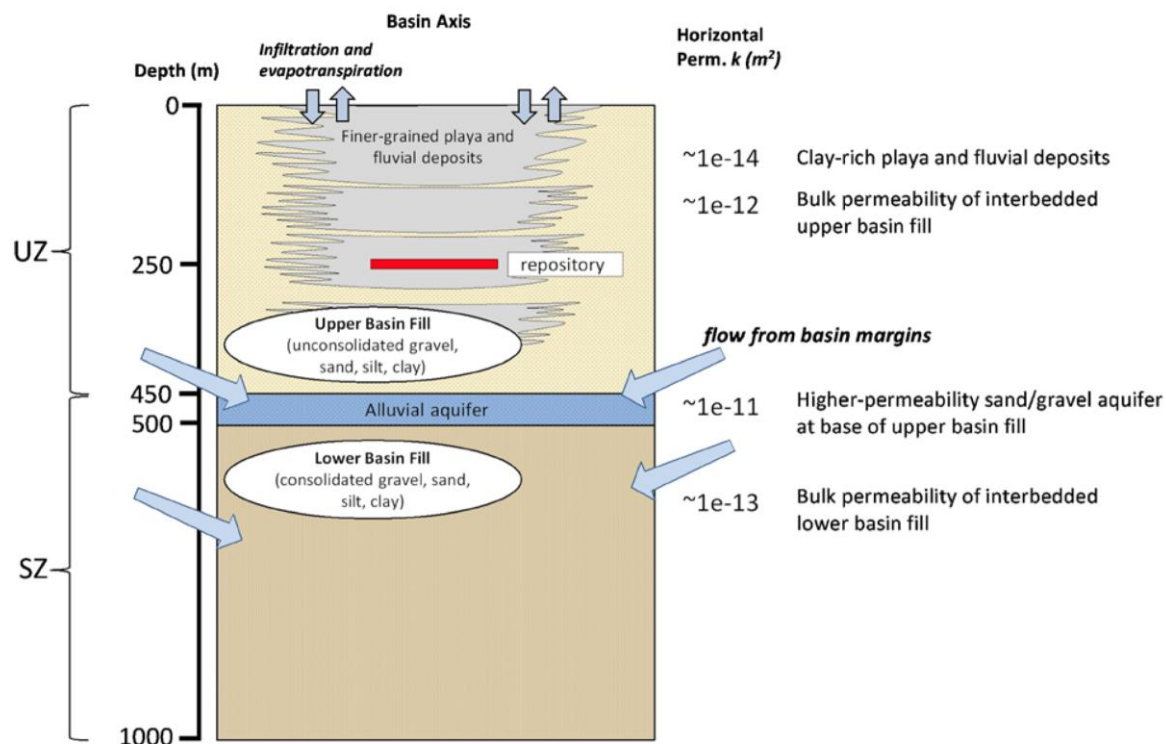
The following sections describe the model of a steady-state postclosure criticality in a hypothetical unsaturated saturated repository. Section 3.1 describes the hypothetical reference unsaturated repository used in these analyses, Section 3.2 outlines improvements and fixes made to the PFLOTRAN model during FY2023, Section 3.3 describes the repository-scale PFLOTRAN model of the hypothetical unsaturated repository, Section 3.4 presents the parameters studied in FY2023 simulations, Section 3.5 gives the results FY2023 simulations, and Section 3.6 provides a summary of needed future work.

#### 3.1 General Repository Description

This section considers the unsaturated zone alluvium reference case described in Section 1.5. This geologic reference case was first introduced in Mariner et al. (2018) and refined in Sevougian et al. (2019a,b) and LaForce et al. (2021).

The reference case considers thick alluvial valleys of the Great Basin in the western United States and the low-permeability playa/lacustrine sediments found there. Several features of this type of host rock are favorable to waste isolation, including low groundwater fluxes, low permeability, and low water saturation. This type of environment is favorable to the disposal of DPCs since low water saturation greatly reduces the possibility of criticality events. Mariner et al. (2018) goes into detail of the natural barrier system, movement of water through sediments, and the physical and chemical characteristics of the host rock. Figure 1-2 in Section 1.5 provides a general schematic of the hydrology and geology of an unsaturated alluvium repository.

Figure 3-1 shows additional detail of the cross section of an unsaturated zone model in which the repository is represented by the red block at a depth of 250 m and lies within the unsaturated zone, which is located between a depth of 0 m and 450 m. Within the unsaturated zone, there are impermeable, fine-grained, playa sediments; fluvial deposits; and the upper basin fill consisting of unconsolidated gravel, sand, silt, and clay. The saturated zone is located below the unsaturated zone at a depth of 450 m to 1,000 m. The saturated zone contains an alluvial aquifer at a depth of 450 m to 500 m. This higher permeability, sand/gravel aquifer lies at the base of the upper basin fill and above the lower basin fill. Located between 500 m and 1,000 m, the lower basin fill consists of consolidated gravel, sand, silt, and clay.



NOTE: perm. = permeability  
 SZ = saturated zone  
 UZ = unsaturated zone

Source: Mariner et al. 2018.

**Figure 3-1. Schematic Cross Section of the Unsaturated Zone Model**

## 3.2 PFLOTRAN Model Developments

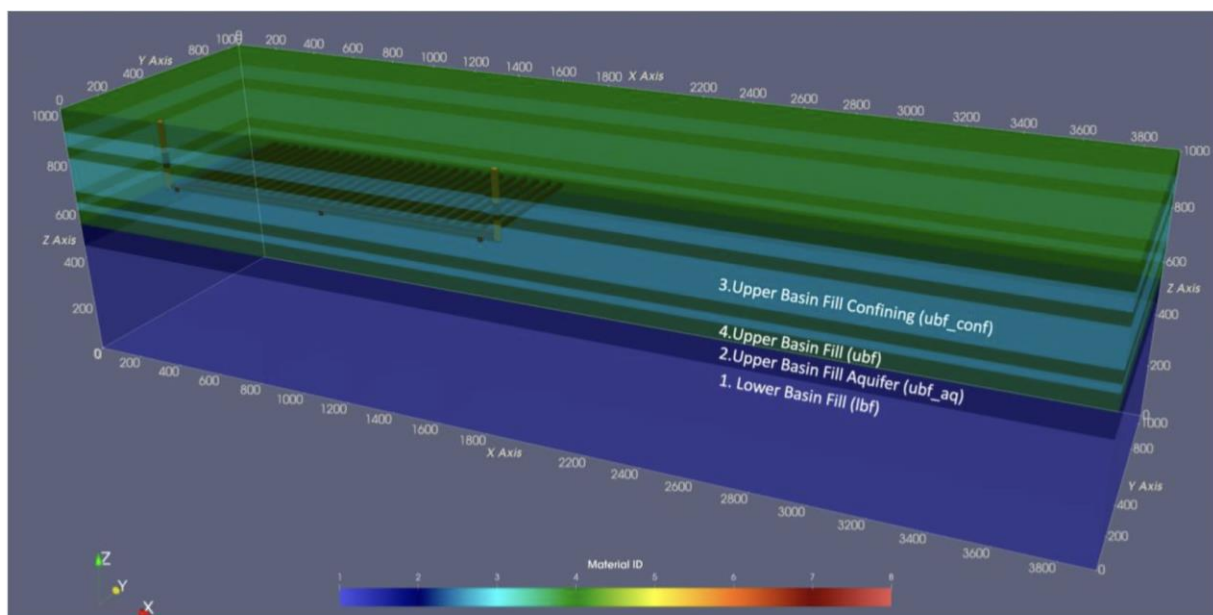
In FY2022, simulations were run with a criticality start time of less than one year and were only able to complete runs for the 10 mm/yr percolation rate and decay heat data for packages 400 years OoR, as the high temperatures were causing convergence issues. During FY2023, those bugs were resolved and the runs were able to complete with more realistic values: criticality start time at 9,000 years and 32-PWR DPCs with 110 years OoR decay heat data. Simulations using a 2 mm/year percolation rate were also successfully completed, but results focus on 10 mm/year percolation rate runs.

The results presented below were obtained using an executable from a development branch in PFLOTRAN (commit c3ee814) compiled with Intel 20.0.1.217 and PETSc v3.17.2 and run on Sandia National Laboratories high-performance computing clusters. No changes were made to allow use of the Waste Form process model without reactive transport, meaning flow-only simulations were run with a dummy tracer.

### 3.3 PFLOTRAN Model

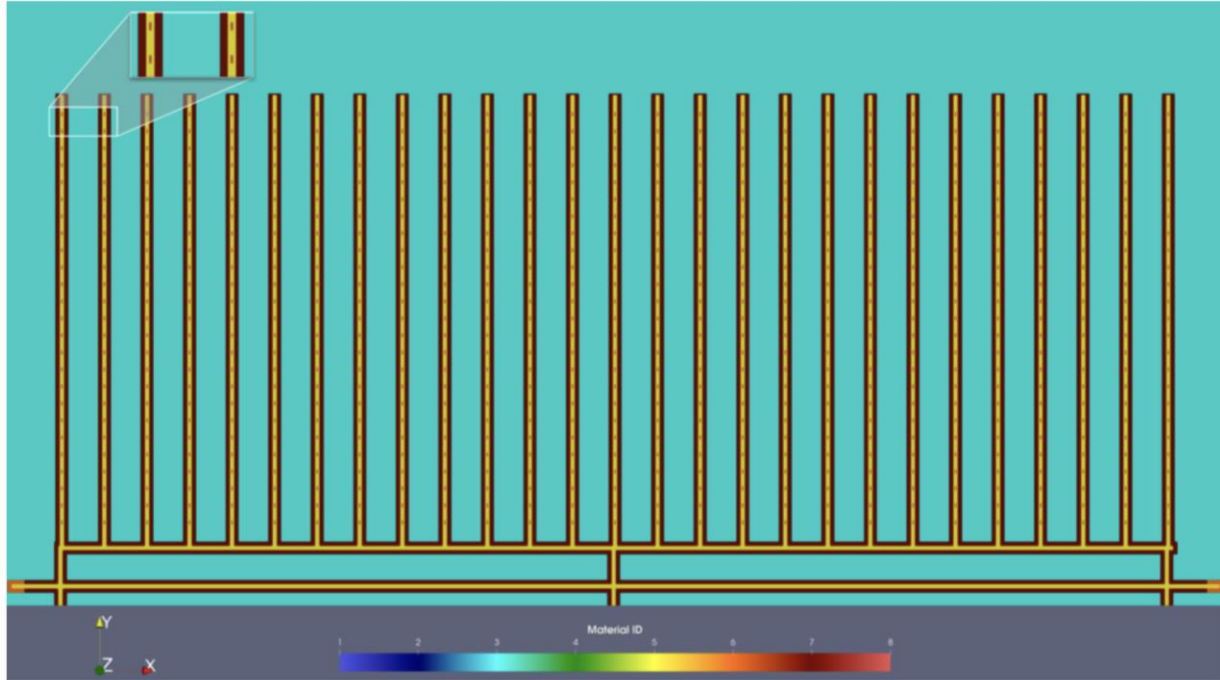
Updates to the model domain originally proposed by Mariner et al. (2018) for field-scale simulations of the unsaturated zone reference case have been slightly modified because of a “zigzag” issue in the DRZ edge that has been resolved in LaForce et al. (2021). Figure 3-2 shows the configuration for the model domain colored by material ID. The model domain has the same domain size of  $3,915 \times 1,065 \times 1,005$  m as in Mariner et al. (2018). The repository lies within the upper basin fill confining (ubf\_conf) sediment, which is material ID 3 denoted by turquoise coloring. Figure 3-3 shows an  $x$ - $y$  slice through the repository that is also colored by material ID. In this model the repository is assumed to be 250 m below the surface. The zoom box on the top left of the figure shows four waste packages in red, buffer in yellow, DRZ in burgundy, and ubf\_conf in turquoise.

The nine varying simulations being compared use 32-PWR, 110 years OoR, decay heat data in a field-scale half-symmetry model with 27 drifts and 25 waste packages per drift (675 32-PWR waste packages for half-symmetry); the decay heat curve for 110 years OoR is shown in Figure 3-4. All simulations were set up with CANISTER\_BREACH\_TIME of 8,999 years and CRIT\_START of 9,000 years. Drift spacing is 50 m, and center-to-center spacing of waste packages along the drift is 20 m. The model has no-flow boundary condition at the south face, which acts as a reflector, meaning the total number of waste packages represented in the model is 1,350. The field-scale PA unstructured mesh used for the final simulations was gridded with Cubit (Skroch et al. 2021) and has 2,996,313 grid cells (LaForce et al. 2021). Simulations are run with PFLOTRAN (Hammond et al. 2014). Model domain visualizations have been generated using ParaView (Ayachit 2015). These simulations were run to 100,000 years on 544 or 540 cores of a parallel, high-performance computing cluster on the unsaturated zone mesh. Successful simulations took an average of 20 hours to complete.



NOTE: Turquoise color (material ID 3) represents the ubf\_conf units (the centermost contains the repository as seen there), green (material ID 4) represents UBF, dark blue (material ID 2) represents the UBF aquifer, and blue (material ID 1) represents LBF. Distances along the axes are in meters, where 1,000 m is land surface and 0 m is the bottom of the model domain. The left side of the figure represents a western direction.

**Figure 3-2. Configuration of the Repository and Natural Barrier System Generated Using Cubit, Simulated in PFLTRAN, and Visualized in ParaView**



NOTE: The repository is assumed to be 250 meters below the surface. The zoom-in box on the top left shows a close-up of four waste packages (WPs) colored in red, buffer in yellow, DRZ in burgundy, and ubf\_conf in turquoise. Visualized using ParaView.

Figure 3-3. x-y Slice through the Repository Colored by Material ID

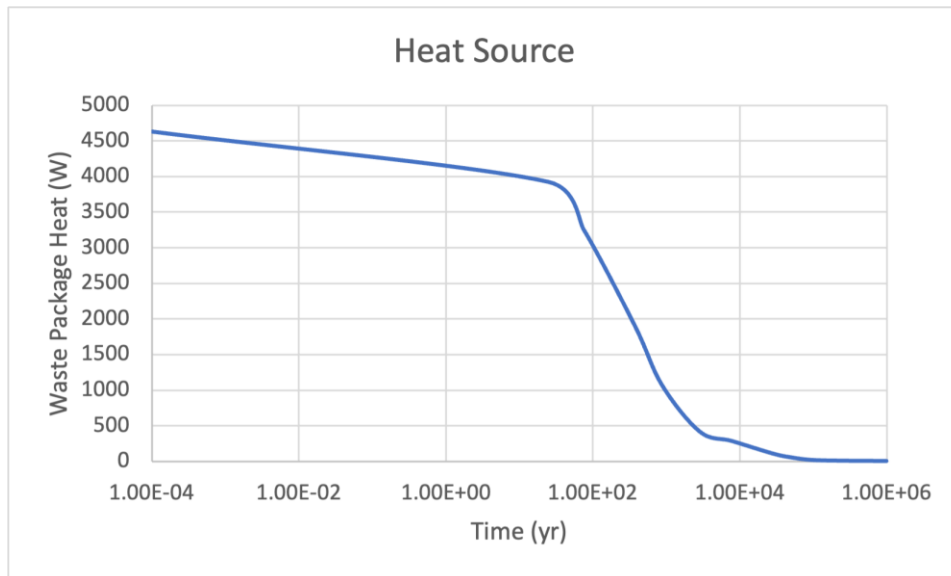


Figure 3-4. Heat Source Curve for 32-PWR, 110-Year OoR Decay Data

### 3.4 Parametric Study of Infiltration, Power Level, and Waste Package Breach Size

The present study is focused on setting up varying runs to examine the conditions under which criticality could occur in the centermost waste package. In accordance with last year's results (Price et al. 2022), in which a Monte Carlo N-Particle Transport (MCNP) study indicated that a water level of 52.2% is necessary for criticality to occur (i.e., the DPC must be at least half full of water for criticality to occur), the criticality water saturation was originally set to 0.5. However, 100,000-year simulations indicated that liquid saturation within the center-most waste package did not exceed 0.43. Therefore, to observe the effects of criticality on the repository, the criticality water saturation was set to 0.35. Table 3-1 lists the variables changed in the model and their values. Table 3-2 lists the run IDs and values for these variables in each run, namely the use of different combinations of infiltration rates (2 mm/yr, 10 mm/yr), criticality power levels (0 W, 50 W, 200 W, 400 W), criticality water saturation (0.5 and 0.35) and maximum time step after 20,000 years (10 years, 5 years, 1 year, 0.25 years).

The decision to change the time step at 20,000 years was made because previous runs showed that the conditions for criticality were not met until roughly 24,000 years, as is discussed later in this section. More fine-tuned results were required around the time of criticality to understand the oscillatory behavior. The simulation remains unchanged until the point of criticality. Therefore, to save computation time, the more fine-tuned time steps began at 20,000 years. As no major changes were observed in the model in the first 20,000 years, the results are unaffected. Infiltration rates and criticality power levels are based on previous analyses (Price et al. 2021, 2022), the criticality water saturation level was set as described above, and the time steps were selected as the analyses progressed. Runs 7, 8, and 9 use different maximum time-step values while other parameters were held constant as part of the study to determine if the smaller time steps resolved instabilities observed in previous runs. The instabilities and time-step study are discussed below in Section 3.5. Runs with a criticality power level of 0 W show the effects of decay heat only (i.e., subcritical conditions are maintained). All runs have been set up to have a canister breach time of 8,999 years and a criticality start time of 9,000 years for the centermost waste package only, as is shown in Figure 3-5, where it can be observed that only the centermost waste package has a heat spike associated with criticality.

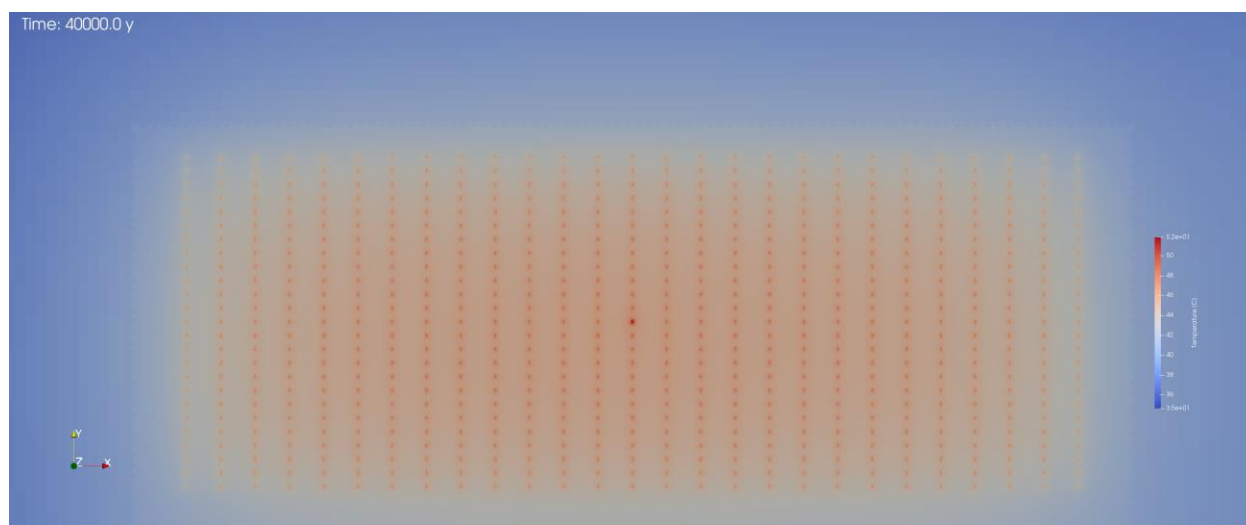


Figure 3-5. Temperature of Repository at 40,000 Years for the 0.25-Year Time-Step Run

**Table 3-1. Model Variables with Varying Values**

Model Variables	Varying Values
Infiltration Rate	2 mm/yr, 10 mm/yr
Criticality Power Level	0 W, 50 W, 200 W, 400 W
Criticality Water Saturation	0.5, 0.35
Maximum Time Step after 20,000 years	10 years, 5 years, 1 year, 0.25 years

**Table 3-2. Breakdown of Different Value Combinations within 10 Unsaturated Zone Simulation Runs**

Run ID	Simulation Combinations <sup>a</sup>
Run 1	10 mm/yr, 400 W, 0.5, NA
Run 2	2 mm/yr, 400 W 0.5, NA
Run 3	10 mm/yr, 400 W, 0.35, 10 years
Run 4	10 mm/yr, 200 W, 0.35, 10 years
Run 5	10 mm/yr, 50 W, 0.35, 10 years
Run 6	10 mm/yr, 0 W, 0.35, 10 years
Run 7	10 mm/yr, 400 W, 0.35, 5 years
Run 8	10 mm/yr, 400 W, 0.35, 1 year
Run 9	10 mm/yr, 400 W, 0.35, 0.25 years

NOTE: <sup>a</sup> Variable order is infiltration rate, criticality power level, criticality water saturation, and maximum time-step size after 20,000 years.

**NA = not applicable**

### 3.5 Modeling Results

After successfully completing of Run 1 to 100,000 years, but observing that the water level never exceeded 0.50, the study team extended the run out to 1 million years to investigate if water saturation would reach 0.50 over the longer time period. As shown in Figure 3-6, water saturation did not reach 0.50 over 1 million years, meaning that criticality did not occur because not enough moderator was present. Run 2 was cancelled 60 years into the simulation, as it would be unlikely for the liquid saturation to be higher for a 2 mm/yr infiltration rate than it was for a 10 mm/yr infiltration rate. However, running the 2 mm/yr problem out to even 60 years is an improvement from last year, when a similar simulation failed immediately because of high temperatures.

It should be noted that, in the figures presented below, the initial liquid saturation is shown as 0.25, representing a waste package that is one-quarter filled with water. This value is not correct, as DPCs are dried prior to being welded shut; the expected quantity of water inside a dried, intact DPC is on the order of 0.0025 (0.25%). However, when this value is used as the initial saturation, PFLOTRAN fails to run. In the analyses described below, any water inside the waste package when it breaches initially evaporates quickly and the liquid saturation drops to 0.00 within months, so the initial value of saturation does not affect the analyses in this section.

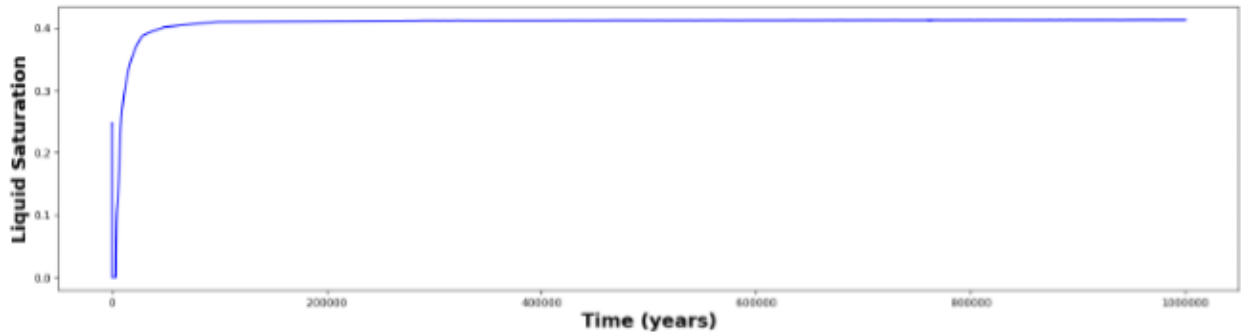


**Figure 3-6. Liquid Saturation in the Centermost Waste Package over 100,000,000 years for Run 1**

The remaining simulations focused on characterizing the potential cyclic nature of criticality from a thermohydrologic perspective. The postulated sequence of events is as follows: water enters a waste package and fills it to a level high enough for steady-state criticality to occur at the assumed power level; enough water evaporates so that criticality ceases; the waste package cools; water enters the waste package and fills it to a level high enough for steady-state criticality to occur, etc.

Runs 3, 4, 5, and 6 were also completed using a 10 mm/yr infiltration rate, but the criticality liquid saturation was set to 0.35 to be able to examine the cyclic nature of a quasi-steady-state criticality. The maximum time step was set to 10 years, and the heats of criticality were varied. Figure 3-7, Figure 3-8, Figure 3-9, and Figure 3-10 show the temperature and liquid saturation of each of these studies. Oscillations can be seen in Figure 3-7, Figure 3-8, and Figure 3-9. No oscillations are seen in Figure 3-10 as the waste package is assumed to remain subcritical in Run 6.

The oscillations can be seen as criticality events characterized by the following sequence: liquid saturation reaches 0.35, criticality begins, water evaporates, then criticality shuts off. However, upon closer inspection, it also appears that there may be numerical instability in the calculation, which is seen especially in Figure 3-7 where liquid saturation appears to bottle-neck and then expand at the end of the simulation. The actual result is likely a numerical instability caused by the cyclic nature of the criticality event. Future work will differentiate between numerical instability and cyclic criticality events. It is also notable that the value around which the liquid saturation is oscillating is higher than the set value of 0.35. This behavior is more clearly seen in Figure 3-11, Figure 3-12, and Figure 3-13, which show liquid saturation from 20,000 to 25,000 years for Runs 3, 4, and 5, respectively.

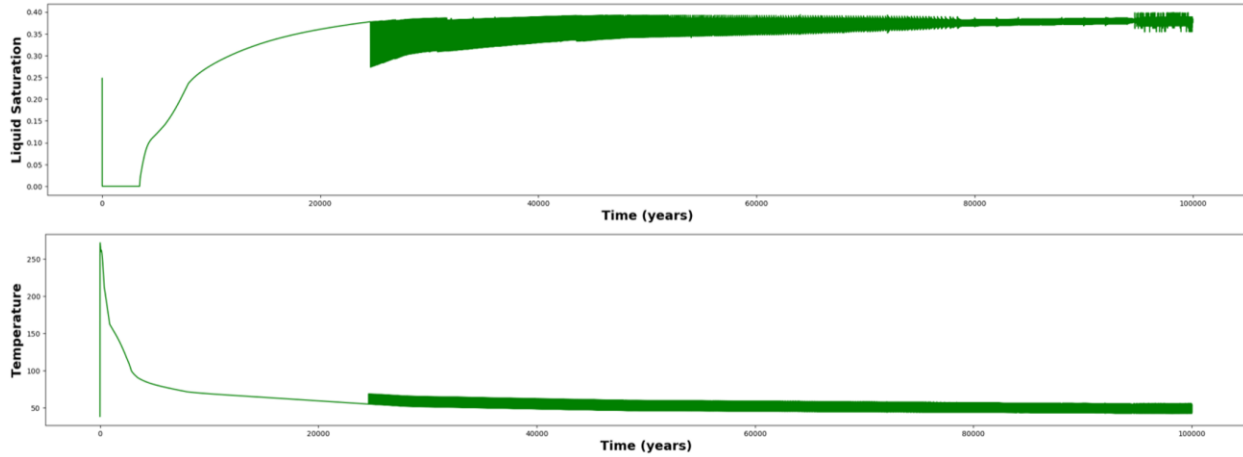


Figure 3-7. Liquid Saturation and Temperature for Centermost Waste Package for Run 3

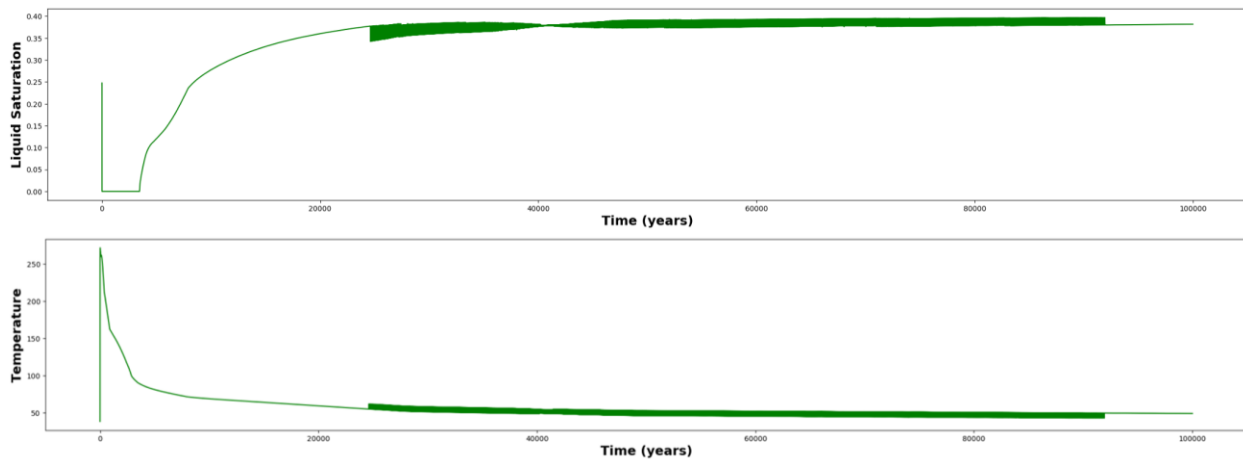


Figure 3-8. Liquid Saturation and Temperature for Centermost Waste Package for Run 4

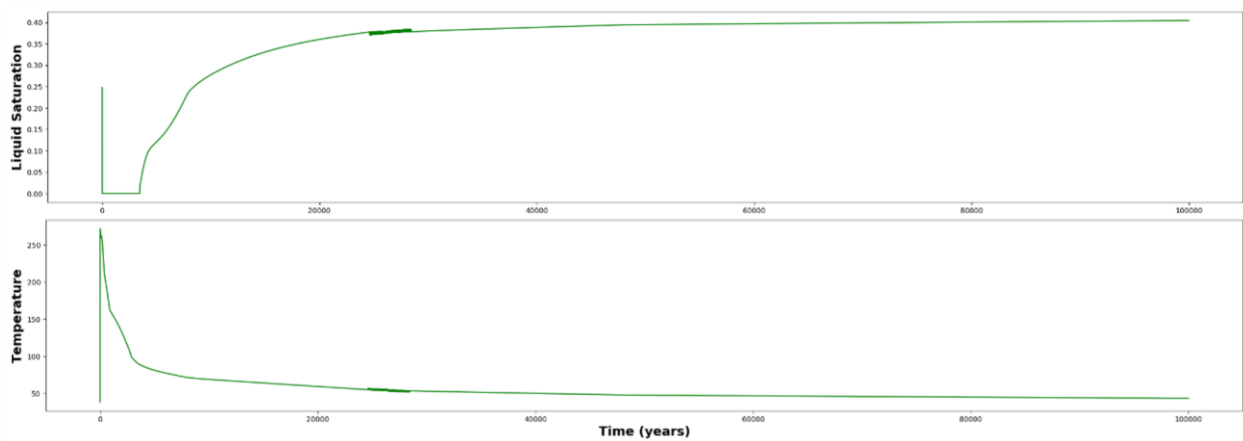


Figure 3-9. Liquid Saturation and Temperature for Centermost Waste Package for Run 5

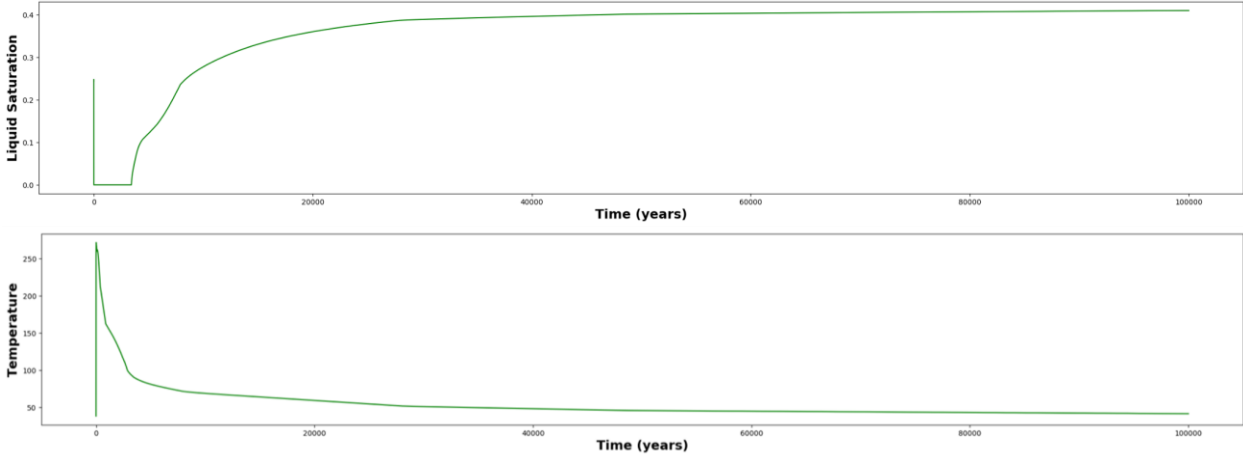


Figure 3-10. Liquid Saturation and Temperature for Centermost Waste Package for Run 6

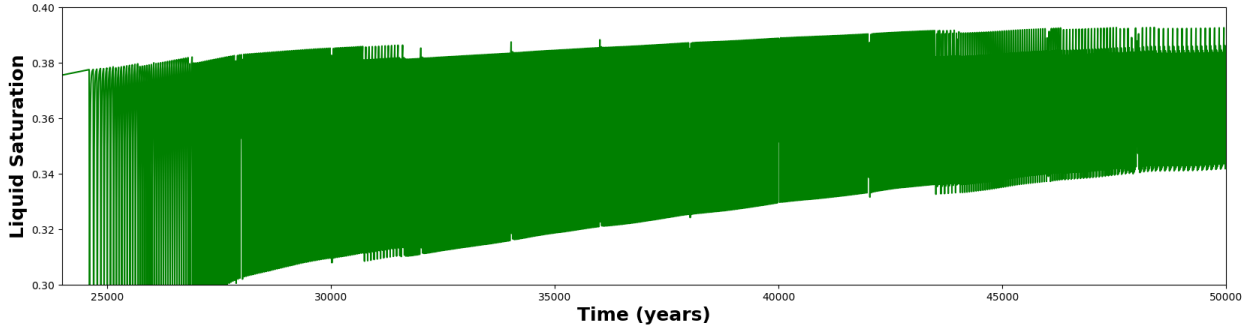


Figure 3-11. Liquid Saturation for Run 3 from 24,000 to 50,000 Years

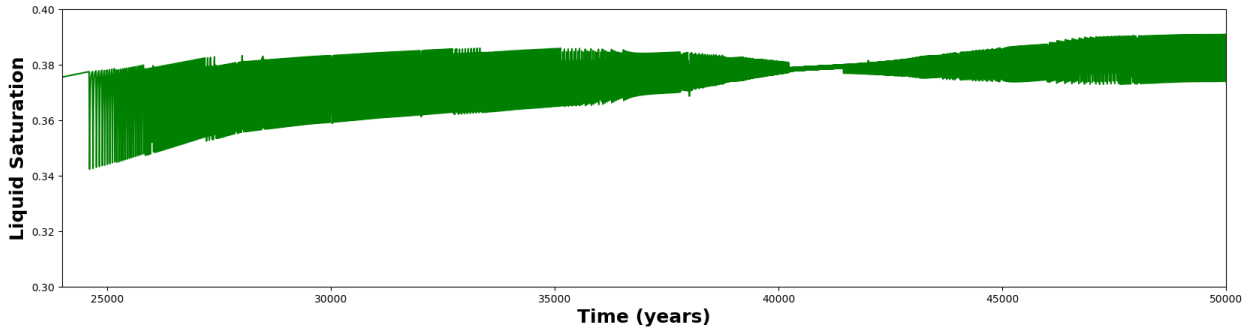
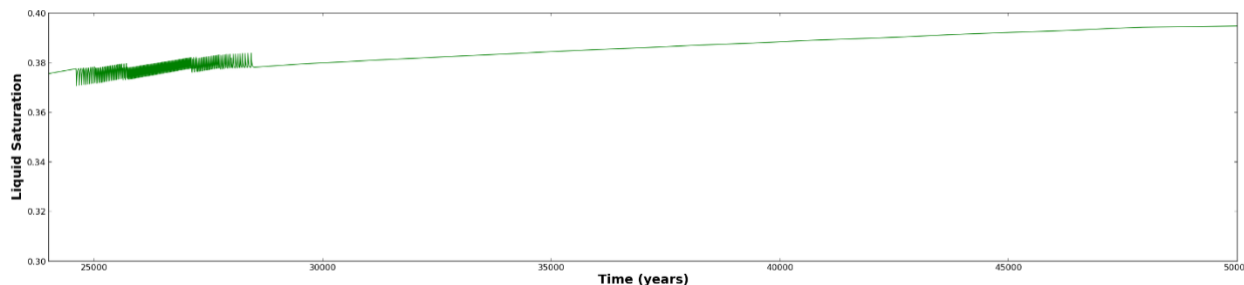


Figure 3-12. Liquid Saturation for Run 4 from 24,000 to 50,000 Years

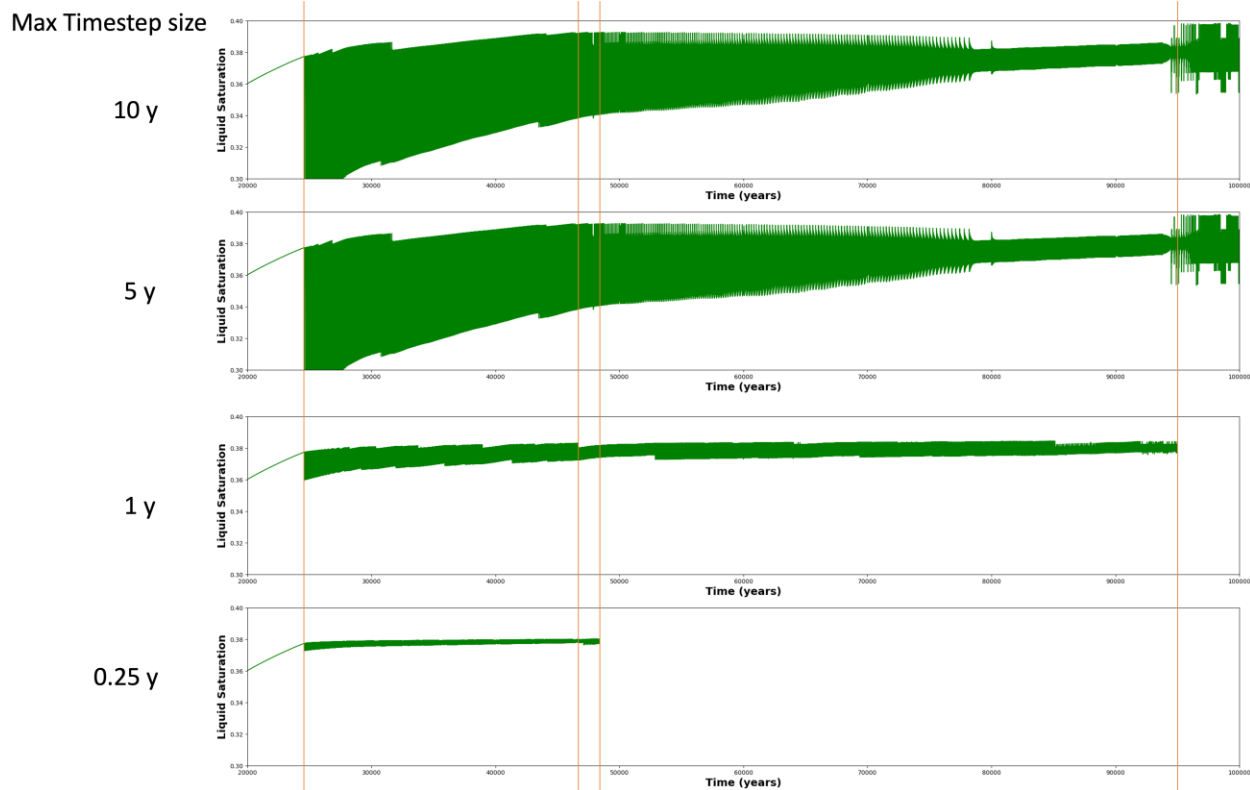


**Figure 3-13. Liquid Saturation for Run 5 from 24,000 to 50,000 Years**

These results necessitated a time-step study to see if the instabilities resolved with smaller time steps. Values of 5, 1, and 0.25 years were used for the time-step study (Runs 8, 9, and 10) with all other parameters constant. The liquid saturation plots for these additional runs, along with the original 10-year time-step run, are shown in Figure 3-14, and the temperature plots are shown in Figure 3-15. Gold lines mark times of interest, as determined by the liquid saturation results, are shown in both figures, with the times of interest being between 20,000 years and 100,000 years.

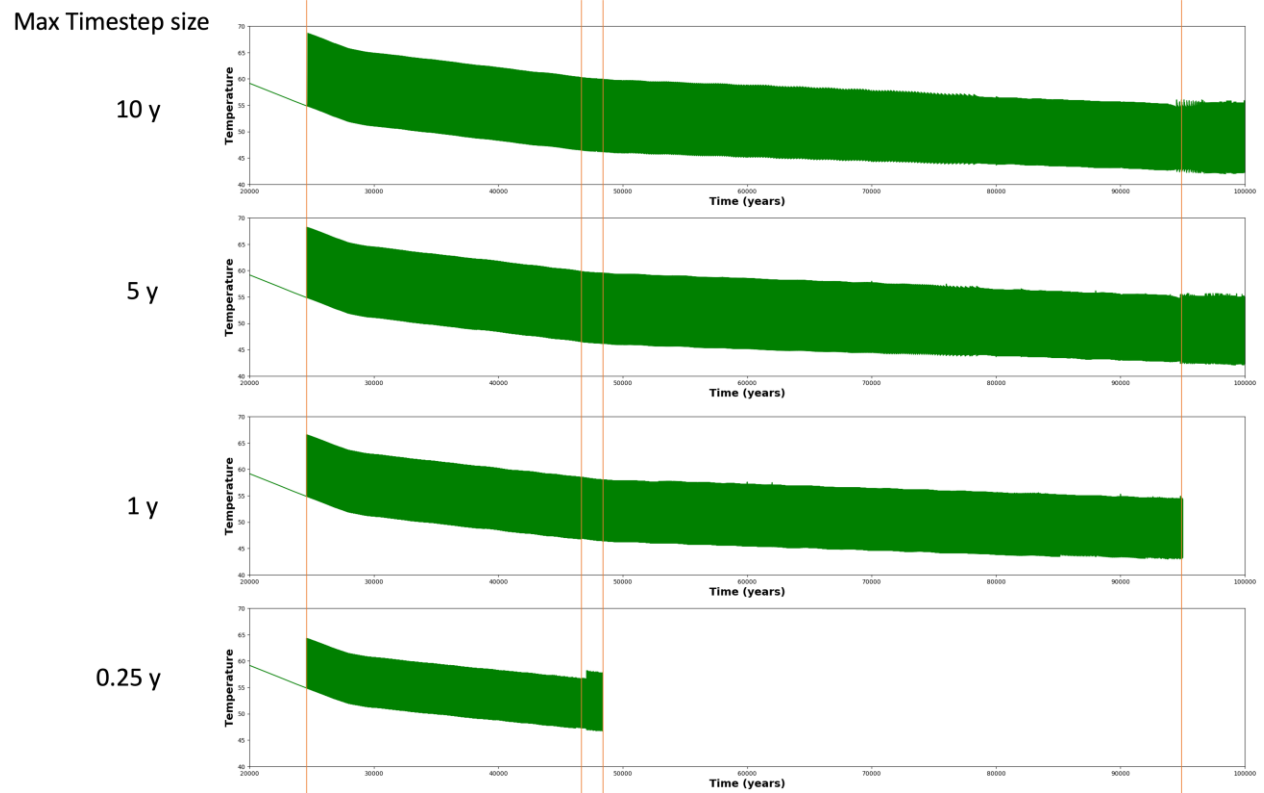
The 1-year and 0.25-year time-step results did not complete within a 48-hour walltime. However, the 1-year time step was only 5,000 years short of the 100,000-year mark, while the 0.25-year time-step run did not get to 50,000 years.

The amplitude of the temperature plots is fairly uniform until the final years of the simulation. Also, the amplitude of the temperature variation decreases by at least 1°C–2°C as time-step size decreases. The effect of the time step is more obvious with the liquid saturation plots. The amplitude of the variability in both temperature and saturation significantly decreases as the time step decreases. Figure 3-16 shows a ParaView visual of the centermost waste package at the time of the first oscillations for the 0.25-year time-step run. It can be seen in the image that three grid cells make up any given waste package in the model. While the observation point in the center of the three grid cells—defined as the center of the centermost waste package (Fwp\_Inside)—has a liquid saturation greater than 0.35, the other two grid cells that make up the waste package have a liquid saturation lower than 0.35. The average liquid saturation value of the three grid cells is taken into consideration within the criticality mechanism block using the critical water saturation option. The oscillations of the plots presented signify the start of the criticality event in these runs.



NOTE: Gold lines mark times of interest between 20,000 years and 100,000 years as determined by the liquid saturation results.

**Figure 3-14. Liquid Saturation Compared by Maximum Time-Step Size (Runs 3, 7, 8, and 9)**



NOTE: Gold lines mark times of interest between 20,000 years and 100,000 years as determined by the liquid saturation results.

**Figure 3-15. Temperature Comparison by Maximum Time Step (Runs 3, 7, 8, and 9)**

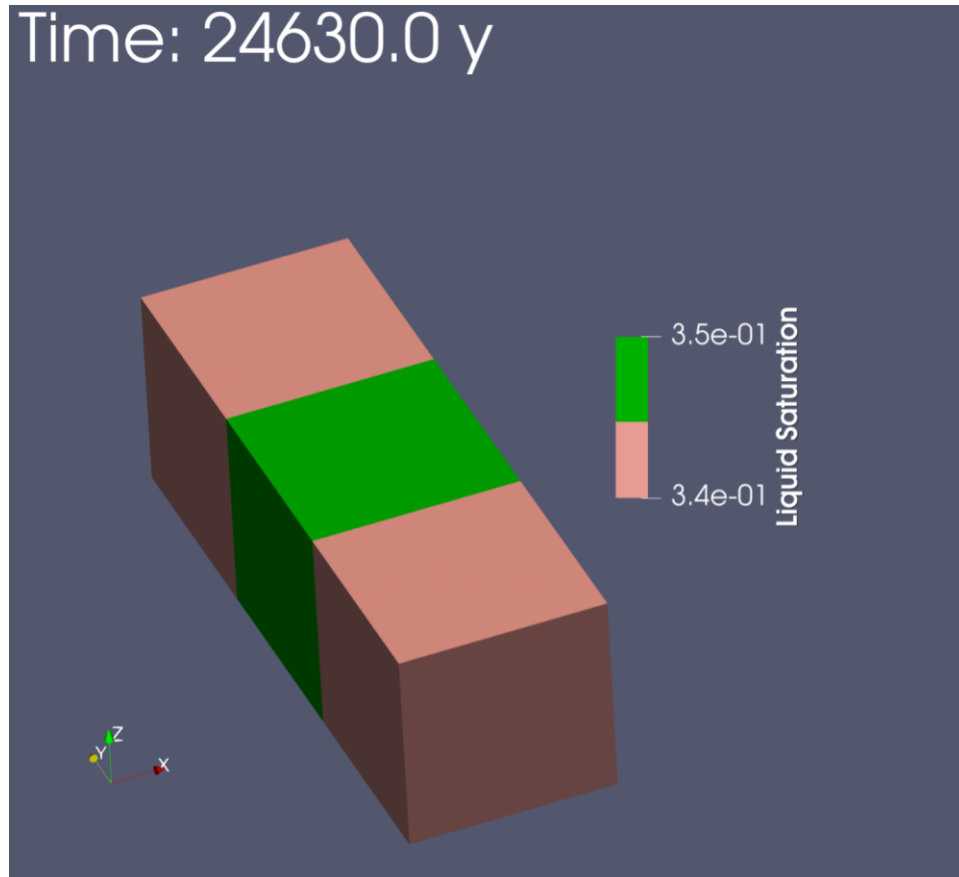


**Figure 3-16. ParaView Visual of Centermost Waste Package at 24,630 Years**

For each run, the average amplitude of changes in temperature and liquid saturation as well as the number of criticality events were calculated (Table 3-3). The number of criticality events was defined by identifying when the temperature increased by more than 5°C from one time step to the next, a criterion that captures the spike from one temperature to another as heat due to the criticality event is added to the system. It can be seen that the amplitudes decrease with the maximum time-step size, but the number of criticality events increases. The number of criticality events for the runs with 1- and 0.25-year maximum time steps more than doubles when compared to the 10- and 5-year maximum time-step runs even though the 1- and 0.25-year runs did not continue for the full simulation time.

**Table 3-3. Average Amplitude of Temperature and Liquid Saturation Changes as well as Number of Criticality Events by Time Step**

<b>Time-Step Size (years)</b>	<b>Average Temperature Amplitude (°C)</b>	<b>Average Liquid Saturation Amplitude</b>	<b>Number of Criticality Events</b>
10	12.40062	0.02071	7,706
5	12.04789	0.01445	8,314
1 <sup>a</sup>	11.28743	0.00614	23,265
0.25 <sup>a</sup>	9.29397	0.00121	17,747

NOTE: <sup>a</sup>These runs did not complete to 100,000 years.

It should also be noted that the temperature increase for these runs, which assume a critical event of 400 W, is on the order of 10°C. This increase is probably not significant in terms of engineered and natural barrier performance.

### 3.6 Further Work

As noted above, in Figure 3-6, Figure 3-7, Figure 3-8, Figure 3-9, and Figure 3-10, initial liquid saturation in the waste package is defined as 0.25, which is incorrect. Waste packages are expected to be very dry, with an initial liquid saturation of 0.0025. However, since the unsaturated zone is extremely dry, the liquid saturation drops to 0 within the first year, so this error has not affected any of the results presented here. Future work will correct this initial value to more accurately reflect the expected initial conditions.

Additional work considered for the future includes investigations into the range of saturation levels needed for criticality to occur, the range of conditions for which the critical saturation level can be achieved (e.g., different infiltrations, different heat output, different waste package spacing), and the increase in radionuclide inventory should criticality occur. Oscillations in PFLOTRAN results for the simulations in which criticality occurs will be addressed to further refine those simulations.

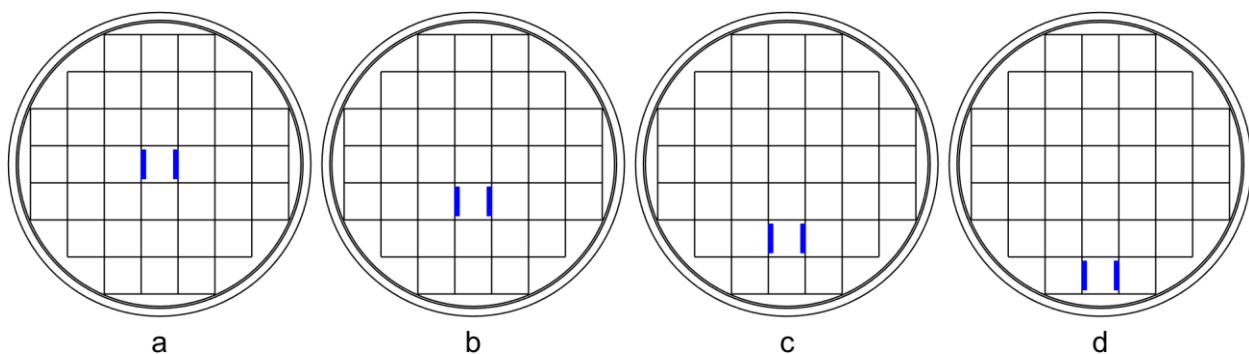
This page is intentionally left blank.

## 4. REACTIVITY INSERTION RATE ANALYSIS FOR TRANSIENT CRITICALITY

A transient criticality marked by a rapid reactivity insertion of large magnitude can result in high power levels, high energy generation, and high temperatures. In the canister evaluated by Salazar et al. (2022), the highest amount of excess reactivity of \$6.67 was observed in a case in which the entirety of the neutron absorber material had dissolved and precipitated out of solution. Although this magnitude of reactivity is very high, one can intuitively see that precipitation or settling  $^{10}\text{B}$  as corrosion products would be a very slow process in the context of neutronic transients, likely on the order of minutes or even hours, and feedback mechanisms would reduce the system-level reactivity increase. A reactivity magnitude in the \$4–\$6 range occurring in less than one second does not reflect a likely or even possible scenario under the conditions anticipated after repository closure.

Efforts to bound reactivity magnitude and rates could look like an analysis of FEPs in which realistic scenarios are considered and modeled in a conservative way. One such example is in the consideration of absorber material falling through a DPC. The falling of absorber material likely represents the fastest rate of insertion that could be achieved, but even that possibility is limited by Newtonian kinetics. In this scenario, a piece of absorber material is degraded and barely held in place in the canister. Something occurs such that the absorber is no longer physically restrained leaving it free to move downwards through the canister.

A highly stylized, albeit unrealistic, scenario was considered in which two full-length absorber plates in the central basket location were allowed to fall unobstructed to the bottom of the canister. Modeled for this analysis was a MCNP model of a 37-PWR DPC with the as-loaded configuration of SNF from the Zion commercial nuclear power station. The inner diameter of the canister is about 90 cm. The two absorber plates in the central-most basket cell are fully intact, and all other absorbers have been removed. In the starting condition, there is just enough  $^{10}\text{B}$  in solution to keep the canister just barely subcritical. The canister reactivity is evaluated for multiple absorber locations, four of which are shown below in Figure 4-1, where the blue rectangles represent the absorber locations. The labels a–d in Figure 4-1 are also used in Figure 4-2 to indicate the data points corresponding to the four locations.

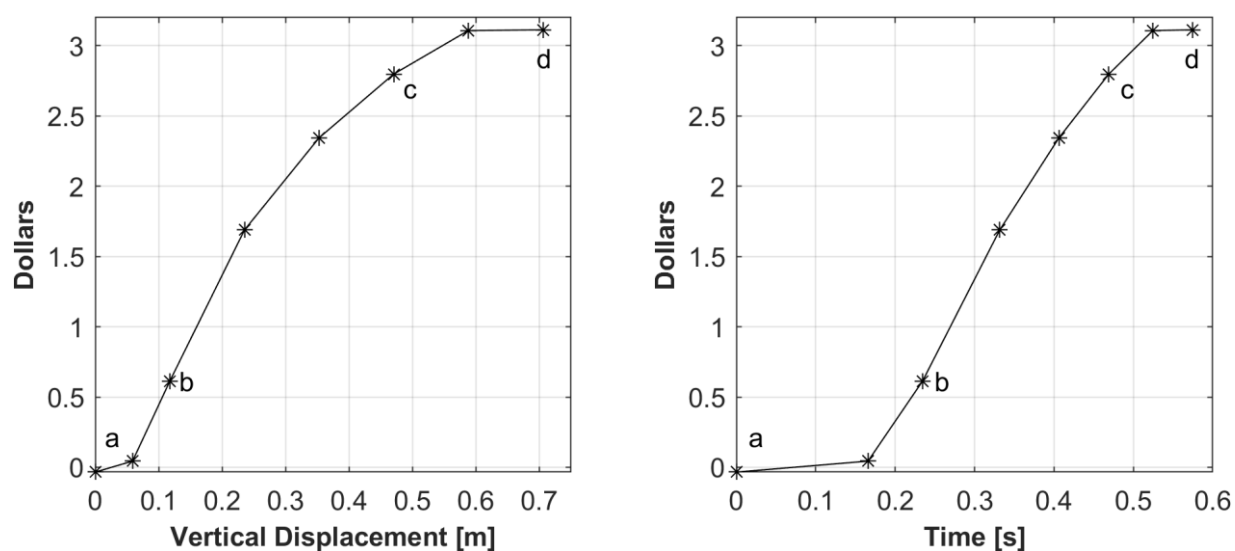


NOTE: Blue rectangles represent absorber locations.

**Figure 4-1. The Four Basket Cell Locations as the Intact Absorber Plates Fall to the Bottom of the Canister**

The absorber position as a function of time is shown in Equation 4-1, which accounts for freefall of the plate accounting for buoyancy of the water. Drag is negligible and ignored. Reactivity as a function of absorber vertical displacement as it falls through the canister and time are plotted in Figure 4-2, left and right graphs respectively.

$$y(t) = -\frac{gV_A(\rho_A - \rho_{H_2O})}{2m_A}t^2 \quad \text{Equation 4-1}$$



NOTE: Absorber position for the vertical displacement is the distance from original position. The labels a–d correspond to the same labels for Figure 4-1 showing four absorber locations used for analysis.

**Figure 4-2. Reactivity as a Function of Absorber Vertical Displacement (left) and Time (right)**

These results are preliminary, and more work to refine the analysis is planned for the future. That said, these preliminary results do illustrate that a reactivity insertion of around \$3 would require on the order of tenths of seconds to progress. It should also be noted that this result is at thermally static conditions without reactivity feedback, and a more complete analysis would result in less reactivity increase. The primary insight provided by this type of analysis is that appreciable reactivity magnitudes require increasingly longer time scales. Future efforts will focus on refining this type of analysis and providing additional support for assumptions.

## 5. MODELING TRANSIENT CRITICALITY IN A SATURATED REPOSITORY

This section presents the results of modeling transient criticality in a saturated repository using the SIMULATE-3K (S3K) code. First, the application of the code to the conditions of interest during the postclosure period are discussed (Section 5.1), followed by a discussion of previous work (Section 5.2), a presentation of results for this year (Section 5.3), and a discussion of further work (Section 5.4).

### 5.1 Application of SIMULATE-3K to a DPC

The S3K code (Studsvik AB n.d.) has been used to evaluate transient criticality events for a DPC containing either PWR or BWR SNF disposed in a saturated shale geologic repository. Characteristics such as peak power, duration, total energy released, and thermodynamic impacts have been previously studied, e.g., Price et al. (2021) and Salazar et al. (2022), as well as in Price et al. (2023), from which particular information is summarized in Section 5.2 and Section 5.3. In Price et al. (2021), a transient criticality event in the DPC was simulated through the rod ejection accident (REA). The cross-section input to S3K is provided by CASMO, a lattice fuel 2D multigroup transport-based Method of Characteristics code (Grandi et al. 2011). CASMO produces a 2D transport solution rooted in a heterogeneous model geometry, which is used for steady-state neutronic analysis in SIMULATE that, in turn, is used for transient neutronic analysis in S3K.

It should be noted that Price et al. (2021), Salazar et al. (2022), and Price et al. (2023) rely on the same control rod ejection methodology. Full-length and partial-length rods are ejected from the center of the core for the local reactivity insertions analysis. For the global reactivity insertions analysis, the control rods are assumed to be uniformly ejected throughout the core.

There are some limitations to the studies in Price et al. (2021), Salazar et al. (2022), and Price et al. (2023) as the intended function of S3K does not consider the modeling of transient analysis of canisters/out-of-reactor conditions. Therefore, control rod movement is restricted based on design of the PWR reactor design. That is, the control rods are inserted from the top in the PWR. Also, the control rod withdraw speed is limited to 9,999 cm/s (translates to 0.0365 seconds), which affects the maximum reactivity insertion rate. Finally, CASMO/SIMULATE captures decay times on the order of tens of years and not the thousands of years (e.g., 9,000) required by the DPC conditions. This situation may make the isotopic composition bounding in nature (i.e., higher excess reactivity in the DPC). With these limitations explained, highlights from FY2021 (Price et al. 2021) and FY20223 (Salazar et al. 2022) are presented below before delving into the results of FY2023 work (Price et al. 2023) in Section 5.2 and Section 5.3.

**Highlights from Previous Years**—Work in FY2021 (Price et al. 2021) and FY2022 (Salazar et al. 2022) focused on topics such as the REA analysis of a PWR DPC (37-PWR SNF assemblies). One area of focus comprised simulating a criticality transient potentially occurring in disposed DPC due to displacement of neutron absorbers or changes in geometry. The reactivity insertion, due to the REA, was modeled in the center of the DPC, referred to as “local reactivity insertion.”

Another focus area concerned the global reactivity insertion analysis for the PWR DPC based on the REA. The same methodology was used as in the localized REA analysis, but the control rods are assumed to be uniformly ejected throughout the DPC in the global scenario. A different global reactivity insertion analysis involved the simulation of the PWR DPC as a re-criticality accident condition in a reactor core with unborated water being injected into the PWR core causing the boron to become diluted.

Finally, a control blade ejection analysis of a BWR DPC (89-BWR SNF assemblies) simulating a criticality transient potentially occurring in a disposed DPC due to displacement of neutron absorbers, or changes in geometry, was examined. This analysis was performed in the same manner as the localized PWR REA.

## 5.2 Approach for FY2023

In FY2023 (Price et al. 2023), the primary scope and approach to evaluate transient criticality events in a saturated repository focused on reducing dependence on axial variations in fuel composition and minimizing the impacts of leakage on modeling by simulating partial-length control rods with uniform absorber composition (Price et al. [2021] and Salazar et al. [2022] used full-length control rod ejection). The partial-length control rods were evaluated for both local and global reactivity insertion scenarios for the PWR DPC (37-PWR SNF assemblies), and these results were then compared with those from the full-length rods.

In addition, the study team investigated a second analysis approach that involved modeling a simplified DPC with essentially fresh fuel to represent (and potentially bound) the population of DPCs. The reasoning for this approach was to reduce modeling dependence on as-loaded PWR DPC characteristics (assembly initial enrichment, burnup, design, location within DPC, etc.). The results of the modeling with the simplified DPC were compared to those obtained using the characteristics of an as-loaded DPC.

In the third approach studied in FY2023, a range of reactivity insertion times representing various insertion mechanisms was evaluated. These insertion time variations represent various DPC abnormal conditions. For instance, the slower insertion times are representative of the settling of corrosion products and dissolved absorbers, while the faster insertion times are representative of geometric changes due to seismic events.

To consider the effects of initiation of transients in DPCs at various conditions, the study team pursued a fourth approach considering a hot package undergoing a steady-state criticality and a “cold” package. This approach evaluated transient parameters of interest (e.g., fuel and moderator temperatures, peak power, total energy generation).

## 5.3 Transient Criticality Results

The following subsections summarize the results from FY2023 transient criticality analyses for a saturated repository documented in Price et al. (2023).

### 5.3.1 Simplified DPC Development

An evaluation was performed to develop a simplified DPC model using various “fresh” fuel enrichments with local reactivity insertions comparing regular-length control rods to partial-length control rods. The initial enrichments evaluated were 2, 3, and 5 wt%  $^{235}\text{U}$  with various reactivity insertion times. That is, all PWR assemblies are modeled with the same initial enrichment (e.g., all PWR assemblies in the entire DPC are modeled at an initial enrichment of 2 wt%  $^{235}\text{U}$ , etc.). Note that the assemblies are modeled with insignificantly low burnup (i.e., a few MWd/MTU) to allow the code to initiate the transient.

The simulations indicate that the partial-length control rod results consistently bound the regular-length control rod results. They also demonstrate that all key transient parameters of interest (e.g., peak power, total energy, peak fuel temperature) are directly proportional to enrichment and insertion time. This observation is illustrated in Figure 5-1 for peak power. The average equivalent enrichment of a DPC

loaded with PWR SNF is not expected to be greater than 3 wt% <sup>235</sup>U. Therefore, the parametric evaluations with the simplified model in the following subsections are based on a DPC loaded with 3 wt% <sup>235</sup>U enriched fuel. Note that assuming a more conservative enrichment of 5 wt% <sup>235</sup>U would not be representative of SNF, and less than 3 wt% <sup>235</sup>U may not be sufficiently conservative. Representative fuel characteristics (e.g., enrichment, design) will be refined in future studies.

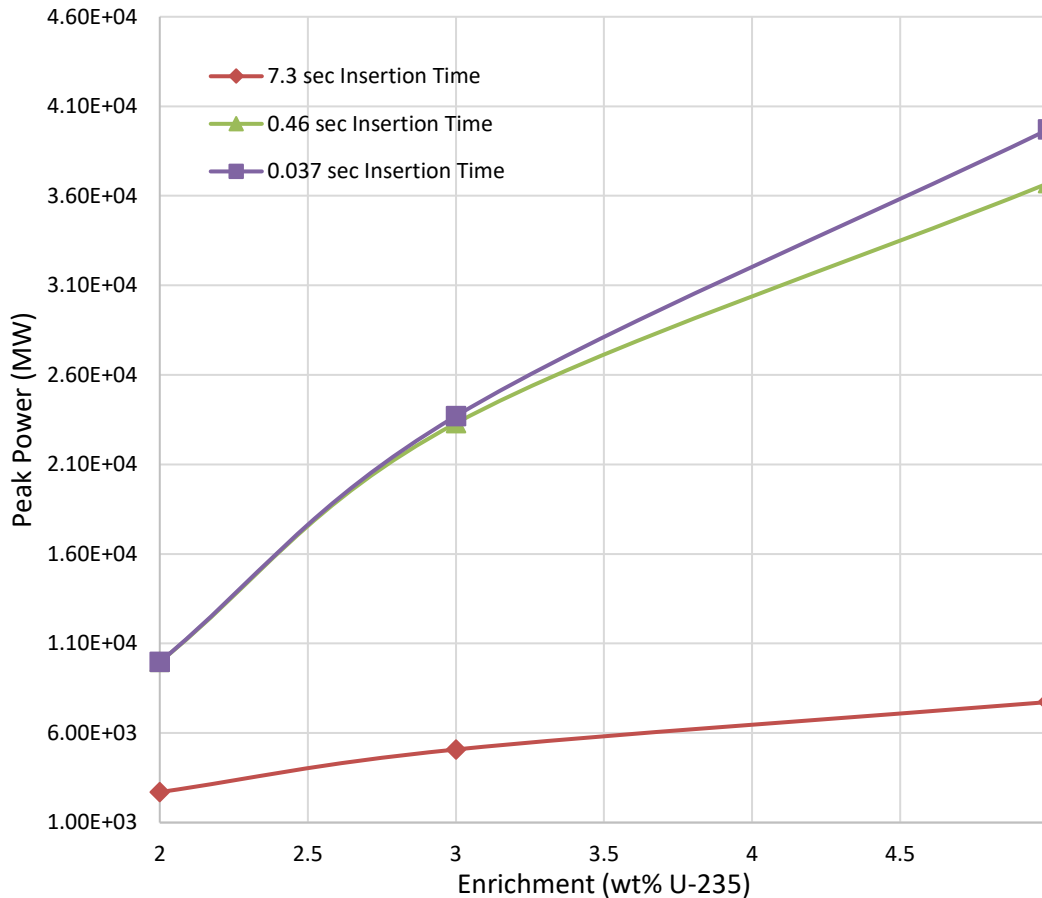


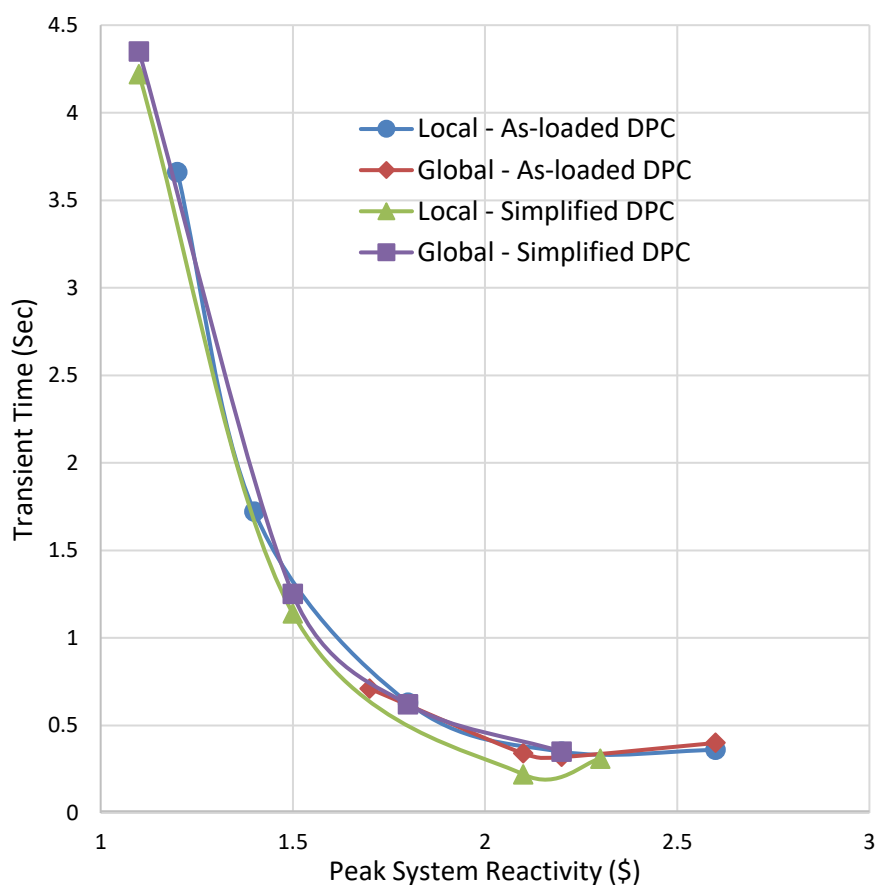
Figure 5-1. Transient Peak Power versus Enrichment—Varied Insertion Times

### 5.3.2 Comparison of Simplified and As-Loaded PWR DPC—Local and Global Reactivity Insertions at a Constant Insertion Rate

To compare the simplified and as-loaded PWR DPC models and to determine the impact of reactivity insertion location on potential transients, a set of calculations for both PWR DPC local and global reactivity insertion were performed at 1-second insertion time. This scenario is expected to be a more representative, but still a conservative choice reflecting processes anticipated to occur during the postclosure period. This 1-second insertion time is based on preliminary evaluations of movement/settling of degrading absorber plates from the middle of a flooded DPC to the bottom. Note that, unlike the cases presented in Section 4, the modeling described in this section is fully coupled (neutronics, kinetics, and TH effects), including reactivity feedback. These calculations were performed for both a simplified

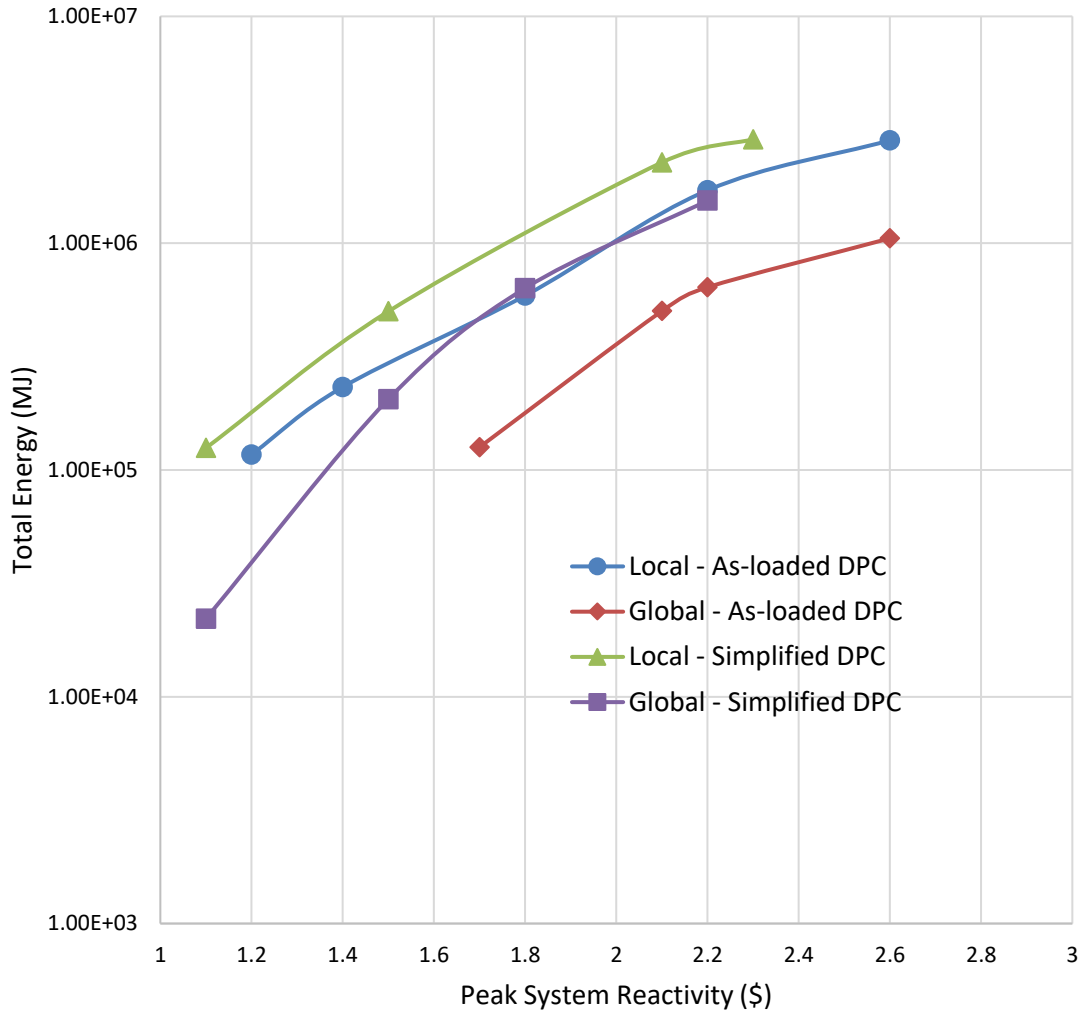
(3 wt%  $^{235}\text{U}$  initial enrichment) and an as-loaded PWR DPC loading. The peak reactivity of the system is defined by the insertion time along with feedback mechanisms (i.e., fuel temperature coefficient). The reactivity insertion time dictates whether the highest reactivity worth is achieved before the completion of the transient.

It can be seen in Figure 5-2 that the peak system reactivity is inversely proportional to transient time (rate at which the reactivity is inserted). Faster transients result in higher peak system reactivity since the fuel and temperature reactivity feedback mechanisms are not instantaneous (i.e., it takes time to heat up the fuel and moderator). Furthermore, as illustrated in Figure 5-3, the total energy increases in a roughly linear fashion with increasing peak system reactivity (while keeping the reactivity insertion time at 1-second for all scenarios). The simplified DPC is consistently bounding for all reactivity insertion amounts evaluated. Similar trends are observed for the core power and temperatures (fuel and moderator).



NOTE: DPC = dual-purpose canister

**Figure 5-2. Transient Time versus Peak System Reactivity—1-Second Reactivity Insertion Time**



NOTE: DPC = dual-purpose canister

**Figure 5-3. Transient Total Energy versus Peak System Reactivity—  
 1-Second Reactivity Insertion Time**

It is worth pointing out that the as-loaded DPC selected for this study is one of the more reactive PWR DPCs loaded and analyzed thus far (Liljenfeldt et al. 2017). Therefore, the reactivity of the simplified PWR DPC loaded with 3 wt% <sup>235</sup>U enriched fuel would likely bound other as-loaded PWR DPCs; this supposition will be further evaluated and confirmed as additional as-loaded DPCs are modeled.

### 5.3.3 Simplified PWR DPC with Partial-Length Control Rods—Local versus Global Reactivity Insertion

A simplified model of the PWR DPC with partial-length control rods was analyzed for local reactivity insertion with the assumption that all PWR assemblies have an initial enrichment of 3 wt% <sup>235</sup>U. The reactivity insertion times were varied from slow (365 seconds) to very fast (~0.04 seconds) to bound potential transients. The local and global reactivity insertion results demonstrate that peak system reactivity is inversely proportional to insertion time.

Another observation is that the parameters of interest including peak system reactivity, peak power, total energy, maximum fuel temperature, maximum water temperature, and peaking factor are relatively similar for both cases. This outcome is expected for the simplified DPC because of the lack of axial or radial variability in fuel composition leaving radial leakage, which is not significant for the relatively large DPC, as the only parameter that could impact system kinetics.

### 5.3.4 As-Loaded PWR DPC with Partial-Length Control Rods—Local versus Global Reactivity Insertion

An as-loaded model of the PWR DPC with partial-length control rods is also analyzed for reactivity insertion with the DPC assemblies, and the results have been included herein. The reactivity insertion times were varied from slow (365 seconds) to very fast (~0.04 seconds) to bound potential transients. The local and global reactivity insertion results demonstrate that peak system reactivity is inversely proportional to insertion time. It can be seen from the results in Table 5-1 through Table 5-4 that fairly similar behavior/values exist for both moderator and fuel temperature when comparing localized and global reactivity insertion for all insertion times. This same trend was noted for the simplified DPC, further supporting the preliminary conclusion that the simplified DPC model could be considered representative of transients in as-loaded DPCs.

**Table 5-1. Summary PWR Local Reactivity Insertion—  
As-Loaded DPC at Slow Reactivity Insertion Times**

As-Loaded DPC Local Reactivity Insertion Partial-Length Control Rods					
Parameter	Insertion Time (second)				
	365	36.5	14.6	7.3	1.83
Peak System Reactivity (\$)	1.0	1.2	1.4	1.6	2.7
Peak Power (MW)	5.34E+01	1.44E+03	5.39E+03	1.53E+04	1.32E+05
Total Energy (MJ)	1.75E+04	1.66E+05	6.00E+05	8.56E+05	3.77E+06
Maximum Fuel Temperature	476°C (749 K)	1,255°C (1,528 K)	1,412°C (1,685 K)	1,486°C (1,759 K)	2,176°C (2,449 K)
Maximum Average Fuel Temperature	244°C (517 K)	309°C (582 K)	325°C (598 K)	334°C (607K)	411°C (684 K)
Maximum Water Temperature	211°C (484 K)	225°C (498 K)	225°C (498 K)	225°C (498K)	225°C (498 K)
Maximum Average Water Temperature	206°C (479 K)	212°C (485 K)	212°C (485 K)	212°C (485K)	212°C (485K)
Transient Time (second)	14.92	3.12	1.38	0.82	0.54
Power Peaking Factor	1.679	1.679	1.679	1.679	1.679

NOTE: DPC = dual-purpose canister

**Table 5-2. Summary PWR Local Reactivity Insertion—  
As-Loaded DPC at Fast Reactivity Insertion Times**

<b>As-Loaded DPC Local Reactivity Insertion Partial-Length Control Rods</b>					
<b>Parameter</b>	<b>Insertion Time (second)</b>				
	<b>0.91</b>	<b>0.46</b>	<b>0.30</b>	<b>0.073</b>	<b>0.037</b>
Peak System Reactivity (\$)	2.8	3.0	3.4	3.6	3.6
Peak Power (MW)	1.46E+05	2.15E+05	2.90E+05	3.82E+05	3.83E+05
Total Energy (MJ)	4.66E+06	7.12E+06	9.36E+06	1.14E+07	1.24E+07
Maximum Fuel Temperature	2,249°C (2,522K)	2,479°C (2,752K)	2,596°C (2,869K)	2,707°C (2,980K)	2,707°C (2,980K)
Maximum Average Fuel Temperature	427°C (700K)	491°C (764K)	532°C (805K)	604°C (877K)	605°C (878K)
Maximum Water Temperature	225°C (498K)	225°C (498K)	225°C (498K)	226°C (499K)	225°C (498K)
Maximum Average Water Temperature	212°C (485K)	212°C (485K)	212°C (485K)	213°C (486K)	213°C (486K)
Transient Time (second)	0.35	0.06	0.05	0.04	0.04
Power Peaking Factor	1.679	1.679	1.679	1.679	1.679

NOTE: DPC = dual-purpose canister

**Table 5-3. Summary PWR Global Reactivity Insertion—  
As-Loaded DPC at Slow Reactivity Insertion Times**

<b>As-Loaded DPC Global Reactivity Insertion Partial-Length Control Rods</b>					
<b>Parameter</b>	<b>Insertion Time (second)</b>				
	<b>365</b>	<b>36.5</b>	<b>14.6</b>	<b>7.3</b>	<b>1.83</b>
Peak System Reactivity (\$)	1.0	1.3	1.5	1.8	2.6
Peak Power (MW)	7.71E+01	2.41E+03	8.88E+03	2.58E+04	1.00E+05
Total Energy (MJ)	5.16E+02	7.46E+04	4.03E+05	9.27E+05	1.41E+06
Maximum Fuel Temperature	557°C (831 K)	1,281°C (1,554 K)	1,387°C (1,660 K)	1,448°C (1,721K)	2,007°C (2,280 K)
Maximum Average Fuel Temperature	247°C (520 K)	304°C (577 K)	315°C (588 K)	326°C (599 K)	385°C (659 K)
Maximum Water Temperature	224°C (497 K)	224°C (497 K)	224°C (497 K)	224°C (497 K)	224°C (497 K)
Maximum Average Water Temperature	211°C (484 K)	212°C (485 K)	212°C (485 K)	212°C (485 K)	212°C (485 K)
Transient Time (second)	16.02	2.15	1.1	1.05	0.54
Power Peaking Factor	1.864	1.864	1.864	1.864	1.864

NOTE: DPC = dual-purpose canister

**Table 5-4. Summary PWR Global Reactivity Insertion—  
As-loaded DPC at Fast Reactivity Insertion Times**

<b>As-Loaded DPC Global Reactivity Insertion Partial-Length Control Rods</b>					
<b>Parameter</b>	<b>Insertion Time (second)</b>				
	<b>0.91</b>	<b>0.46</b>	<b>0.30</b>	<b>0.073</b>	<b>0.037</b>
Peak System Reactivity (\$)	2.7	3.0	3.2	3.4	3.5
Peak Power (MW)	1.17E+05	2.35E+05	2.58E+05	3.52E+05	3.54E+05
Total Energy (MJ)	1.30E+06	3.89E+06	4.61E+06	7.46E+06	7.59E+06
Maximum Fuel Temperature	2,101°C (2,374K)	2,453°C (2,726 K)	2,512°C (2,785 K)	2,631°C (2,904 K)	3,393°C (2,906 K)
Maximum Average Fuel Temperature	403°C (676 K)	483°C (757 K)	512°C (785K)	589°C (862 K)	589°C (863 K)
Maximum Water Temperature	224°C (498 K)	227°C (500K)	227°C (500 K)	228°C (501 K)	238°C (501 K)
Maximum Average Water Temperature	212°C (485 K)	213°C (486 K)	213°C (486 K)	214°C (487K)	214°C (487 K)
Transient Time (second)	0.37	0.06	0.05	0.04	0.05
Power Peaking Factor	1.864	1.864	1.864	1.864	1.864

NOTE: DPC = dual-purpose canister

### 5.3.5 Varied Starting Temperatures

As disposed DPCs can potentially vary in internal temperature prior to the initiation of the criticality transient either because of the time at which the transient occurs (decay heat) or the condition of the DPC (e.g., an ongoing steady-state criticality), an evaluation was performed that considered two initial temperatures, “warm” and “cold”. Note that the same control rod characteristics were modeled for both cases (e.g., control rod withdrawal location, reactivity insertion time). As shown in Table 5-5, the peak system reactivity for the transient in the cooler DPC is higher than it is for the warmer DPC. The table also shows that the total transient time is inversely proportional to the peak system reactivity. The transients in the cooler DPCs result in higher maximum fuel temperature, peak power, and total energy generation. Further investigations of criticality transients initiating in cooler DPCs is warranted since these preliminary results indicate that they may be more limiting than transients in warmer DPCs.

**Table 5-5. Summary Simplified DPC at Constant Reactivity Insertion Time at Varied Transient Starting Temperatures**

Parameters	Simplified DPC—Local Reactivity Insertion Partial-Length Control Rods 1-Second Insertion Time	
Peak System Reactivity (\$)	1.3	1.9
<b>Start of Transient</b>		
Core Power (MW)	7.25E-07	4.70E-06
Maximum Fuel Temperature	264°C (537K)	38°C (311K)
Core Average Fuel Temperature	169°C (442K)	38°C (311K)
Core Average Moderator Temperature	168°C (441K)	38°C (311K)
<b>Transient Peak Values</b>		
Peak Power (MW)	5.35E+03	6.41E+04
Total Energy (MJ)	1.16E+05	1.49E+06
Maximum Fuel Temperature	660°C (933K)	1449°C (1722K)
Average Fuel Temperature	258°C (531)	303°C (576K)
Maximum Water Temperature	188°C (461K)	182°C (455K)
Average Water Temperature	178°C (451K)	110°C (383K)
Total Transient Time (second)	2.07	1.0

NOTE: DPC = dual-purpose canister

## 5.4 Further Work

Based on the work performed during FY2023 (Price et al. 2023), the following areas warrant further investigation:

- Evaluate the impact of DPC initial temperatures/conditions (e.g., critical versus subcritical package) on transient characteristics
- Evaluate reactivity insertion time on transient characteristics
- Evaluate secondary transient pulses, especially for slower transients
- Evaluate representativeness of simplified DPC models to the population of DPCs
- Demonstrate that the conclusions and trends for BWR DPCs are consistent with those for PWR DPCs

- Develop lookup tables for transient in a multidimensional matrix for a variety of fuels, reactivity insertion magnitudes, locations, times, etc.
- Develop a study to determine reactivity insertion mechanisms (e.g., using a what-if, HAZOP, or a fault/event tree process) and magnitudes (using MCNP)
- Evaluate transients with different control rod compositions (e.g., boron, gadolinium) to achieve a wider range of reactivity insertions
- Evaluate transients with control rods that have a nonuniform composition with absorber material concentrated in a portion of the rod simulating the dislocation of an absorber plate

This page is intentionally left blank.

## 6. MODELING TRANSIENT CRITICALITY IN AN UNSATURATED REPOSITORY

### 6.1 Application of Razorback to a DPC

RAZORBACK (Talley 2017a,b, 2018) is a reactor transient computer code designed to simulate operations of the Annular Core Research Reactor (ACRR) at Sandia National Laboratories. Previous studies applied the code to transient events in DPCs in an unsaturated repository to evaluate kinetics parameters of interest such as the power profile, the fuel temperature profile (localized and global), and the water temperature profile (localized and global) (Price et al. 2021; Salazar et al. 2022).

RAZORBACK provides a coupled numerical solution of the point reactor kinetics equations; the energy conservation equation for fuel element heat transfer; the equation of motion for fuel element thermal expansion; and the mass, momentum, and energy conservation equations for cooling of the fuel elements by water. To account for reactivity feedback parameters, a series of steady-state criticality calculations with MCNP were performed to characterize reactivity feedback, provided the conditions for baseline criticality were achieved.

**Previous Work**—In the previous studies, an MCNP model was developed for a 37-PWR DPC with the as-loaded configuration of SNF from the Zion commercial nuclear power station (Price et al. 2021). The DPC contains 37 Westinghouse  $15 \times 15$  PWR SNF assemblies with the as-loaded configuration of cask stored at the Zion Nuclear Power Station. The fuel composition was provided by Oak Ridge National Laboratory from depletion calculations on an assembly basis for the cask at Zion using information from UNF-ST&DARDS (Clarity et al. 2017).

Reactivity of the canister was evaluated at different configurations to represent how reactivity of the DPC might change temporally because of groundwater infiltration and degradation of DPC component internals (Price et al. 2021). The analysis comprised various stylized scenarios to account for the flooding of the DPC, dissolution of the absorber materials, collapse of the basket structure, and collapse of the fuel assembly grid spacers. In Salazar et al. (2022), the analysis was expanded to investigate the dissolution and precipitation of  $^{10}\text{B}$  from the neutron absorber plates and system reactivity as a function of water level in the canister. It was shown that complete removal of the DPC absorber plates could result in a reactivity insertion as high as  $\$6.67$  assuming no other changes to the DPC that could affect reactivity (i.e., constant fuel temperature, constant water temperature, density). It was also shown that the canister could achieve criticality at just over halfway full of fresh water. These estimates provide the parameter space that a transient analysis should cover.

The reactivity feedback mechanisms derived from MCNP calculations were then fed into RAZORBACK for transient analysis. In Price et al. (2021), reactivity was inserted into the DPC by means of movement of a control rod bank with a total worth of  $\$5.40$ . RAZORBACK was unable to complete simulations involving high total reactivity insertions or rapid reactivity insertions. Reactivity insertions of  $\$3$  were achieved for transients  $\geq 0.1$  seconds though some inconsistencies in coolant temperature were noted. In Salazar et al. (2022), reactivity was introduced globally to the DPC as opposed to the use of control rods. Reactivity insertions between  $\$1$  and  $\$3$  were analyzed for periods of 10 milliseconds, 100 milliseconds, 500 milliseconds, 1 second, 5 seconds, and 10 seconds. RAZORBACK was unable to complete the 10-millisecond calculations.

The key takeaways of the previous studies (Price et al. 2021; Salazar et al. 2022) are the following:

- If corrosion products from the degraded absorbers settle (or are removed from solution) within a short time period, the resulting reactivity insertions could result in rapid releases of energy on the order of  $10^8$ – $10^9$  J within a span of seconds.
- Results indicate that peak fuel temperatures do not rise to the extent that the SNF is damaged, the  $\text{UO}_2$  fuel does not melt, and the cladding does not approach temperature at which melting is possible.
- Criticality could occur when just over 50% of the DPC internal volume is filled with fresh water.
- The value of  $\beta_{eff}$  represents a higher bound for reactivity associated with the removal of  $^{10}\text{B}$  from the system given thermally static conditions.

## 6.2 Attempted Continuation with RAZORBACK

It was previously noted that the RAZORBACK code was unable to complete simulations involving rapid reactivity insertions with magnitudes larger than about  $\beta_{eff}$ . This limitation was treated with increased scrutiny, and further investigations into the difficulties the code has with modeling transient events in a DPC indicated the TH solver employed in RAZORBACK is unable to resolve the rapid heat transfer characteristics associated with anticipated transients in a DPC. Although RAZORBACK is able to run some of the more moderate transients to completion, there is some indication that stability issues in the TH solver could be affecting the evaluated results.

RAZORBACK was developed to model the ACRR at Sandia National Laboratories. The  $\text{UO}_2$ -BeO that fuels the ACRR is unique in that it was specifically designed to have a large heat capacity. This characteristic coupled with the fact that the fuel elements are 3.8 cm in diameter means the ACRR fuel has a large thermal mass. Typical PWR or BWR SNF is composed of  $\text{UO}_2$ , which is less thermally capacitive with fuel rods less than  $1/4^{\text{th}}$  the diameter of the ACRR fuel, so the fuel in a DPC has a much lower thermal mass by volume than the ACRR. A transient in a DPC containing typical PWR or BWR SNF similar in energy density to the ACRR would result in greater heat flux from the fuel to the coolant. The ACRR also resides in a 10 m deep pool, which helps to suppress boiling, whereas a DPC in an unsaturated repository is essentially at atmospheric pressure. The heat transfer rates associated with a supercritical DPC in an unsaturated environment are simply beyond the design basis of the RAZORBACK code. Initial attempts to modify the code to enable TH solver convergence were unsuccessful, leading to a re-evaluation of this development path. In the end, the level of effort required was deemed too high to continue.

It was therefore determined best to pursue alternative tools with the right combination of neutronics and TH capabilities. As a DPC contains SNF and resembles a reactor core, a logical candidate for a modeling tool would be a code designed for a commercial power reactor. As PWRs and BWRs operate at pressures much greater than ambient, reactor codes generally do not contain constitutive relations required for modeling criticality at atmospheric conditions. This reasoning explains why RAZORBACK, designed for modeling pool type reactors, was chosen in the first place. Critically configured, water-moderated commercial power fuel assemblies at atmospheric pressure represent a niche modeling environment.

Migrating to a new analysis tool also affords the opportunity to address another limitation when applying reactor core codes to disposal conditions, that is DPCs will likely be emplaced horizontally while reactor cores are primarily oriented vertically. TH core modeling often employs the subchannel analysis method, which is an effective simplification when the coolant streamline velocity aligns axially with the fuel rods.

In a horizontally emplaced DPC, however, convective flow induced from the heat generated from a transient will experience considerable cross-flow between the fuel rods. Criticality transients evolve quite rapidly and can even come to completion before any convective flow can develop, so it is unclear what impact this situation has on the parameters of interest. This observation is especially true for the saturated case for which boiling is unlikely to occur because of the increased pressure from the hydrostatic head. For the unsaturated case, boiling is more likely to occur, and boiling heat transfer between vertically oriented rods versus horizontally oriented ones can be quite different.

The ideal analysis tool (1) can accommodate a wide range of operating pressures including ambient, (2) can model boiling heat transfer including thermal stratification, (3) is not strictly subchannel based and can accommodate horizontal orientation, and (4) is fully coupled to neutronics and kinetics. Two such codes are available: GOTHIC™, which is developed and maintained by Zachary Nuclear Engineering, and TRACE, which is the NRC's flagship TH analysis tool. Further evaluation of both codes is desired to determine suitability, but currently only TRACE has been acquired. The effort to acquire GOTHIC™ is still ongoing.

### 6.3 Further Work

The TRACE code has already been acquired and a TH model of a 37-PWR DPC is currently under development. Once the TH model is more mature and verified to produce reasonable results, the kinetics parameters will be added to enable transient criticality evaluation. TRACE has a built-in point reactor kinetics module with inputs for reactivity feedback coefficients similar to that implemented in RAZORBACK, so the previously conducted neutronics analysis can serve as input into TRACE. This similarity between the codes should also allow direct comparison to prior years transient analysis with RAZORBACK. With a more robust TH solver, TRACE is expected to be able to model the transients that proved problematic in RAZORBACK, i.e., transients greater in reactivity magnitude and rates of insertion.

TRACE is built on a more generalized TH solver and does not suffer limits on the orientation of gravity with control volumes. The model is being developed to represent a horizontally emplaced waste package, but it should be relatively trivial to modify the gravity vector and model the canister in a vertical orientation. The two cases can then be compared to determine if there is an appreciable impact of orientation on the transient parameters of interest (peak power, total energy, peak temperatures, average temperatures, and transient duration).

TRACE also has the capability to be fully coupled with the kinetics code PARCS, which solves the time-dependent two-group neutron diffusion equation in 3D cartesian geometry. The level of detail available with the use of PARCS may not be required for transient analysis of DPCs, but the flexibility of spatially and temporally resolved reactivity insertion mechanisms may prove valuable.

This page is intentionally left blank.

## 7. SUMMARY AND CONCLUSIONS

A multiyear study was initiated to examine the potential consequences of criticality with respect to long-term repository performance. In these analyses, criticality is postulated to occur during the postclosure period in a hypothetical repository containing DPCs. In the first phase (a scoping phase), the study team developed an approach to creating the modeling tools and techniques that may eventually be required to either exclude criticality from or include criticality in a PA as appropriate; this effort is documented in Price et al. (2019a). In the second phase, the study team implemented this modeling approach and identified future work, as documented in Price et al. (2019b). The next step was a repository-scale PA examining the potential consequences of postclosure steady-state criticality, an effort that included the development of information, modeling tools, and techniques to support such a PA (Price et al. 2021, 2022). In addition, work on building the capability to model transient criticality progressed, though the effort focused on modeling a single canister rather than multiple canisters under anticipated repository conditions. This report represents the continuation of work on modeling postclosure steady-state and transient criticality and documents the expansion of the information, modeling tools, and techniques featured in Price et al. (2021, 2022).

Section 2 describes further developments in modeling steady-state criticality in a DPC disposed of in a hypothetical saturated repository. With respect to modeling the neutronics and the TH processes inside a critical DPC under boiling conditions, it was found that RELAP5-3D does not provide the necessary modeling capabilities for predicting the water level's spatial location and its impact on canister performance given the geometric configuration of this system. A review of the capabilities of a variety of TH codes determined that TRACE provides modeling features more suitable for resolving these phenomena in a critical DPC in which boiling can occur and can provide negative reactivity feedback. Several test problems were run and analyzed, comparing the results from Star-CCM+ and from TRACE. Several discrepancies were noted and will be investigated as a part of verifying whether TRACE is an adequate tool for TH calculations in simulating boiling in a critical DPC. Progress was also made with respect to modeling postclosure criticality in a DPC full of water and surrounded by low-permeability backfill such that water cannot expand and boil on the time scales relevant to a criticality event (i.e., seconds). Temperatures, neutron multiplication factors, and pressures were calculated and will be used in conjunction with a geomechanics model to investigate the hypothesis that the material outside the waste package (i.e., the backfill, the emplacement disturbed zone, and the host rock) could fracture as a result of the pressure build-up in the waste package.

The study team successfully built a repository-scale model of steady-state criticality in a DPC disposed of in a hypothetical saturated repository. This model includes (1) DPCs containing both PWR and BWR SNF, (2) grid spacer degradation (which can lead to permanent criticality termination), (3) the material transform model in both the buffer and the DRZ (which accounts for changes in transport properties in these materials as a result of the heat generated by the criticality event), and (4) varied times of criticality initiation. The model ran successfully for a little more than 500 years simulation time and then failed. This failure will be investigated in the future. Future work includes extending the material transport model into the host rock, including transport of  $^{79}\text{Se}$  for dose calculations, and examining ways to reduce temperatures in the repository.

Section 3 presents results from modeling steady-state criticality in a hypothetical unsaturated repository. The results indicate that the decay heat in a DPC evaporates water entering the waste package such that, for a 10 mm/yr infiltration rate and the assumed repository design, the maximum saturation level (an indication of the water level inside the DPC) is about 0.43. Previous analyses indicated that a saturation

level of at least 0.5 was necessary for criticality to occur. Although further analyses are required, based on these results it may be possible to provide a technical basis for excluding steady-state criticality in an unsaturated repository from a PA on the basis of low probability. In case such an exclusion is not possible or the decision is made not to pursue excluding steady-state criticality in an unsaturated repository on the basis of low probability, the study team also worked toward understanding the cyclical nature of this type of criticality. These results indicate that, should postclosure criticality occur in an unsaturated repository, its consequences would be minimal because of the limited power that can be generated and because of the limited increase in temperature. Limited power means limited increase in radionuclide inventory, particularly  $^{129}\text{I}$ , and limited temperature rise means limited effects on engineered and natural barriers in the vicinity of the waste package. This topic will be investigated further.

Section 4 describes an effort to bound reactivity insertion magnitude and rates for transient criticality events. One approach to bounding reactivity insertion magnitude and rates is to analyze the FEPs involved in various what-if scenarios. A study by Salazar et al. (2022) points to the falling of absorber material through a DPC as a scenario warranting further investigation. The falling of absorber material likely represents the fastest rate of insertion that could be achieved, but even that possibility is limited by Newtonian kinetics. An MCNP model was used to consider a highly stylized, albeit unrealistic, scenario involving a 37-PWR DPC with the as-loaded configuration of SNF from the Zion commercial nuclear power station. Two full-length absorber plates in the central basket location were allowed to fall unobstructed to the bottom of the canister. While more work to refine the analysis is planned for the future, the preliminary results indicate that a reactivity insertion of around \$3 would require on the order of tenths of seconds to progress. It should also be noted that these results are at thermally static conditions without reactivity feedback, and a more complete analysis would yield a lower reactivity increase. The primary insight provided by this type of analysis is that appreciable reactivity magnitudes require increasingly longer time scales.

Section 5 presents results from modeling transient criticality in a saturated repository. These studies provide a basis for simplifying transient criticality calculations by assuming an initial enrichment of 3 wt%  $^{235}\text{U}$ , rather than using the as-loaded fuel information. Other simplifications include assuming local reactivity insertion with partial-length control rods to represent or bound variations in DPC loading, fuel designs, initial enrichments, burnup, axial burnup profiles, time of criticality transient during disposal, and location of reactivity insertion. This preliminary finding will need further evaluation by modeling additional transient conditions in various as-loaded DPCs. The initial study performed for local reactivity insertion in a simplified DPC comparing regular-length control rods to partial-length control rods showed that the results of the partial-length control rod cases consistently bound those with full-length control rods. The investigation of reactivity insertion location (local versus global) indicates a relatively small dependence on reactivity and parameters of interest (e.g., peak power, total energy generation, maximum fuel temperature) with local reactivity insertions being more limiting. The results from the set of calculations for both local and global reactivity insertion with varied reactivity insertion times indicate that the primary variable impacting the peak reactivity of the system is the insertion time. The preliminary results for transients initiating in warmer DPCs (e.g., ones with an ongoing steady-state criticality) versus cooler DPCs indicate that the peak system reactivity for the cooler DPCs as well as the maximum fuel temperature and total energy generation are greater than the parameter values for the warmer DPCs with a shorter transient time.

Section 6 discusses the investigation into transient criticality in an unsaturated repository as well as the magnitude of reactivity and reactivity insertion rates that might be reasonable under anticipated repository conditions. It was determined that RAZORBACK, a code used previously to model transient

criticality in an unsaturated repository, could not capture some of the processes important to modeling transient criticality. In particular, it was found that the heat transfer rates associated with a supercritical DPC in an unsaturated environment are simply beyond the design basis of the RAZORBACK code. Therefore, a search for a new code was initiated resulting in the identification of two codes warranting further study, i.e., TRACE and GOTHIC™.

This page is intentionally left blank.

## 8. REFERENCES

10 CFR 63. *Disposal of High-Level Radioactive Wastes in a Geologic Repository at Yucca Mountain, Nevada.*

10 CFR 71. *Packaging and Transportation of Radioactive Material.*

10 CFR 72. *Licensing Requirements for the Independent Storage of Spent Nuclear Fuel, High-level Radioactive Waste, and Reactor-related Greater than Class C Waste.*

2017-000045. U.S. Department of Energy, Office of Spent Fuel and Waste Science and Technology. 40 CFR 197. *Public Health and Environmental Radiation Protection Standards for Yucca Mountain, Nevada.*

73 FR 61256. *Public Health and Environmental Radiation Protection Standards for Yucca Mountain, Nevada.*

Alsaed, A.A. and L.L. Price. 2020. *Features, Events, and Processes Relevant to DPC Criticality Analysis.* SAND2020-9165. Albuquerque, NM: Sandia National Laboratories.

Ayachit, U. 2015. *The ParaView Guide: A Parallel Visualization Application.* ISBN 978-1930934306. Clifton Park, NY: Kitware, Inc.

Benavides, J., G. Jimenez, S. Lopez, M. Galban, and M. Lloret. 2020. Modeling and results of the dry cask simulator (DCS) with STAR-CCM+. *Nuclear Engineering and Design* 369:110820. doi: <https://doi.org/10.1016/j.nucengdes.2020.110820>.

Clarity, J.B., K. Banerjee, H.K. Liljenfeldt, and W.J. Marshall. 2017. As-Loaded Criticality Margin Assessment of Dual-Purpose Canisters Using UNF-ST&DARDS. *Nuclear Technology* 199:245–275. <https://doi.org/10.1080/00295450.2017.1361250>.

Cooper, J.R. and R.B. Dooley. 2007. *Revised Release on the IAPWS Industrial Formulation 1997 for the Thermodynamic Properties of Water and Steam.* IAPWS R7-97(2012). Lucerne, Switzerland: International Association for the Properties of Water and Steam. <http://www.iapws.org/relguide/IF97-Rev.pdf>.

DOE. 2008a. *Yucca Mountain Repository License Application.* DOE/RW-0573, Rev. 0. Las Vegas, NV: US Department of Energy, Office of Civilian Radioactive Waste Management.

DOE. 2008b. *Yucca Mountain Repository License Application.* DOE/RW-0573, Rev. 1. Las Vegas, NV: US Department of Energy, Office of Civilian Radioactive Waste Management.

E. Kalinina, T. Hadgu, A. Ilgen, C. Bryan, J. Carter, T. Severynse and F. Perry 2017a. *Summary of Grandi, G.M., K.S. Smith, J.D. Rhodes, III. 2011. SIMULATE-3K Models and Methodology.* SSP9813r7. Studsvik Scandpower, Inc. (proprietary document).

Hammond, G.E., P.C. Lichtner, and R.T. Mills. 2014. Evaluating the performance of parallel subsurface simulators: An illustrative example with PFLOTRAN. *Water Resources Research* 50:208–228. doi: 10.1002/2012WR013483.

Hardin, E., L. Price, E. Kalinina, T. Hadgu, A. Ilgen, C. Bryan, J. Scaglione, K. Banerjee, J. Clarity, R. Jubin, V. Sobes, R. Howard, J. Carter, T. Severynse, and F. Perry. 2015. *Summary of Investigations on Technical Feasibility of Direct Disposal of Dual-Purpose Canisters*. FCRD-UFD-2015-000129, Rev. 0; SAND2015-8712R. Albuquerque, NM: Sandia National Laboratories. doi: 10.2172/1504860.

Jones, K., B. Dunsford, J. Rothe, and D. Ulshafer. 2021. *TRACE Plug-in Users Manual: Symbolic Nuclear Analysis Package (SNAP)*. Version 4.3.0. Bloomsburg, PA: Applied Programming Technology, Inc.

LaForce, T., E. Basurto, K.W. Chang, R. Jayne, R. Leone, M. Nole, F.V. Perry, and E. Stein. 2021. *GDSA Repository Systems Analysis Investigations in FY2021*. M2SF-20SN010304062. Albuquerque, NM: Sandia National Laboratories.

Liljenfeldt, H., K. Banerjee, J. Clarity, J. Scaglione, R. Jubin, V. Sobes, R. Howard, E. Hardin, L. Price, Mariner, P.E., E.R. Stein, J.M. Frederick, S.D. Sevougian, and G.E. Hammond. 2017. *Advances in Geologic Disposal System Modeling and Shale Reference Case*. SFWD-SFWST-2017-000044; SAND2017-10304R. Albuquerque, NM: Sandia National Laboratories.

Mariner, P.E., E.R. Stein, J.M. Frederick, S.D. Sevougian, and G.E. Hammond. 2017. *Advances in Geologic Disposal System Modeling and Shale Reference Case*. SFWD-SFWST-2017-000044; SAND2017-10304R. Albuquerque, NM: Sandia National Laboratories.

Mariner, P.E., E.R. Stein, S.D. Sevougian, L.J. Cunningham, J.M. Frederick, G.E. Hammond, T.S. Lowry, S. Jordan, and E. Basurto. 2018. *Advances in Geologic Disposal Safety Assessment and an Unsaturated Alluvium Reference Case*. SFWD-SFWST-2018-000509; SAND2018-11858R. Albuquerque, NM: Sandia National Laboratories.

Nole, M., G.D. Beskardes, D. Fukuyama, R.C. Leone, H.D. Park, M. Paul, A. Salazar, G.E. Hammond, P.C. Lichtner. 2023. *Recent Advancements in PFLOTRAN Development for the GDSA Framework*. M3SF-23SN010304101; SAND2023-07655. Albuquerque, NM: Sandia National Laboratories.

Nuclear Waste Policy Act of 1982. 42 U.S.C. 10101 et seq.

Pandya, T.M., S.R. Johnson, T.M. Evans, G.G. Davidson, S.P. Hamilton, and A.T. Godfrey. 2016. Implementation, capabilities, and benchmarking of Shift, a massively parallel Monte Carlo radiation transport code. *Journal of Computational Physics* 308:239–272. <https://doi.org/10.1016/j.jcp.2015.12.037>.

Price, L., A.A. Alsaed, P. Jones, C. Sanders, and J. Prouty. 2023. *Analysis of Transient Postclosure Criticality*. SAND2023-10092R. Albuquerque, NM: Sandia National Laboratories.

Price, L.L., A. Salazar, E. Basurto, A.A. Alsaed, J. Cardoni, M. Nole, J. Prouty, C. Sanders, G. Davidson, M. Swinney, S. Bhatt, E. Gonzalez, B. Kiedrowski. 2021. *Repository-Scale Performance Assessment Incorporating Postclosure Criticality*. SAND2022-7932 R. Albuquerque, NM: Sandia National Laboratories.

Price, L.L., A.A. Alsaed, A. Barela, P.V. Brady, F. Gelbard, M.B. Gross, M. Nole, J.L. Prouty, K. Banerjee, S. Bhatt, G.G. Davidson, Z. Fang, R. Howard, S.R. Johnson, S.L. Painter, M. Swinney, E. Gonzalez. 2019b. *Preliminary Analysis of Postclosure DPC Criticality Consequences*. M2SF-20SN010305061; SAND2020-4106. Albuquerque, NM: Sandia National Laboratories.

- Price, L.L., A.A. Alsaed, A.C. Barela, E. Basurto, J.L. Prouty, A. Salazar, C. Sanders, A. Taconi, M. Swinney, G. Davidson, N. Kucinski, N. Panicker, E. Gonzalez, and B. Kiedrowski. 2022. *Effects of Postclosure Criticality on Repository Performance*. SAND2022-10297 R. Albuquerque, NM: Sandia National Laboratories.
- Price, L.L., A.A. Alsaed, P.V. Brady, M.B. Gross, E.L. Hardin, M. Nole, J.L. Prouty, K. Banerjee, and G.G. Davidson. 2019a. *Postclosure Criticality Consequence Analysis – Scoping Phase*. M3SF-19SN010305061; SAND2019-4644R. Albuquerque, NM: Sandia National Laboratories.
- Pruess, K. 2004. The TOUGH Codes—A Family of Simulation Tools for Multiphase Flow and Transport Processes in Permeable Media. *Vadose Zone Journal* 3 (3):738–746. doi: <https://doi.org/10.2113/3.3.738>.
- Salazar, A., III, C. Sanders, A.A. Alsaed, and J. Prouty. 2022. *Transient Criticality Model Development*. M4SF-22SN010305123; SAND2022-13081 R. Albuquerque, NM: Sandia National Laboratories.
- Sevougian, S.D., E.R. Stein, T. LaForce, F.V. Perry, M. Nole, and K.W. Chang. 2019a. *GDSA Repository Systems Analysis FY19 Update*. M3SF-19SN010304052; SAND2019-1194R. Albuquerque, NM: Sandia National Laboratories.
- Sevougian, S.D., E.R. Stein, T. LaForce, F.V. Perry, T.S. Lowry, L. Cunningham, M. Nole, C.B. Haukwa, K.W. Chang, and P.E. Mariner. 2019b. *GDSA Repository Systems Analysis Progress Report*. M2SF-19SN010304051; SAND2019-5189R. Albuquerque, NM: Sandia National Laboratories.
- Skroch, M., S.J. Owen, M.L. Staten, R.W. Quadros, B. Hanks, B. Clark, T. Hensley, C. Ernst, R. Morris, C. McBride, C. Stimpson, J. Perry, M. Richardson, and K. Merkley. 2021. *CUBIT geometry and mesh generation toolkit 15.9 user documentation*. SAND2021-12663 W. Albuquerque, NM: Sandia National Laboratories.
- Swinney, M., S. Bhatt, N. Panicker, G. Davidson, N. Kucinski, M. Nole, K. Banerjee, E. Gonzalez, and B. Kiedrowski. 2021. *Steady-State and Time-Dependent Coupled Simulations of a Critical Dual-Purpose Canister in a Saturated Repository*. ORNL/SPR-2021/229. Oak Ridge, TN: Oak Ridge National Laboratory.
- Swinney, M.W., N. Panicker, G. Davidson, N. Kucinski, and A.J. Wysocki. 2022. *Development of Coupled Simulations for Critical Dual-Purpose Canisters in a Saturated Repository*. ORNL/SPR-2022/2624. Oak Ridge, TN: Oak Ridge National Laboratory.
- Talley, D.G. 2017a. *RAZORBACK – A Research Reactor Transient Analysis Code v. 1.0 vol. 1: User’s Manual*. SAND2017-10561. Albuquerque, NM: Sandia National Laboratories.
- Talley, D.G. 2017b. *RAZORBACK – A Research Reactor Transient Analysis Code v. 1.0 vol. 3: Verification and Validation Report*. SAND2017-3372. Albuquerque, NM: Sandia National Laboratories.
- Talley, D.G., 2018. *RAZORBACK – A Research Reactor Transient Analysis Code, Version 1.0 – Volume 2: Software Design and Development Report*. SAND2018-4507. Albuquerque, NM: Sandia National Laboratories.
- The RELAP5-3D Code Development Team. 2018. *RELAP5-3D Code Manual Volume I: Code Structure, System Models, and Solution Methods*. INL/MIS-15-36723, Revision 4.4. Idaho Falls, ID: Idaho National Laboratory.

Weast, R.C., and M.J. Astle. 1979. *CRC Handbook of Chemistry and Physics*. Boca Raton, FL: CRC Press.

YMP (Yucca Mountain Project). 2003. *Disposal Criticality Analysis Methodology Topical Report*. YMP/TR-004Q, Rev. 2. Las Vegas, NV: Yucca Mountain Site Characterization Office.

## **APPENDIX A**

### **PFLOTRAN Input Deck Files for Shale Half-Symmetry Steady-State Criticality with both BWR and PWR Waste Packages**

This page is intentionally left blank.

## A-1. PFLOTRAN Input File

```
# BWR and PWR half-symmetry shale model
# 8 criticality start times
# 3 constant powers
# 89-BWR decay heat
# 32-PWR decay heat
# Grid Spacer Degredation Model
# Smectite-to-illite transition MATERIAL_TRANSFORM_GENERAL
# WASTE_FORM
# CRITICALITY_MECH
# MECHANISM_CUSTOM
# CANISTER_DEGREDATION_MODEL
#===== flow mode =====

SIMULATION
SIMULATION_TYPE SUBSURFACE
PROCESS_MODELS
  SUBSURFACE_FLOW flow
  MODE GENERAL
  OPTIONS
  /
  /
  SUBSURFACE_TRANSPORT transport
  MODE GIRT
  /
  MATERIAL_TRANSFORM smectite_illite
  /
  UFD_DECAY ufd_decay
  /
  WASTE_FORM wf_general
  TYPE GENERAL
  /
  UFD_BIOSPHERE bio
  /
  /
CHECKPOINT
  TIMES y 499. 999. 4999. 9999. 19999. 49999. 99999. 499999.
  FORMAT HDF5
  /
END

SUBSURFACE

#===== EOS =====

EOS WATER
  DENSITY IF97
  ENTHALPY IF97
  STEAM_DENSITY IF97
  STEAM_ENTHALPY IF97
  SATURATION_PRESSURE IF97
  /
```

```

===== numerical methods =====
NUMERICAL_METHODS FLOW

  TIMESTEPPER
    TS_ACCELERATION 9
    DT_FACTOR 2.d0 1.5d0 1.25d0 1.d0 1.d0 0.8d0 0.6d0 0.4d0 0.33d0
  /

  NEWTON_SOLVER
    USE_INFINITY_NORM_CONVERGENCE
    PRESSURE_CHANGE_LIMIT 5.d6
  /

  LINEAR_SOLVER
    MAXIMUM_NUMBER_OF_ITERATIONS 1000
    PRECONDITIONER CPR
    SOLVER FGMRES
  /
END

NUMERICAL_METHODS TRANSPORT

  NEWTON_SOLVER
    RTOL 1.d-08
    ATOL 1.d-12
    MINIMUM_NEWTON_ITERATIONS 3
  /

END

===== datasets =====
#these are used for initial and boundary conditions
DATASET 1d_temperature
  FILENAME reggrad0013_clay4pwr.h5
  HDF5_DATASET_NAME hydrostatic_boundary_T
/
DATASET 1d_pressure
  FILENAME reggrad0013_clay4pwr.h5
  HDF5_DATASET_NAME hydrostatic_boundary_P
/
===== chemistry =====
CHEMISTRY
  PRIMARY_SPECIES
    Am241
    Am242
    Pu238
    Pu240
    Np237
    U233
    Th229
    I129
    Cs137
    Sr90
  /
  MINERALS
    Am241(s)
    Am242(s)
    Pu238(s)
    Pu240(s)
    Np237(s)
    U233(s)
    Th229(s)
    I129(s)
    Cs137(s)
    Sr90(s)
  /
  MINERAL_KINETICS
    Am241(s)
    RATE_CONSTANT 0.0d0
  /

```

```
Am242(s)
  RATE_CONSTANT 0.0d0
/
Pu238(s)
  RATE_CONSTANT 0.0d0
/
Pu240(s)
  RATE_CONSTANT 0.0d0
/
Np237(s)
  RATE_CONSTANT 0.0d0
/
U233(s)
  RATE_CONSTANT 0.0d0
/
Th229(s)
  RATE_CONSTANT 0.0d0
/
I129(s)
  RATE_CONSTANT 0.d0
/
Cs137(s)
  RATE_CONSTANT 0.d0
/
Sr90(s)
  RATE_CONSTANT 0.d0
/
/

TRUNCATE_CONCENTRATION 1.d-20
DATABASE ufd-decay.dat

OUTPUT
  TOTAL
  TOTAL_SORBED
  all
/

END
#===== discretization =====
GRID
  TYPE unstructured clay12pwr_grid1a_usg.h5
END
#===== times =====
TIME
  FINAL_TIME 1.d6 y
  INITIAL_Timestep_SIZE 1.d-6 y
  MAXIMUM_Timestep_SIZE 1. y at 1. y
  MAXIMUM_Timestep_SIZE 5. y at 10. y
  MAXIMUM_Timestep_SIZE 50. y at 100. y
  MAXIMUM_Timestep_SIZE 10. y at 450. y
  MAXIMUM_Timestep_SIZE 5. y at 470. y
  MAXIMUM_Timestep_SIZE 1. y at 495. y

  MAXIMUM_Timestep_SIZE 1.d-2 y at 499. y
  MAXIMUM_Timestep_SIZE 1. y at 499.01 y
  MAXIMUM_Timestep_SIZE 1.d-3 y at 500. y
  MAXIMUM_Timestep_SIZE 1. y at 500.001 y

  MAXIMUM_Timestep_SIZE 5. y at 510. y
  MAXIMUM_Timestep_SIZE 10. y at 530. y
  MAXIMUM_Timestep_SIZE 50. y at 700. y
  MAXIMUM_Timestep_SIZE 100. y at 800. y

  MAXIMUM_Timestep_SIZE 1.d-2 y at 999. y
  MAXIMUM_Timestep_SIZE 1. y at 999.01 y
  MAXIMUM_Timestep_SIZE 1.d-3 y at 1000. y
  MAXIMUM_Timestep_SIZE 1. y at 1000.001 y

  MAXIMUM_Timestep_SIZE 5. y at 1010. y
  MAXIMUM_Timestep_SIZE 10. y at 1030. y
```

```
MAXIMUM_Timestep_SIZE 50. y at 1700. y
MAXIMUM_Timestep_SIZE 100. y at 1800. y

MAXIMUM_Timestep_SIZE 1.d-2 y at 4999. y
MAXIMUM_Timestep_SIZE 1. y at 4999.01 y
MAXIMUM_Timestep_SIZE 1.d-3 y at 5000. y
MAXIMUM_Timestep_SIZE 1. y at 5000.001 y

MAXIMUM_Timestep_SIZE 5. y at 5010. y
MAXIMUM_Timestep_SIZE 10. y at 5030. y
MAXIMUM_Timestep_SIZE 50. y at 5700. y
MAXIMUM_Timestep_SIZE 100. y at 5800. y

MAXIMUM_Timestep_SIZE 1.d-2 y at 9999. y
MAXIMUM_Timestep_SIZE 1. y at 9999.01 y
MAXIMUM_Timestep_SIZE 1.d-3 y at 10000. y
MAXIMUM_Timestep_SIZE 1. y at 10000.001 y

MAXIMUM_Timestep_SIZE 5. y at 10010. y
MAXIMUM_Timestep_SIZE 10. y at 10030. y
MAXIMUM_Timestep_SIZE 50. y at 10700. y
MAXIMUM_Timestep_SIZE 100. y at 10800. y

MAXIMUM_Timestep_SIZE 1.d-2 y at 19999. y
MAXIMUM_Timestep_SIZE 1. y at 19999.01 y
MAXIMUM_Timestep_SIZE 1.d-3 y at 20000. y
MAXIMUM_Timestep_SIZE 1. y at 20000.001 y

MAXIMUM_Timestep_SIZE 5. y at 20010. y
MAXIMUM_Timestep_SIZE 10. y at 20030. y
MAXIMUM_Timestep_SIZE 50. y at 20700. y
MAXIMUM_Timestep_SIZE 100. y at 20800. y
MAXIMUM_Timestep_SIZE 500. y at 22000. y

MAXIMUM_Timestep_SIZE 1.d-2 y at 49999. y
MAXIMUM_Timestep_SIZE 1. y at 49999.01 y
MAXIMUM_Timestep_SIZE 1.d-3 y at 50000. y
MAXIMUM_Timestep_SIZE 1. y at 50000.001 y

MAXIMUM_Timestep_SIZE 5. y at 50010. y
MAXIMUM_Timestep_SIZE 10. y at 50030. y
MAXIMUM_Timestep_SIZE 50. y at 50100. y
MAXIMUM_Timestep_SIZE 100. y at 51000. y
MAXIMUM_Timestep_SIZE 500. y at 52000. y

MAXIMUM_Timestep_SIZE 1.d-2 y at 99999. y
MAXIMUM_Timestep_SIZE 1. y at 99999.01 y
MAXIMUM_Timestep_SIZE 1.d-3 y at 100000. y
MAXIMUM_Timestep_SIZE 1. y at 100000.001 y

MAXIMUM_Timestep_SIZE 5. y at 100010. y
MAXIMUM_Timestep_SIZE 10. y at 100030. y
MAXIMUM_Timestep_SIZE 100. y at 100100. y
MAXIMUM_Timestep_SIZE 500. y at 101000. y
MAXIMUM_Timestep_SIZE 1000. y at 102000. y

MAXIMUM_Timestep_SIZE 1.d-2 y at 499999. y
MAXIMUM_Timestep_SIZE 1. y at 499999.01 y
MAXIMUM_Timestep_SIZE 1.d-3 y at 500000. y
MAXIMUM_Timestep_SIZE 1. y at 500000.001 y

MAXIMUM_Timestep_SIZE 5. y at 500010. y
MAXIMUM_Timestep_SIZE 10. y at 500030. y
MAXIMUM_Timestep_SIZE 100. y at 500100. y
MAXIMUM_Timestep_SIZE 1000. y at 501000. y
```

END

```
#===== output options =====
OUTPUT
OBSERVATION_FILE
```

```
PERIODIC TIMESTEP 1
/
MASS_BALANCE_FILE
TIMES y 499. 999. 4999. 9999. 19999. 49999. 99999. 499999.
/
SNAPSHOT_FILE
FORMAT HDF5
PERIODIC TIME 0.1 y between 0. y and 1. y
PERIODIC TIME 1. y between 0. y and 10. y
PERIODIC TIME 10. y between 0. y and 100. y
PERIODIC TIME 1. y between 499. y and 510. y # crit event starts
PERIODIC TIME 100. y between 0. y and 1000. y
PERIODIC TIME 1. y between 999. y and 1010. y # crit event starts
PERIODIC TIME 1. y between 4999. y and 5010. y # crit event starts
PERIODIC TIME 1. y between 9999. y and 10010. y # crit event starts
PERIODIC TIME 1. y between 19999. y and 20010. y # crit event starts
PERIODIC TIME 1000. y between 0. y and 30000. y
PERIODIC TIME 1. y between 49999. y and 50010. y # crit event starts
PERIODIC TIME 10000. y between 0. y and 100000. y
PERIODIC TIME 1. y between 99999. y and 100010. y # crit event starts
PERIODIC TIME 1. y between 499999. y and 500010. y # crit event starts
PERIODIC TIME 100000. y between 0. y and 1000000. y
/
VELOCITY_AT_CENTER
VARIABLES
MATERIAL_ID
TEMPERATURE
LIQUID_PRESSURE
PERMEABILITY
LIQUID_SATURATION
GAS_PRESSURE
GAS_SATURATION
/
END
#===== observation points =====
EXTERNAL_FILE obs_points-mod-BWR-PWR.txt
#===== fluid properties =====
FLUID_PROPERTY
PHASE LIQUID
DIFFUSION_COEFFICIENT 1.d-9
END

FLUID_PROPERTY
PHASE GAS
DIFFUSION_COEFFICIENT 2.1d-5
END

#===== material properties =====
##### natural #####
MATERIAL_PROPERTY shale
ID 1
CHARACTERISTIC_CURVES shale
POROSITY 0.20
TORTUOSITY_FUNCTION_OF_POROSITY 1.4
SOIL_COMPRESSIBILITY 1.6d-8
SOIL_COMPRESSIBILITY_FUNCTION LEIJNSE
SOIL_REFERENCE_PRESSURE INITIAL_PRESSURE
ROCK_DENSITY 2700.
THERMAL_CONDUCTIVITY_DRY 0.6d0
THERMAL_CONDUCTIVITY_WET 1.2d0
HEAT_CAPACITY 830.
#MATERIAL_TRANSFORM ilt_bentonite # extending material transform module to shale to ensure
# temperature-related changes to transport properties of
# the backfill and host rock are captured.

PERMEABILITY
PERM_ISO 1.d-19
/
/
```

```

MATERIAL_PROPERTY drz
  ID 8
  CHARACTERISTIC_CURVES shale
  POROSITY 0.20
  TORTUOSITY_FUNCTION_OF_POROSITY 1.4
  SOIL_COMPRESSIBILITY 1.6d-8
  SOIL_COMPRESSIBILITY_FUNCTION LEIJNSE
  SOIL_REFERENCE_PRESSURE INITIAL_PRESSURE
  ROCK_DENSITY 2700.
  THERMAL_CONDUCTIVITY_DRY 0.6d0
  THERMAL_CONDUCTIVITY_WET 1.2d0
  HEAT_CAPACITY 830.
# MATERIAL_TRANSFORM ilt_bentonite # extending material transform module to shale to ensure
#                                     # temperature-related changes to transport properties of
#                                     # the backfill and host rock are captured.

  PERMEABILITY
    PERM_ISO 1.d-18
  /
/

MATERIAL_PROPERTY overburden # top of domain slab
  ID 2
  CHARACTERISTIC_CURVES default
  POROSITY 0.20
  TORTUOSITY_FUNCTION_OF_POROSITY 1.4
  SOIL_COMPRESSIBILITY 1.6d-8
  SOIL_COMPRESSIBILITY_FUNCTION LEIJNSE
  SOIL_REFERENCE_PRESSURE INITIAL_PRESSURE
  ROCK_DENSITY 2700.
  THERMAL_CONDUCTIVITY_DRY 0.9d0
  THERMAL_CONDUCTIVITY_WET 1.7d0
  HEAT_CAPACITY 830.
  PERMEABILITY
    PERM_ISO 1.d-15
  /
/

MATERIAL_PROPERTY overburden_drz
  ID 9
  CHARACTERISTIC_CURVES default
  POROSITY 0.20
  TORTUOSITY_FUNCTION_OF_POROSITY 1.4
  SOIL_COMPRESSIBILITY 1.6d-8
  SOIL_COMPRESSIBILITY_FUNCTION LEIJNSE
  SOIL_REFERENCE_PRESSURE INITIAL_PRESSURE
  ROCK_DENSITY 2700.
  THERMAL_CONDUCTIVITY_DRY 0.9d0
  THERMAL_CONDUCTIVITY_WET 1.7d0
  HEAT_CAPACITY 830.
  PERMEABILITY
    PERM_ISO 1.d-14
  /
/

MATERIAL_PROPERTY siltstone
  ID 3
  CHARACTERISTIC_CURVES shale
  POROSITY 0.20
  TORTUOSITY_FUNCTION_OF_POROSITY 1.4
  SOIL_COMPRESSIBILITY 1.6d-8
  SOIL_COMPRESSIBILITY_FUNCTION LEIJNSE
  SOIL_REFERENCE_PRESSURE INITIAL_PRESSURE
  ROCK_DENSITY 2700.
  THERMAL_CONDUCTIVITY_DRY 0.8d0
  THERMAL_CONDUCTIVITY_WET 1.4d0
  HEAT_CAPACITY 830.
  PERMEABILITY
    PERM_ISO 1.d-17
  /
/

```

```
MATERIAL_PROPERTY silt_drz
  ID 10
  CHARACTERISTIC_CURVES shale
  POROSITY 0.20
  TORTUOSITY_FUNCTION_OF_POROSITY 1.4
  SOIL_COMPRESSIBILITY 1.6d-8
  SOIL_COMPRESSIBILITY_FUNCTION LEIJNSE
  SOIL_REFERENCE_PRESSURE INITIAL_PRESSURE
  ROCK_DENSITY 2700.
  THERMAL_CONDUCTIVITY_DRY 0.8d0
  THERMAL_CONDUCTIVITY_WET 1.4d0
  HEAT_CAPACITY 830.
  PERMEABILITY
    PERM_ISO 1.d-16
  /
/
```

```
MATERIAL_PROPERTY sandstone
  ID 4
  CHARACTERISTIC_CURVES default
  POROSITY 0.20
  TORTUOSITY_FUNCTION_OF_POROSITY 0.333
  SOIL_COMPRESSIBILITY 3.2d-9
  SOIL_COMPRESSIBILITY_FUNCTION LEIJNSE
  SOIL_REFERENCE_PRESSURE INITIAL_PRESSURE
  ROCK_DENSITY 2700.
  THERMAL_CONDUCTIVITY_DRY 1.0d0
  THERMAL_CONDUCTIVITY_WET 3.1d0
  HEAT_CAPACITY 830.
  PERMEABILITY
    PERM_ISO 1.d-13
  /
/
```

```
MATERIAL_PROPERTY sand_drz
  ID 11
  CHARACTERISTIC_CURVES default
  POROSITY 0.20
  TORTUOSITY_FUNCTION_OF_POROSITY 0.333
  SOIL_COMPRESSIBILITY 3.2d-9
  SOIL_COMPRESSIBILITY_FUNCTION LEIJNSE
  SOIL_REFERENCE_PRESSURE INITIAL_PRESSURE
  ROCK_DENSITY 2700.
  THERMAL_CONDUCTIVITY_DRY 1.0d0
  THERMAL_CONDUCTIVITY_WET 3.1d0
  HEAT_CAPACITY 830.
  PERMEABILITY
    PERM_ISO 1.d-12
  /
/
```

```
MATERIAL_PROPERTY limestone
  ID 5
  CHARACTERISTIC_CURVES default
  POROSITY 0.10
  TORTUOSITY_FUNCTION_OF_POROSITY 1.4
  SOIL_COMPRESSIBILITY 3.2d-9
  SOIL_COMPRESSIBILITY_FUNCTION LEIJNSE
  SOIL_REFERENCE_PRESSURE INITIAL_PRESSURE
  ROCK_DENSITY 2700.
  THERMAL_CONDUCTIVITY_DRY
  THERMAL_CONDUCTIVITY_WET 2.6d0
  HEAT_CAPACITY 830.
  PERMEABILITY
    PERM_ISO 1.d-14
  /
/
```

```
MATERIAL_PROPERTY lower_shale
  ID 6
  CHARACTERISTIC_CURVES shale
  POROSITY 0.10
  TORTUOSITY_FUNCTION_OF_POROSITY 1.4
  SOIL_COMPRESSIBILITY 1.6d-8
  SOIL_COMPRESSIBILITY_FUNCTION LEIJNSE
  SOIL_REFERENCE_PRESSURE INITIAL_PRESSURE
  ROCK_DENSITY 2700.
  THERMAL_CONDUCTIVITY_DRY 0.6d0
  THERMAL_CONDUCTIVITY_WET 1.2d0
  HEAT_CAPACITY 830.
  PERMEABILITY
    PERM_ISO 1.d-20
  /
/
```

```
MATERIAL_PROPERTY lower_sand
  ID 7
  CHARACTERISTIC_CURVES default
  POROSITY 0.20
  TORTUOSITY_FUNCTION_OF_POROSITY 0.333
  SOIL_COMPRESSIBILITY_FUNCTION LEIJNSE
  SOIL_REFERENCE_PRESSURE INITIAL_PRESSURE
  ROCK_DENSITY 2700.
  THERMAL_CONDUCTIVITY_DRY 1.d0
  THERMAL_CONDUCTIVITY_WET 3.1d0
  HEAT_CAPACITY 830.
  PERMEABILITY
    PERM_ISO 1.d-13
  /
/
```

##### engineered #####

```
MATERIAL_PROPERTY buffer
  ID 12
  CHARACTERISTIC_CURVES bentonite
  POROSITY 0.35
  TORTUOSITY_FUNCTION_OF_POROSITY 1.4
  SOIL_COMPRESSIBILITY 1.6d-8
  SOIL_COMPRESSIBILITY_FUNCTION LEIJNSE
  SOIL_REFERENCE_PRESSURE INITIAL_PRESSURE
  ROCK_DENSITY 2700.
  THERMAL_CONDUCTIVITY_DRY 0.6d0
  THERMAL_CONDUCTIVITY_WET 1.5d0
  HEAT_CAPACITY 830.
  MATERIAL_TRANSFORM ilt_bentonite
  PERMEABILITY
    PERM_ISO 1.d-20
  /
/
```

```
MATERIAL_PROPERTY wp
  ID 13
  CHARACTERISTIC_CURVES default
  POROSITY 0.50
  TORTUOSITY 1.0
  SOIL_COMPRESSIBILITY_FUNCTION LEIJNSE
  SOIL_COMPRESSIBILITY 0.d0
  SOIL_REFERENCE_PRESSURE INITIAL_PRESSURE
  ROCK_DENSITY 5000.d0
  THERMAL_CONDUCTIVITY_DRY 16.7d0
  THERMAL_CONDUCTIVITY_WET 16.7d0
  HEAT_CAPACITY 466.
  PERMEABILITY
    PERM_ISO 1.d-16
  /
/
```

#===== characteristic curves =====

```
CHARACTERISTIC_CURVES default
  SATURATION_FUNCTION VAN_GENUCHTEN
    LOOP_INVARIANT
    UNSATURATED_EXTENSION ECPC
    ALPHA 1.d-4
    M 0.5
    LIQUID_RESIDUAL_SATURATION 0.1d0
    MAX_CAPILLARY_PRESSURE 1.d7
  /
  PERMEABILITY_FUNCTION MUALEM_VG_LIQ
    PHASE LIQUID
    M 0.5
    LIQUID_RESIDUAL_SATURATION 0.1d0
  /
  PERMEABILITY_FUNCTION MUALEM_VG_GAS
    PHASE GAS
    M 0.5
    LIQUID_RESIDUAL_SATURATION 0.1d0
    GAS_RESIDUAL_SATURATION 0.1d0
  /
END
```

```
CHARACTERISTIC_CURVES bentonite
  SATURATION_FUNCTION VAN_GENUCHTEN
    LOOP_INVARIANT
    UNSATURATED_EXTENSION ECPC
    ALPHA 6.25d-8
    M 0.375
    LIQUID_RESIDUAL_SATURATION 0.1d0
    MAX_CAPILLARY_PRESSURE 1.d8
  /
  PERMEABILITY_FUNCTION MUALEM_VG_LIQ
    PHASE LIQUID
    M 0.375
    LIQUID_RESIDUAL_SATURATION 0.1d0
  /
  PERMEABILITY_FUNCTION MUALEM_VG_GAS
    PHASE GAS
    M 0.375
    LIQUID_RESIDUAL_SATURATION 0.1d0
    GAS_RESIDUAL_SATURATION 0.1d0
  /
END
```

```
CHARACTERISTIC_CURVES shale #and drz
  SATURATION_FUNCTION VAN_GENUCHTEN
    LOOP_INVARIANT
    UNSATURATED_EXTENSION ECPC
    ALPHA 6.67d-7
    M 0.333
    LIQUID_RESIDUAL_SATURATION 0.1d0
    MAX_CAPILLARY_PRESSURE 1.d8
  /
  PERMEABILITY_FUNCTION MUALEM_VG_LIQ
    PHASE LIQUID
    M 0.333
    LIQUID_RESIDUAL_SATURATION 0.1d0
  /
  PERMEABILITY_FUNCTION MUALEM_VG_GAS
    PHASE GAS
    M 0.333
    LIQUID_RESIDUAL_SATURATION 0.1d0
    GAS_RESIDUAL_SATURATION 0.1d0
  /
END
```

```

#===== flow conditions =====
#hydrostatic pressure gradient and geothermal gradient for initial conditions
FLOW_CONDITION initial
  TYPE
    LIQUID_PRESSURE DIRICHLET
    MOLE_FRACTION DIRICHLET
    TEMPERATURE DIRICHLET
  /
  LIQUID_PRESSURE DATASET 1d_pressure
  MOLE_FRACTION 1.d-8
  TEMPERATURE DATASET 1d_temperature
END

FLOW_CONDITION bottom
  TYPE
    LIQUID_PRESSURE DIRICHLET
    MOLE_FRACTION DIRICHLET
    TEMPERATURE DIRICHLET
  /
  LIQUID_PRESSURE DATASET 1d_pressure
  MOLE_FRACTION 1.d-8
  TEMPERATURE DATASET 1d_temperature
END

#Add the heatsource for each waste package
FLOW_CONDITION wp_heatsource_PWR
  TYPE
    RATE SCALED_MASS_RATE VOLUME
  /
  INTERPOLATION LINEAR
  RATE FILE decay_heat_MPC_32_rescaled_110y-Tab-delimited.txt
END

#New heatsource being specified for BWR WPs
FLOW_CONDITION wp_heatsource_BWR
  TYPE
    RATE SCALED_MASS_RATE VOLUME
  /
  INTERPOLATION LINEAR
  RATE FILE decay_heat_MPC_89_rescaled_110y_heatsource.txt
END

#sink for well
FLOW_CONDITION well
  TYPE
    RATE SCALED_VOLUMETRIC_RATE VOLUME
  /
  RATE -500.d0 0.d0 0.d0 gal/day gal/day W
END

#===== transport conditions and constraints =====

TRANSPORT_CONDITION bottom
  TYPE zero_gradient
  CONSTRAINT_LIST
    0.d0 initial
  /
END

TRANSPORT_CONDITION initial
  TYPE dirichlet_zero_gradient
  CONSTRAINT_LIST
    0.d0 initial
  /
END

CONSTRAINT initial
  CONCENTRATIONS
    Am241 1.d-21 T

```

```

Am242  1.d-21  T
Pu238  1.d-21  T
Pu240  1.d-21  T
Np237  1.d-21  T
U233   1.d-21  T
Th229  1.d-21  T
I129   1.d-21  T
Cs137  1.d-21  T
Sr90   1.d-21  T
/
MINERALS
Am241(s) 0.d0  1.d0
Am242(s) 0.d0  1.d0
Pu238(s) 0.d0  1.d0
Pu240(s) 0.d0  1.d0
Np237(s) 0.d0  1.d0
U233(s)  0.d0  1.d0
Th229(s) 0.d0  1.d0
I129(s)  0.d0  1.d0
Cs137(s) 0.d0  1.d0
Sr90(s)  0.d0  1.d0
/
END

#===== regions =====
#Add a region for the well and the ERB1B_well
REGION well_far
COORDINATES
  6765. 570. 1110.
  6780. 585. 1170.
/
END

REGION fake_well
COORDINATES
  1770. 570. 1110.
  1785. 585. 1170.
/
END

#Observation points
EXTERNAL_FILE obs_regions-mod-BWR-PWR.txt

#All regions are defined in:
EXTERNAL_FILE regions.txt

#===== boundary condition couplers =====
BOUNDARY_CONDITION top
FLOW_CONDITION initial
TRANSPORT_CONDITION initial
REGION top
END

BOUNDARY_CONDITION bottom
FLOW_CONDITION bottom
TRANSPORT_CONDITION initial
REGION bottom
END

BOUNDARY_CONDITION west
FLOW_CONDITION initial
TRANSPORT_CONDITION initial
REGION west
END

```

```

BOUNDARY_CONDITION east
  FLOW_CONDITION initial
  TRANSPORT_CONDITION initial
  REGION east
END

##### initial condition couplers #####

INITIAL_CONDITION all
  FLOW_CONDITION initial
  TRANSPORT_CONDITION initial
  REGION all
END

##### source_sink couplers #####
#applying decay heat for BWR and PWR WPs not having a critical event
EXTERNAL_FILE source_sink-BWR-PWR-48crit-corrected.txt

#add sink for REGION well
SOURCE_SINK
  REGION well_far
  FLOW_CONDITION well
  TRANSPORT_CONDITION initial
END

##### strata #####

EXTERNAL_FILE strata.txt

END_SUBSURFACE

WASTE_FORM_GENERAL
  EXTERNAL_FILE wfg_modified-BWR-PWR-csnf-canister-deg.txt

  PRINT_MASS_BALANCE

##### PWR's going through a critical event #####
# need 24 PWR WPs going to critical event that will make up combinations for
# 8 start times (50,1000,5000,10000,20000,50000,100000,500000) and
# 3 constant powers (1,2,4 kW)

#      1kW
# 1      b 499 c 500 cp 1
# obs point 'wp1_PWR'
WASTE_FORM
  REGION wp28_15
  EXPOSURE_FACTOR 1.d0
  VOLUME 1.830d0 m^3
  MECHANISM_NAME csnf
  CANISTER_BREACH_TIME 499. y
  CRITICALITY_MECHANISM_NAME ss_criticality-32-PWR-1
  SPACER_MECHANISM_NAME spc_01
/
CRITICALITY_MECH
  NAME ss_criticality-32-PWR-1
  CRIT_START 500.0 y
  CRIT_END 1.0d6 y
  HEAT_OF_CRITICALITY
    CONSTANT_POWER 1.0 kW
  /
DECAY_HEAT TOTAL
  DATASET decay_heat_MPC_32_rescaled_110y.txt
/
INVENTORY
  EXPANDED_DATASET MPC-32-162_crit_inv_v1.txt
  OPTION
    USE_LOOKUP_AND_IMPLICIT
  /
/
/

```

```
# 2      b 999 c 1000 cp 1
WASTE_FORM
  REGION wp26_20
  EXPOSURE_FACTOR 1.d0
  VOLUME 1.830d0 m^3
  MECHANISM_NAME csnf
  CANISTER_BREACH_TIME 999. y
  CRITICALITY_MECHANISM_NAME ss_criticality-32-PWR-2
  SPACER_MECHANISM_NAME spc_01
/
CRITICALITY_MECH
  NAME ss_criticality-32-PWR-2
  CRIT_START 1000.0 y
  CRIT_END 1.0d6 y
  HEAT_OF_CRITICALITY
    CONSTANT_POWER 1.0 kW
  /
DECAY_HEAT TOTAL
  DATASET decay_heat_MPC_32_rescaled_110y.txt
/
INVENTORY
  EXPANDED_DATASET MPC-32-162_crit_inv_v1.txt
  OPTION
    USE_LOOKUP_AND_IMPLICIT
  /
/
/

#3      b 4999 c 5000 cp 1
WASTE_FORM
  REGION wp39_17
  EXPOSURE_FACTOR 1.d0
  VOLUME 1.830d0 m^3
  MECHANISM_NAME csnf
  CANISTER_BREACH_TIME 4999. y
  CRITICALITY_MECHANISM_NAME ss_criticality-32-PWR-3
  SPACER_MECHANISM_NAME spc_01
/
CRITICALITY_MECH
  NAME ss_criticality-32-PWR-3
  CRIT_START 5000.0 y
  CRIT_END 1.0d6 y
  HEAT_OF_CRITICALITY
    CONSTANT_POWER 1.0 kW
  /
DECAY_HEAT TOTAL
  DATASET decay_heat_MPC_32_rescaled_110y.txt
/
INVENTORY
  EXPANDED_DATASET MPC-32-162_crit_inv_v1.txt
  OPTION
    USE_LOOKUP_AND_IMPLICIT
  /
/
/

#4      b 9,999 c 10,000 cp 1
WASTE_FORM
  REGION wp31_32
  EXPOSURE_FACTOR 1.d0
  VOLUME 1.830d0 m^3
  MECHANISM_NAME csnf
  CANISTER_BREACH_TIME 9999. y
  CRITICALITY_MECHANISM_NAME ss_criticality-32-PWR-4
  SPACER_MECHANISM_NAME spc_01
/
CRITICALITY_MECH
  NAME ss_criticality-32-PWR-4
  CRIT_START 10000.0 y
  CRIT_END 1.0d6 y
  HEAT_OF_CRITICALITY
    CONSTANT_POWER 1.0 kW
  /
DECAY_HEAT TOTAL
  DATASET decay_heat_MPC_32_rescaled_110y.txt
/
INVENTORY
  EXPANDED_DATASET MPC-32-162_crit_inv_v1.txt
  OPTION
    USE_LOOKUP_AND_IMPLICIT
  /
/
/
```

```

#5      b 19,999 c 20,000 cp 1
WASTE_FORM
REGION wp39_33
EXPOSURE_FACTOR 1.d0
VOLUME 1.830d0 m^3
MECHANISM_NAME csnf
CANISTER_BREACH_TIME 19999. y
CRITICALITY_MECHANISM_NAME ss_criticality-32-PWR-5
SPACER_MECHANISM_NAME spc_01
/
CRITICALITY_MECH
NAME ss_criticality-32-PWR-5
CRIT_START 20000.0 y
CRIT_END 1.0d6 y
HEAT_OF_CRITICALITY
  CONSTANT_POWER 1.0 kW
/
DECAY_HEAT TOTAL
  DATASET decay_heat_MPC_32_rescaled_110y.txt
/
INVENTORY
  EXPANDED_DATASET MPC-32-162_crit_inv_v1.txt
  OPTION
    USE_LOOKUP_AND_IMPLICIT
  /
/
/
#6      b 49,999 c 50,000 cp 1
WASTE_FORM
REGION wp33_43
EXPOSURE_FACTOR 1.d0
VOLUME 1.830d0 m^3
MECHANISM_NAME csnf
CANISTER_BREACH_TIME 49999. y
CRITICALITY_MECHANISM_NAME ss_criticality-32-PWR-6
SPACER_MECHANISM_NAME spc_01
/
CRITICALITY_MECH
NAME ss_criticality-32-PWR-6
CRIT_START 50000.0 y
CRIT_END 1.0d6 y
HEAT_OF_CRITICALITY
  CONSTANT_POWER 1.0 kW
/
DECAY_HEAT TOTAL
  DATASET decay_heat_MPC_32_rescaled_110y.txt
/
INVENTORY
  EXPANDED_DATASET MPC-32-162_crit_inv_v1.txt
  OPTION
    USE_LOOKUP_AND_IMPLICIT
  /
/
/
#7      b 99,999 c 100,000 cp 1
WASTE_FORM
REGION wp38_18
EXPOSURE_FACTOR 1.d0
VOLUME 1.830d0 m^3
MECHANISM_NAME csnf
CANISTER_BREACH_TIME 99999. y
CRITICALITY_MECHANISM_NAME ss_criticality-32-PWR-7
SPACER_MECHANISM_NAME spc_01
/
CRITICALITY_MECH
NAME ss_criticality-32-PWR-7
CRIT_START 100000.0 y
CRIT_END 1.0d6 y
HEAT_OF_CRITICALITY
  CONSTANT_POWER 1.0 kW
/
DECAY_HEAT TOTAL
  DATASET decay_heat_MPC_32_rescaled_110y.txt
/
INVENTORY
  EXPANDED_DATASET MPC-32-162_crit_inv_v1.txt
  OPTION
    USE_LOOKUP_AND_IMPLICIT
  /
/
/

```

```
#8      b 499,999 c 500,000 cp 1
WASTE_FORM
  REGION wp26_0
  EXPOSURE_FACTOR 1.d0
  VOLUME 1.830d0 m^3
  MECHANISM_NAME csnf
  CANISTER_BREACH_TIME 499999. y
  CRITICALITY_MECHANISM_NAME ss_criticality-32-PWR-8
  SPACER_MECHANISM_NAME spc_01
/
CRITICALITY_MECH
  NAME ss_criticality-32-PWR-8
  CRIT_START 500000.0 y
  CRIT_END 1.0d6 y
  HEAT_OF_CRITICALITY
    CONSTANT_POWER 1.0 kw
  /
DECAY_HEAT TOTAL
  DATASET decay_heat_MPC_32_rescaled_110y.txt
/
INVENTORY
  EXPANDED_DATASET MPC-32-162_crit_inv_v1.txt
  OPTION
    USE_LOOKUP_AND_IMPLICIT
  /
/
/
#      2 kw
#9      b 499 c 500 cp 2
WASTE_FORM
  REGION wp20_27
  EXPOSURE_FACTOR 1.d0
  VOLUME 1.830d0 m^3
  MECHANISM_NAME csnf
  CANISTER_BREACH_TIME 499. y
  CRITICALITY_MECHANISM_NAME ss_criticality-32-PWR-9
  SPACER_MECHANISM_NAME spc_01
/
CRITICALITY_MECH
  NAME ss_criticality-32-PWR-9
  CRIT_START 500.0 y
  CRIT_END 1.0d6 y
  HEAT_OF_CRITICALITY
    CONSTANT_POWER 2.0 kw
  /
DECAY_HEAT TOTAL
  DATASET decay_heat_MPC_32_rescaled_110y.txt
/
INVENTORY
  EXPANDED_DATASET MPC-32-162_crit_inv_v1.txt
  OPTION
    USE_LOOKUP_AND_IMPLICIT
  /
/
/
#10
WASTE_FORM
  REGION wp37_6
  EXPOSURE_FACTOR 1.d0
  VOLUME 1.830d0 m^3
  MECHANISM_NAME csnf
  CANISTER_BREACH_TIME 999. y
  CRITICALITY_MECHANISM_NAME ss_criticality-32-PWR-10
  SPACER_MECHANISM_NAME spc_01
/
CRITICALITY_MECH
  NAME ss_criticality-32-PWR-10
  CRIT_START 1000.0 y
  CRIT_END 1.0d6 y
  HEAT_OF_CRITICALITY
    CONSTANT_POWER 2.0 kw
  /
DECAY_HEAT TOTAL
  DATASET decay_heat_MPC_32_rescaled_110y.txt
/
INVENTORY
  EXPANDED_DATASET MPC-32-162_crit_inv_v1.txt
  OPTION
    USE_LOOKUP_AND_IMPLICIT
  /
/
/
```

```

#11
WASTE_FORM
  REGION wp32_18
  EXPOSURE_FACTOR 1.d0
  VOLUME 1.830d0 m^3
  MECHANISM_NAME csnf
  CANISTER_BREACH_TIME 4999. y
  CRITICALITY_MECHANISM_NAME ss_criticality-32-PWR-11
  SPACER_MECHANISM_NAME spc_01
/
CRITICALITY_MECH
  NAME ss_criticality-32-PWR-11
  CRIT_START 5000.0 y
  CRIT_END 1.0d6 y
  HEAT_OF_CRITICALITY
    CONSTANT_POWER 2.0 kW
  /
DECAY_HEAT TOTAL
  DATASET decay_heat_MPC_32_rescaled_110y.txt
/
INVENTORY
  EXPANDED_DATASET MPC-32-162_crit_inv_v1.txt
  OPTION
    USE_LOOKUP_AND_IMPLICIT
  /
/
/
#12
WASTE_FORM
  REGION wp19_15
  EXPOSURE_FACTOR 1.d0
  VOLUME 1.830d0 m^3
  MECHANISM_NAME csnf
  CANISTER_BREACH_TIME 9999. y
  CRITICALITY_MECHANISM_NAME ss_criticality-32-PWR-12
  SPACER_MECHANISM_NAME spc_01
/
CRITICALITY_MECH
  NAME ss_criticality-32-PWR-12
  CRIT_START 10000.0 y
  CRIT_END 1.0d6 y
  HEAT_OF_CRITICALITY
    CONSTANT_POWER 2.0 kW
  /
DECAY_HEAT TOTAL
  DATASET decay_heat_MPC_32_rescaled_110y.txt
/
INVENTORY
  EXPANDED_DATASET MPC-32-162_crit_inv_v1.txt
  OPTION
    USE_LOOKUP_AND_IMPLICIT
  /
/
/
#13
WASTE_FORM
  REGION wp27_9
  EXPOSURE_FACTOR 1.d0
  VOLUME 1.830d0 m^3
  MECHANISM_NAME csnf
  CANISTER_BREACH_TIME 19999. y
  CRITICALITY_MECHANISM_NAME ss_criticality-32-PWR-13
  SPACER_MECHANISM_NAME spc_01
/
CRITICALITY_MECH
  NAME ss_criticality-32-PWR-13
  CRIT_START 20000.0 y
  CRIT_END 1.0d6 y
  HEAT_OF_CRITICALITY
    CONSTANT_POWER 2.0 kW
  /
DECAY_HEAT TOTAL
  DATASET decay_heat_MPC_32_rescaled_110y.txt
/
INVENTORY
  EXPANDED_DATASET MPC-32-162_crit_inv_v1.txt
  OPTION
    USE_LOOKUP_AND_IMPLICIT
  /
/
/

```

```
#14
WASTE_FORM
  REGION wp38_30
  EXPOSURE_FACTOR 1.d0
  VOLUME 1.830d0 m^3
  MECHANISM_NAME csnf
  CANISTER_BREACH_TIME 49999. y
  CRITICALITY_MECHANISM_NAME ss_criticality-32-PWR-14
  SPACER_MECHANISM_NAME spc_01
/
CRITICALITY_MECH
  NAME ss_criticality-32-PWR-14
  CRIT_START 50000.0 y
  CRIT_END 1.0d6 y
  HEAT_OF_CRITICALITY
    CONSTANT_POWER 2.0 kW
  /
DECAY_HEAT TOTAL
  DATASET decay_heat_MPC_32_rescaled_110y.txt
/
INVENTORY
  EXPANDED_DATASET MPC-32-162_crit_inv_v1.txt
  OPTION
    USE_LOOKUP_AND_IMPLICIT
  /
/
/

#15
WASTE_FORM
  REGION wp24_48
  EXPOSURE_FACTOR 1.d0
  VOLUME 1.830d0 m^3
  MECHANISM_NAME csnf
  CANISTER_BREACH_TIME 99999. y
  CRITICALITY_MECHANISM_NAME ss_criticality-32-PWR-15
  SPACER_MECHANISM_NAME spc_01
/
CRITICALITY_MECH
  NAME ss_criticality-32-PWR-15
  CRIT_START 100000.0 y
  CRIT_END 1.0d6 y
  HEAT_OF_CRITICALITY
    CONSTANT_POWER 2.0 kW
  /
DECAY_HEAT TOTAL
  DATASET decay_heat_MPC_32_rescaled_110y.txt
/
INVENTORY
  EXPANDED_DATASET MPC-32-162_crit_inv_v1.txt
  OPTION
    USE_LOOKUP_AND_IMPLICIT
  /
/
/

#16
WASTE_FORM
  REGION wp38_40
  EXPOSURE_FACTOR 1.d0
  VOLUME 1.830d0 m^3
  MECHANISM_NAME csnf
  CANISTER_BREACH_TIME 499999. y
  CRITICALITY_MECHANISM_NAME ss_criticality-32-PWR-16
  SPACER_MECHANISM_NAME spc_01
/
CRITICALITY_MECH
  NAME ss_criticality-32-PWR-16
  CRIT_START 500000.0 y
  CRIT_END 1.0d6 y
  HEAT_OF_CRITICALITY
    CONSTANT_POWER 2.0 kW
  /
DECAY_HEAT TOTAL
  DATASET decay_heat_MPC_32_rescaled_110y.txt
/
INVENTORY
  EXPANDED_DATASET MPC-32-162_crit_inv_v1.txt
  OPTION
    USE_LOOKUP_AND_IMPLICIT
  /
/
/
```

```

#           2 kW
#17
WASTE_FORM
  REGION wp36_36
  EXPOSURE_FACTOR 1.d0
  VOLUME 1.830d0 m^3
  MECHANISM_NAME csnf
  CANISTER_BREACH_TIME 499. y
  CRITICALITY_MECHANISM_NAME ss_criticality-32-PWR-17
  SPACER_MECHANISM_NAME spc_01
/
CRITICALITY_MECH
  NAME ss_criticality-32-PWR-17
  CRIT_START 500.0 y
  CRIT_END 1.0d6 y
  HEAT_OF_CRITICALITY
    CONSTANT_POWER 3.0 kW
  /
DECAY_HEAT TOTAL
  DATASET decay_heat_MPC_32_rescaled_110y.txt
/
INVENTORY
  EXPANDED_DATASET MPC-32-162_crit_inv_v1.txt
  OPTION
    USE_LOOKUP_AND_IMPLICIT
  /
/
#18
WASTE_FORM
  REGION wp14_8
  EXPOSURE_FACTOR 1.d0
  VOLUME 1.830d0 m^3
  MECHANISM_NAME csnf
  CANISTER_BREACH_TIME 999. y
  CRITICALITY_MECHANISM_NAME ss_criticality-32-PWR-18
  SPACER_MECHANISM_NAME spc_01
/
CRITICALITY_MECH
  NAME ss_criticality-32-PWR-18
  CRIT_START 1000.0 y
  CRIT_END 1.0d6 y
  HEAT_OF_CRITICALITY
    CONSTANT_POWER 3.0 kW
  /
DECAY_HEAT TOTAL
  DATASET decay_heat_MPC_32_rescaled_110y.txt
/
INVENTORY
  EXPANDED_DATASET MPC-32-162_crit_inv_v1.txt
  OPTION
    USE_LOOKUP_AND_IMPLICIT
  /
/
#19
WASTE_FORM
  REGION wp20_31
  EXPOSURE_FACTOR 1.d0
  VOLUME 1.830d0 m^3
  MECHANISM_NAME csnf
  CANISTER_BREACH_TIME 4999. y
  CRITICALITY_MECHANISM_NAME ss_criticality-32-PWR-19
  SPACER_MECHANISM_NAME spc_01
/
CRITICALITY_MECH
  NAME ss_criticality-32-PWR-19
  CRIT_START 5000.0 y
  CRIT_END 1.0d6 y
  HEAT_OF_CRITICALITY
    CONSTANT_POWER 3.0 kW
  /
DECAY_HEAT TOTAL
  DATASET decay_heat_MPC_32_rescaled_110y.txt
/
INVENTORY
  EXPANDED_DATASET MPC-32-162_crit_inv_v1.txt
  OPTION
    USE_LOOKUP_AND_IMPLICIT
  /
/
/

```

```
#20
WASTE_FORM
  REGION wp40_13
  EXPOSURE_FACTOR 1.d0
  VOLUME 1.830d0 m^3
  MECHANISM_NAME csnf
  CANISTER_BREACH_TIME 9999. y
  CRITICALITY_MECHANISM_NAME ss_criticality-32-PWR-20
  SPACER_MECHANISM_NAME spc_01
/
CRITICALITY_MECH
  NAME ss_criticality-32-PWR-20
  CRIT_START 10000.0 y
  CRIT_END 1.0d6 y
  HEAT_OF_CRITICALITY
    CONSTANT_POWER 3.0 kW
  /
DECAY_HEAT TOTAL
  DATASET decay_heat_MPC_32_rescaled_110y.txt
/
INVENTORY
  EXPANDED_DATASET MPC-32-162_crit_inv_v1.txt
  OPTION
    USE_LOOKUP_AND_IMPLICIT
  /
/
/
#21
WASTE_FORM
  REGION wp35_23
  EXPOSURE_FACTOR 1.d0
  VOLUME 1.830d0 m^3
  MECHANISM_NAME csnf
  CANISTER_BREACH_TIME 19999. y
  CRITICALITY_MECHANISM_NAME ss_criticality-32-PWR-21
  SPACER_MECHANISM_NAME spc_01
/
CRITICALITY_MECH
  NAME ss_criticality-32-PWR-21
  CRIT_START 20000.0 y
  CRIT_END 1.0d6 y
  HEAT_OF_CRITICALITY
    CONSTANT_POWER 3.0 kW
  /
DECAY_HEAT TOTAL
  DATASET decay_heat_MPC_32_rescaled_110y.txt
/
INVENTORY
  EXPANDED_DATASET MPC-32-162_crit_inv_v1.txt
  OPTION
    USE_LOOKUP_AND_IMPLICIT
  /
/
/
#22
WASTE_FORM
  REGION wp23_37
  EXPOSURE_FACTOR 1.d0
  VOLUME 1.830d0 m^3
  MECHANISM_NAME csnf
  CANISTER_BREACH_TIME 49999. y
  CRITICALITY_MECHANISM_NAME ss_criticality-32-PWR-22
  SPACER_MECHANISM_NAME spc_01
/
CRITICALITY_MECH
  NAME ss_criticality-32-PWR-22
  CRIT_START 50000.0 y
  CRIT_END 1.0d6 y
  HEAT_OF_CRITICALITY
    CONSTANT_POWER 3.0 kW
  /
DECAY_HEAT TOTAL
  DATASET decay_heat_MPC_32_rescaled_110y.txt
/
INVENTORY
  EXPANDED_DATASET MPC-32-162_crit_inv_v1.txt
  OPTION
    USE_LOOKUP_AND_IMPLICIT
  /
/
/
```

```
#23
WASTE_FORM
  REGION wp21_47
  EXPOSURE_FACTOR 1.d0
  VOLUME 1.830d0 m^3
  MECHANISM_NAME csnf
  CANISTER_BREACH_TIME 99999. y
  CRITICALITY_MECHANISM_NAME ss_criticality-32-PWR-23
  SPACER_MECHANISM_NAME spc_01
/
CRITICALITY_MECH
  NAME ss_criticality-32-PWR-23
  CRIT_START 100000.0 y
  CRIT_END 1.0d6 y
  HEAT_OF_CRITICALITY
    CONSTANT_POWER 3.0 kW
  /
DECAY_HEAT TOTAL
  DATASET decay_heat_MPC_32_rescaled_110y.txt
/
INVENTORY
  EXPANDED_DATASET MPC-32-162_crit_inv_v1.txt
  OPTION
    USE_LOOKUP_AND_IMPLICIT
  /
/
/
```

```
#24
WASTE_FORM
  REGION wp34_14
  EXPOSURE_FACTOR 1.d0
  VOLUME 1.830d0 m^3
  MECHANISM_NAME csnf
  CANISTER_BREACH_TIME 499999. y
  CRITICALITY_MECHANISM_NAME ss_criticality-32-PWR-24
  SPACER_MECHANISM_NAME spc_01
/
CRITICALITY_MECH
  NAME ss_criticality-32-PWR-24
  CRIT_START 500000.0 y
  CRIT_END 1.0d6 y
  HEAT_OF_CRITICALITY
    CONSTANT_POWER 3.0 kW
  /
DECAY_HEAT TOTAL
  DATASET decay_heat_MPC_32_rescaled_110y.txt
/
INVENTORY
  EXPANDED_DATASET MPC-32-162_crit_inv_v1.txt
  OPTION
    USE_LOOKUP_AND_IMPLICIT
  /
/
/
```

```
##### BWR's going through a critical event #####
# need 24 BWR WPs going to critical event that will make up combinations for
# 8 start times (50,1000,5000,10000,20000,50000,100000,500000) and
# 3 constant powers (1,2,4 kW)
```

```
# 1      b 499 c 500 cp 1
# obs point 'wp1_BWR'
WASTE_FORM
  REGION wp12_24
  EXPOSURE_FACTOR 1.d0
  VOLUME 2.10d0 m^3
  MECHANISM_NAME csnf
  CANISTER_BREACH_TIME 499. y
  CRITICALITY_MECHANISM_NAME 1-ss_criticality-89-BWR
  SPACER_MECHANISM_NAME spc_01
/
CRITICALITY_MECH
  NAME 1-ss_criticality-89-BWR
  CRIT_START 500.0 y
  CRIT_END 1.0d6 y
  HEAT_OF_CRITICALITY
    CONSTANT_POWER 1.0 kW
  /
/
```

```

    DECAY_HEAT TOTAL
      DATASET decay_heat_MPC_89_rescaled_110y.txt
    /
    INVENTORY
      EXPANDED_DATASET MPC-89-W047_crit_inv.txt
      OPTION
        USE_LOOKUP_AND_IMPLICIT
    /
  /
#2
WASTE_FORM
  REGION wp7_36
  EXPOSURE_FACTOR 1.d0
  VOLUME 2.10d0 m^3
  MECHANISM_NAME csnf
  CANISTER_BREACH_TIME 999. y
  CRITICALITY_MECHANISM_NAME 2-ss_criticality-89-BWR
  SPACER_MECHANISM_NAME spc_01
/
CRITICALITY_MECH
  NAME 2-ss_criticality-89-BWR
  CRIT_START 1000.0 y
  CRIT_END 1.0d6 y
  HEAT_OF_CRITICALITY
    CONSTANT_POWER 1.0 kW
  /
  DECAY_HEAT TOTAL
    DATASET decay_heat_MPC_89_rescaled_110y.txt
  /
  INVENTORY
    EXPANDED_DATASET MPC-89-W047_crit_inv.txt
    OPTION
      USE_LOOKUP_AND_IMPLICIT
  /
/
#3
WASTE_FORM
  REGION wp10_27
  EXPOSURE_FACTOR 1.d0
  VOLUME 2.10d0 m^3
  MECHANISM_NAME csnf
  CANISTER_BREACH_TIME 4999. y
  CRITICALITY_MECHANISM_NAME 3-ss_criticality-89-BWR
  SPACER_MECHANISM_NAME spc_01
/
CRITICALITY_MECH
  NAME 3-ss_criticality-89-BWR
  CRIT_START 5000.0 y
  CRIT_END 1.0d6 y
  HEAT_OF_CRITICALITY
    CONSTANT_POWER 1.0 kW
  /
  DECAY_HEAT TOTAL
    DATASET decay_heat_MPC_89_rescaled_110y.txt
  /
  INVENTORY
    EXPANDED_DATASET MPC-89-W047_crit_inv.txt
    OPTION
      USE_LOOKUP_AND_IMPLICIT
  /
/
/

```

```

#4
WASTE_FORM
  REGION wp5_25
  EXPOSURE_FACTOR 1.d0
  VOLUME 2.10d0 m^3
  MECHANISM_NAME csnf
  CANISTER_BREACH_TIME 9999. y
  CRITICALITY_MECHANISM_NAME 4-ss_criticality-89-BWR
  SPACER_MECHANISM_NAME spc_01
/
CRITICALITY_MECH
  NAME 4-ss_criticality-89-BWR
  CRIT_START 10000.0 y
  CRIT_END 1.0d6 y
  HEAT_OF_CRITICALITY
    CONSTANT_POWER 1.0 kW
  /
DECAY_HEAT TOTAL
  DATASET decay_heat_MPC_89_rescaled_110y.txt
/
INVENTORY
  EXPANDED_DATASET MPC-89-W047_crit_inv.txt
  OPTION
    USE_LOOKUP_AND_IMPLICIT
  /
/
/
#5
WASTE_FORM
  REGION wp3_12
  EXPOSURE_FACTOR 1.d0
  VOLUME 2.10d0 m^3
  MECHANISM_NAME csnf
  CANISTER_BREACH_TIME 19999. y
  CRITICALITY_MECHANISM_NAME 5-ss_criticality-89-BWR
  SPACER_MECHANISM_NAME spc_01
/
CRITICALITY_MECH
  NAME 5-ss_criticality-89-BWR
  CRIT_START 20000.0 y
  CRIT_END 1.0d6 y
  HEAT_OF_CRITICALITY
    CONSTANT_POWER 1.0 kW
  /
DECAY_HEAT TOTAL
  DATASET decay_heat_MPC_89_rescaled_110y.txt
/
INVENTORY
  EXPANDED_DATASET MPC-89-W047_crit_inv.txt
  OPTION
    USE_LOOKUP_AND_IMPLICIT
  /
/
/
#6
WASTE_FORM
  REGION wp12_47
  EXPOSURE_FACTOR 1.d0
  VOLUME 2.10d0 m^3
  MECHANISM_NAME csnf
  CANISTER_BREACH_TIME 49999. y
  CRITICALITY_MECHANISM_NAME 6-ss_criticality-89-BWR
  SPACER_MECHANISM_NAME spc_01
/
CRITICALITY_MECH
  NAME 6-ss_criticality-89-BWR
  CRIT_START 50000.0 y
  CRIT_END 1.0d6 y
  HEAT_OF_CRITICALITY
    CONSTANT_POWER 1.0 kW
  /
DECAY_HEAT TOTAL
  DATASET decay_heat_MPC_89_rescaled_110y.txt
/
INVENTORY
  EXPANDED_DATASET MPC-89-W047_crit_inv.txt
  OPTION
    USE_LOOKUP_AND_IMPLICIT
  /
/
/

```

```
#7
WASTE_FORM
  REGION wp10_37
  EXPOSURE_FACTOR 1.d0
  VOLUME 2.10d0 m^3
  MECHANISM_NAME csnf
  CANISTER_BREACH_TIME 99999. y
  CRITICALITY_MECHANISM_NAME 7-ss_criticality-89-BWR
  SPACER_MECHANISM_NAME spc_01
/
CRITICALITY_MECH
  NAME 7-ss_criticality-89-BWR
  CRIT_START 100000.0 y
  CRIT_END 1.0d6 y
  HEAT_OF_CRITICALITY
    CONSTANT_POWER 1.0 kw
  /
DECAY_HEAT TOTAL
  DATASET decay_heat_MPC_89_rescaled_110y.txt
/
INVENTORY
  EXPANDED_DATASET MPC-89-W047_crit_inv.txt
  OPTION
    USE_LOOKUP_AND_IMPLICIT
  /
/
/
#8
WASTE_FORM
  REGION wp8_16
  EXPOSURE_FACTOR 1.d0
  VOLUME 2.10d0 m^3
  MECHANISM_NAME csnf
  CANISTER_BREACH_TIME 499999. y
  CRITICALITY_MECHANISM_NAME 8-ss_criticality-89-BWR
  SPACER_MECHANISM_NAME spc_01
/
CRITICALITY_MECH
  NAME 8-ss_criticality-89-BWR
  CRIT_START 500000.0 y
  CRIT_END 1.0d6 y
  HEAT_OF_CRITICALITY
    CONSTANT_POWER 1.0 kw
  /
DECAY_HEAT TOTAL
  DATASET decay_heat_MPC_89_rescaled_110y.txt
/
INVENTORY
  EXPANDED_DATASET MPC-89-W047_crit_inv.txt
  OPTION
    USE_LOOKUP_AND_IMPLICIT
  /
/
/
#
  2kw
#9
WASTE_FORM
  REGION wp1_34
  EXPOSURE_FACTOR 1.d0
  VOLUME 2.10d0 m^3
  MECHANISM_NAME csnf
  CANISTER_BREACH_TIME 499. y
  CRITICALITY_MECHANISM_NAME 9-ss_criticality-89-BWR
  SPACER_MECHANISM_NAME spc_01
/
CRITICALITY_MECH
  NAME 9-ss_criticality-89-BWR
  CRIT_START 500.0 y
  CRIT_END 1.0d6 y
  HEAT_OF_CRITICALITY
    CONSTANT_POWER 2.0 kw
  /
DECAY_HEAT TOTAL
  DATASET decay_heat_MPC_89_rescaled_110y.txt
/
INVENTORY
  EXPANDED_DATASET MPC-89-W047_crit_inv.txt
  OPTION
    USE_LOOKUP_AND_IMPLICIT
  /
/
/
```

```

WASTE_FORM
  REGION wp4_18
  EXPOSURE_FACTOR 1.d0
  VOLUME 2.10d0 m^3
  MECHANISM_NAME csnf
  CANISTER_BREACH_TIME 999. y
  CRITICALITY_MECHANISM_NAME 10-ss_criticality-89-BWR
  SPACER_MECHANISM_NAME spc_01
/
CRITICALITY_MECH
  NAME 10-ss_criticality-89-BWR
  CRIT_START 1000.0 y
  CRIT_END 1.0d6 y
  HEAT_OF_CRITICALITY
    CONSTANT_POWER 2.0 kW
  /
  DECAy_HEAT TOTAL
    DATASET decay_heat_MPC_89_rescaled_110y.txt
  /
  INVENTORY
    EXPANDED_DATASET MPC-89-W047_crit_inv.txt
    OPTION
      USE_LOOKUP_AND_IMPLICIT
  /
/
WASTE_FORM
  REGION wp13_22
  EXPOSURE_FACTOR 1.d0
  VOLUME 2.10d0 m^3
  MECHANISM_NAME csnf
  CANISTER_BREACH_TIME 4999. y
  CRITICALITY_MECHANISM_NAME 11-ss_criticality-89-BWR
  SPACER_MECHANISM_NAME spc_01
/
CRITICALITY_MECH
  NAME 11-ss_criticality-89-BWR
  CRIT_START 5000.0 y
  CRIT_END 1.0d6 y
  HEAT_OF_CRITICALITY
    CONSTANT_POWER 2.0 kW
  /
  DECAy_HEAT TOTAL
    DATASET decay_heat_MPC_89_rescaled_110y.txt
  /
  INVENTORY
    EXPANDED_DATASET MPC-89-W047_crit_inv.txt
    OPTION
      USE_LOOKUP_AND_IMPLICIT
  /
/
WASTE_FORM
  REGION wp5_49
  EXPOSURE_FACTOR 1.d0
  VOLUME 2.10d0 m^3
  MECHANISM_NAME csnf
  CANISTER_BREACH_TIME 9999. y
  CRITICALITY_MECHANISM_NAME 12-ss_criticality-89-BWR
  SPACER_MECHANISM_NAME spc_01
/
CRITICALITY_MECH
  NAME 12-ss_criticality-89-BWR
  CRIT_START 10000.0 y
  CRIT_END 1.0d6 y
  HEAT_OF_CRITICALITY
    CONSTANT_POWER 2.0 kW
  /
  DECAy_HEAT TOTAL
    DATASET decay_heat_MPC_89_rescaled_110y.txt
  /
  INVENTORY
    EXPANDED_DATASET MPC-89-W047_crit_inv.txt
    OPTION
      USE_LOOKUP_AND_IMPLICIT
  /
/
/

```

```
WASTE_FORM
  REGION wp1_17
  EXPOSURE_FACTOR 1.d0
  VOLUME 2.10d0 m^3
  MECHANISM_NAME csnf
  CANISTER_BREACH_TIME 19999. y
  CRITICALITY_MECHANISM_NAME 13-ss_criticality-89-BWR
  SPACER_MECHANISM_NAME spc_01
/
CRITICALITY_MECH
  NAME 13-ss_criticality-89-BWR
  CRIT_START 20000.0 y
  CRIT_END 1.0d6 y
  HEAT_OF_CRITICALITY
    CONSTANT_POWER 2.0 kW
  /
  DECAy_HEAT TOTAL
    DATASET decay_heat_MPC_89_rescaled_110y.txt
  /
  INVENTORY
    EXPANDED_DATASET MPC-89-W047_crit_inv.txt
    OPTION
      USE_LOOKUP_AND_IMPLICIT
  /
/
WASTE_FORM
  REGION wp8_45
  EXPOSURE_FACTOR 1.d0
  VOLUME 2.10d0 m^3
  MECHANISM_NAME csnf
  CANISTER_BREACH_TIME 49999. y
  CRITICALITY_MECHANISM_NAME 14-ss_criticality-89-BWR
  SPACER_MECHANISM_NAME spc_01
/
CRITICALITY_MECH
  NAME 14-ss_criticality-89-BWR
  CRIT_START 50000.0 y
  CRIT_END 1.0d6 y
  HEAT_OF_CRITICALITY
    CONSTANT_POWER 2.0 kW
  /
  DECAy_HEAT TOTAL
    DATASET decay_heat_MPC_89_rescaled_110y.txt
  /
  INVENTORY
    EXPANDED_DATASET MPC-89-W047_crit_inv.txt
    OPTION
      USE_LOOKUP_AND_IMPLICIT
  /
/
WASTE_FORM
  REGION wp3_7
  EXPOSURE_FACTOR 1.d0
  VOLUME 2.10d0 m^3
  MECHANISM_NAME csnf
  CANISTER_BREACH_TIME 99999. y
  CRITICALITY_MECHANISM_NAME 15-ss_criticality-89-BWR
  SPACER_MECHANISM_NAME spc_01
/
CRITICALITY_MECH
  NAME 15-ss_criticality-89-BWR
  CRIT_START 100000.0 y
  CRIT_END 1.0d6 y
  HEAT_OF_CRITICALITY
    CONSTANT_POWER 2.0 kW
  /
  DECAy_HEAT TOTAL
    DATASET decay_heat_MPC_89_rescaled_110y.txt
  /
  INVENTORY
    EXPANDED_DATASET MPC-89-W047_crit_inv.txt
    OPTION
      USE_LOOKUP_AND_IMPLICIT
  /
/
```

```

WASTE_FORM
  REGION wp6_0
  EXPOSURE_FACTOR 1.d0
  VOLUME 2.10d0 m^3
  MECHANISM_NAME csnf
  CANISTER_BREACH_TIME 499999. y
  CRITICALITY_MECHANISM_NAME 16-ss_criticality-89-BWR
  SPACER_MECHANISM_NAME spc_01
/
CRITICALITY_MECH
  NAME 16-ss_criticality-89-BWR
  CRIT_START 500000.0 y
  CRIT_END 1.0d6 y
  HEAT_OF_CRITICALITY
    CONSTANT_POWER 2.0 kW
  /
  DECAy_HEAT TOTAL
    DATASET decay_heat_MPC_89_rescaled_110y.txt
  /
  INVENTORY
    EXPANDED_DATASET MPC-89-W047_crit_inv.txt
    OPTION
      USE_LOOKUP_AND_IMPLICIT
  /
/
# 3kW
#17
WASTE_FORM
  REGION wp11_6
  EXPOSURE_FACTOR 1.d0
  VOLUME 2.10d0 m^3
  MECHANISM_NAME csnf
  CANISTER_BREACH_TIME 499. y
  CRITICALITY_MECHANISM_NAME 17-ss_criticality-89-BWR
  SPACER_MECHANISM_NAME spc_01
/
CRITICALITY_MECH
  NAME 17-ss_criticality-89-BWR
  CRIT_START 500.0 y
  CRIT_END 1.0d6 y
  HEAT_OF_CRITICALITY
    CONSTANT_POWER 3.0 kW
  /
  DECAy_HEAT TOTAL
    DATASET decay_heat_MPC_89_rescaled_110y.txt
  /
  INVENTORY
    EXPANDED_DATASET MPC-89-W047_crit_inv.txt
    OPTION
      USE_LOOKUP_AND_IMPLICIT
  /
/
WASTE_FORM
  REGION wp13_20
  EXPOSURE_FACTOR 1.d0
  VOLUME 2.10d0 m^3
  MECHANISM_NAME csnf
  CANISTER_BREACH_TIME 999. y
  CRITICALITY_MECHANISM_NAME 18-ss_criticality-89-BWR
  SPACER_MECHANISM_NAME spc_01
/
CRITICALITY_MECH
  NAME 18-ss_criticality-89-BWR
  CRIT_START 1000.0 y
  CRIT_END 1.0d6 y
  HEAT_OF_CRITICALITY
    CONSTANT_POWER 3.0 kW
  /
  DECAy_HEAT TOTAL
    DATASET decay_heat_MPC_89_rescaled_110y.txt
  /
  INVENTORY
    EXPANDED_DATASET MPC-89-W047_crit_inv.txt
    OPTION
      USE_LOOKUP_AND_IMPLICIT
  /
/
/

```

```
WASTE_FORM
  REGION wp12_27
  EXPOSURE_FACTOR 1.d0
  VOLUME 2.10d0 m^3
  MECHANISM_NAME csnf
  CANISTER_BREACH_TIME 4999. y
  CRITICALITY_MECHANISM_NAME 19-ss_criticality-89-BWR
  SPACER_MECHANISM_NAME spc_01
/
CRITICALITY_MECH
  NAME 19-ss_criticality-89-BWR
  CRIT_START 5000.0 y
  CRIT_END 1.0d6 y
  HEAT_OF_CRITICALITY
    CONSTANT_POWER 3.0 kW
  /
  DECAy_HEAT TOTAL
    DATASET decay_heat_MPC_89_rescaled_110y.txt
  /
  INVENTORY
    EXPANDED_DATASET MPC-89-W047_crit_inv.txt
    OPTION
      USE_LOOKUP_AND_IMPLICIT
  /
/
/
WASTE_FORM
  REGION wp8_31
  EXPOSURE_FACTOR 1.d0
  VOLUME 2.10d0 m^3
  MECHANISM_NAME csnf
  CANISTER_BREACH_TIME 9999. y
  CRITICALITY_MECHANISM_NAME 20-ss_criticality-89-BWR
  SPACER_MECHANISM_NAME spc_01
/
CRITICALITY_MECH
  NAME 20-ss_criticality-89-BWR
  CRIT_START 10000.0 y
  CRIT_END 1.0d6 y
  HEAT_OF_CRITICALITY
    CONSTANT_POWER 3.0 kW
  /
  DECAy_HEAT TOTAL
    DATASET decay_heat_MPC_89_rescaled_110y.txt
  /
  INVENTORY
    EXPANDED_DATASET MPC-89-W047_crit_inv.txt
    OPTION
      USE_LOOKUP_AND_IMPLICIT
  /
/
/
WASTE_FORM
  REGION wp10_5
  EXPOSURE_FACTOR 1.d0
  VOLUME 2.10d0 m^3
  MECHANISM_NAME csnf
  CANISTER_BREACH_TIME 19999. y
  CRITICALITY_MECHANISM_NAME 21-ss_criticality-89-BWR
  SPACER_MECHANISM_NAME spc_01
/
CRITICALITY_MECH
  NAME 21-ss_criticality-89-BWR
  CRIT_START 20000.0 y
  CRIT_END 1.0d6 y
  HEAT_OF_CRITICALITY
    CONSTANT_POWER 3.0 kW
  /
  DECAy_HEAT TOTAL
    DATASET decay_heat_MPC_89_rescaled_110y.txt
  /
  INVENTORY
    EXPANDED_DATASET MPC-89-W047_crit_inv.txt
    OPTION
      USE_LOOKUP_AND_IMPLICIT
  /
/
/
```

```

WASTE_FORM
  REGION wp8_38
  EXPOSURE_FACTOR 1.d0
  VOLUME 2.10d0 m^3
  MECHANISM_NAME csnf
  CANISTER_BREACH_TIME 49999. y
  CRITICALITY_MECHANISM_NAME 22-ss_criticality-89-BWR
  SPACER_MECHANISM_NAME spc_01
/
CRITICALITY_MECH
  NAME 22-ss_criticality-89-BWR
  CRIT_START 50000.0 y
  CRIT_END 1.0d6 y
  HEAT_OF_CRITICALITY
    CONSTANT_POWER 3.0 kW
  /
  DECAF_HEAT TOTAL
    DATASET decay_heat_MPC_89_rescaled_110y.txt
  /
  INVENTORY
    EXPANDED_DATASET MPC-89-W047_crit_inv.txt
    OPTION
      USE_LOOKUP_AND_IMPLICIT
  /
/
/
WASTE_FORM
  REGION wp3_14
  EXPOSURE_FACTOR 1.d0
  VOLUME 2.10d0 m^3
  MECHANISM_NAME csnf
  CANISTER_BREACH_TIME 99999. y
  CRITICALITY_MECHANISM_NAME 23-ss_criticality-89-BWR
  SPACER_MECHANISM_NAME spc_01
/
CRITICALITY_MECH
  NAME 23-ss_criticality-89-BWR
  CRIT_START 100000.0 y
  CRIT_END 1.0d6 y
  HEAT_OF_CRITICALITY
    CONSTANT_POWER 3.0 kW
  /
  DECAF_HEAT TOTAL
    DATASET decay_heat_MPC_89_rescaled_110y.txt
  /
  INVENTORY
    EXPANDED_DATASET MPC-89-W047_crit_inv.txt
    OPTION
      USE_LOOKUP_AND_IMPLICIT
  /
/
/
WASTE_FORM
  REGION wp1_18
  EXPOSURE_FACTOR 1.d0
  VOLUME 2.10d0 m^3
  MECHANISM_NAME csnf
  CANISTER_BREACH_TIME 499999. y
  CRITICALITY_MECHANISM_NAME 24-ss_criticality-89-BWR
  SPACER_MECHANISM_NAME spc_01
/
CRITICALITY_MECH
  NAME 24-ss_criticality-89-BWR
  CRIT_START 500000.0 y
  CRIT_END 1.0d6 y
  HEAT_OF_CRITICALITY
    CONSTANT_POWER 3.0 kW
  /
  DECAF_HEAT TOTAL
    DATASET decay_heat_MPC_89_rescaled_110y.txt
  /
  INVENTORY
    EXPANDED_DATASET MPC-89-W047_crit_inv.txt
    OPTION
      USE_LOOKUP_AND_IMPLICIT
  /
/
/

```

```
MECHANISM CUSTOM
NAME csnf
FRACTIONAL DISSOLUTION_RATE 1.d-7 1/y
MATRIX_DENSITY 10970.
SPECIES
#isotope, atomic wt (g/mol), 1/s, g/g waste, instant release fraction, daughter
# For importing from neutronics dataset:
I129 128.90d0 1.29d-15 0.d0 0.1d0
Am241 241.06d0 5.08d-11 0.d0 0.0d0 Np237
Np237 237.05d0 1.03d-14 0.d0 0.0d0 U233
U233 233.04d0 1.38d-13 0.d0 0.0d0 Th229
Th229 229.03d0 2.78d-12 0.d0 0.0d0
Pu238 238.05d0 2.56d-10 0.d0 0.0d0
Pu240 240.05d0 3.34d-12 0.d0 0.0d0
Cs137 136.91d0 7.31d-10 0.d0 0.0d0
Sr90 89.91d0 7.61d-10 0.d0 0.0d0
Am242 242.06d0 1.56d-10 0.d0 0.0d0
/
CANISTER_DEGRADATION_MODEL
CANISTER_MATERIAL_CONSTANT 1500.
/
END #MECHANISM CUSTOM

MECHANISM CUSTOM
NAME csnf-no-crit
FRACTIONAL DISSOLUTION_RATE 1.d-7 1/y
MATRIX_DENSITY 10970.
SPECIES
#isotope, atomic wt (g/mol), 1/s, g/g waste, instant release fraction, daughter
I129 128.90d0 1.29d-15 1.862671d-4 0.10d0
/
CANISTER_DEGRADATION_MODEL
VITALITY_LOG10_MEAN -4.5
VITALITY_LOG10_STDEV 0.5
VITALITY_UPPER_TRUNCATION -3.0
CANISTER_MATERIAL_CONSTANT 1500.
/
END #MECHANISM CUSTOM csnf-no-crit

SPACER_DEGRADATION_MECHANISM
NAME spc_01
METAL_LOSS_RATIO 4.42953d-04 m^3/kg
THICKNESS 5.00000d-04 m
EXPOSURE_LEVEL 9.93317d-01
C 3.47000d+07 mg/day-dm^2
Q 2.27570d+04 cal/mol
RAD_FACTOR 2.00000d+00
/

END_WASTE_FORM_GENERAL

UFD_DECAY
IMPLICIT_SOLUTION

ELEMENT I
SOLUBILITY 1.d4
KD
wp 0.d0
buffer 0.d0 #kg water/m^3 bulk
shale 0.d0 #kg water/m^3 bulk
drz 0.d0 #kg water/m^3 bulk
overburden 0.d0
overburden_drz 0.d0
siltstone 0.d0 #kg water/m^3 bulk
silt_drz 0.d0
sandstone 0.d0
sand_drz 0.d0
limestone 0.d0
lower_shale 0.d0
lower_sand 0.d0
/
/
ISOTOPE I129
ELEMENT I
DECAY_RATE 1.29d-15
/
```

```

ELEMENT Am
SOLUBILITY 4.d-7
KD
  wp 0.d0
  buffer 2.11d7
  shale 1.08d8
  drz 1.08d8
  siltstone 1.08d8
  silt_drz 1.08d8
  sandstone 2.17d5
  sand_drz 2.17d5
  limestone 2.17d5
  lower_shale 1.08d8
  overburden 1.08d8
  overburden_drz 1.08d8
  lower_sand 2.17d5
/
/
ISOTOPE Am241
ELEMENT Am
DECAY_RATE 5.08d-11
DAUGHTER Np237 1.d0
/
ISOTOPE Am242
ELEMENT Am
DECAY_RATE 1.56d-10
/
/
ELEMENT Pu
SOLUBILITY 2.d-7
KD
  wp 0.d0
  buffer 1.76d6
  shale 1.94d6
  drz 1.94d6
  siltstone 1.94d6
  silt_drz 1.94d6
  sandstone 1.09d6
  sand_drz 1.09d6
  limestone 1.09d6
  lower_shale 1.94d6
  overburden 1.94d6
  overburden_drz 1.94d6
  lower_sand 1.09d6
/
/
ISOTOPE Pu238
ELEMENT Pu
DECAY_RATE 2.56d-10
/
ISOTOPE Pu240
ELEMENT Pu
DECAY_RATE 3.34d-12
/
/
ELEMENT Np
SOLUBILITY 4.d-9
KD
  wp 0.d0
  buffer 1.76d6
  shale 1.94d6
  drz 1.94d6
  siltstone 1.94d6
  silt_drz 1.94d6
  sandstone 3.44d4
  sand_drz 3.44d4
  limestone 3.44d4
  lower_shale 1.94d6
  overburden 1.94d6
  overburden_drz 1.94d6
  lower_sand 3.44d4
/
/
ISOTOPE Np237
ELEMENT Np
DECAY_RATE 1.03d-14
DAUGHTER U233 1.d0
/

```

```
ELEMENT U
SOLUBILITY 7.d-7
KD
  wp 0.d0
  buffer 1.76d8
  shale 1.73d7
  drz 1.73d7
  siltstone 1.73d7
  silt_drz 1.73d7
  sandstone 1.88d3
  sand_drz 1.88d3
  limestone 1.88d3
  lower_shale 1.73d7
  overburden 1.73d7
  overburden_drz 1.73d7
  lower_sand 1.88d3
/
/
ISOTOPE U233
ELEMENT U
DECAY_RATE 1.38d-13
DAUGHTER Th229 1.d0
/
ELEMENT Th
SOLUBILITY 6.d-7
KD
  wp 0.d0
  buffer 5.27d6
  shale 1.73d7
  drz 1.73d7
  siltstone 1.73d7
  silt_drz 1.73d7
  sandstone 6.43d6
  sand_drz 6.43d6
  limestone 6.43d6
  lower_shale 1.73d7
  overburden 1.73d7
  overburden_drz 1.73d7
  lower_sand 6.43d6
/
/
ISOTOPE Th229
ELEMENT Th
DECAY_RATE 2.78d-12
/
ELEMENT Cs
SOLUBILITY 1.d4
KD
  wp 0.d0
  buffer 6.67d5
  shale 8.64d5
  drz 8.64d5
  siltstone 8.64d5
  silt_drz 8.64d5
  sandstone 1.22d6
  sand_drz 1.22d6
  limestone 1.22d6
  lower_shale 8.64d5
  overburden 8.64d5
  overburden_drz 8.64d5
  lower_sand 1.22d6
/
/
ISOTOPE Cs137
ELEMENT Cs
DECAY_RATE 7.31d-10
/
```

```

ELEMENT Sr
  SOLUBILITY 1.d4
  KD
    wp 0.d0
    buffer 0.0d0
    shale 0.d0 #kg water/m^3 bulk
    drz 0.d0 #kg water/m^3 bulk
    siltstone 0.d0 #kg water/m^3 bulk
    silt_drz 0.d0
    sandstone 0.d0
    sand_drz 0.d0
    limestone 0.d0
    lower_shale 0.d0
    overburden 0.d0
    overburden_drz 0.d0
    lower_sand 0.d0
  /
  /
ISOTOPE Sr90
  ELEMENT Sr
  DECAY_RATE 7.61d-10
  /
END #UFD

#===== ufd biosphere =====
UFD_BIOSPHERE

  ERB_1A A_model1
  REGION well_far
  INDIVIDUAL_CONSUMPTION_RATE 2.d0 L/day
  /

  SUPPORTED_RADIONUCLIDES
  RADIONUCLIDE I129
  ELEMENT_KD 0.d0
  DECAY_RATE 1.40d-15 1/sec
  INGESTION_DOSE_COEF 1.1d-7 Sv/Bq
  /
  /
  OUTPUT_START_TIME 1.d0 yr

END

MATERIAL_TRANSFORM_GENERAL

  MATERIAL_TRANSFORM ilt_bentonite
  ILLITIZATION
  ILLITIZATION_FUNCTION DEFAULT
  THRESHOLD_TEMPERATURE 2.5000d+1 C
  EA 1.17152d+5 J/mol
  FREQ 8.0800d+4 L/mol-s
  K_CONC 2.1600d-3 M
  SMECTITE_INITIAL 0.9500d+0
  SHIFT_PERM DEFAULT 9.9900d+2
  END
  TEST
  END
END

END # MATERIAL_TRANSFORM_GENERAL

```

## A-2. PFLOTRAN Waste Form General File (clips)

# BWRs (drifts 0 - 13)

```
WASTE_FORM
REGION wp0_0
EXPOSURE_FACTOR 1.d0
VOLUME 2.10d0 m^3 #89*0.179MTHM*1.44e3kgwaste/MTHM*(m3/10970kgUO2), 89 BWRs, Carter et al 2012 Table 3-7
MECHANISM_NAME csnf-no-crit
SPACER_MECHANISM_NAME spc_01
/
```

```
WASTE_FORM
REGION wp0_1
EXPOSURE_FACTOR 1.d0
VOLUME 2.10d0 m^3 #89*0.179MTHM*1.44e3kgwaste/MTHM*(m3/10970kgUO2), 89 BWRs, Carter et al 2012 Table 3-7
MECHANISM_NAME csnf-no-crit
SPACER_MECHANISM_NAME spc_01
/
```

```
WASTE_FORM
REGION wp0_2
EXPOSURE_FACTOR 1.d0
VOLUME 2.10d0 m^3 #89*0.179MTHM*1.44e3kgwaste/MTHM*(m3/10970kgUO2), 89 BWRs, Carter et al 2012 Table 3-7
MECHANISM_NAME csnf-no-crit
SPACER_MECHANISM_NAME spc_01
/
```

```
WASTE_FORM
REGION wp0_3
EXPOSURE_FACTOR 1.d0
VOLUME 2.10d0 m^3 #89*0.179MTHM*1.44e3kgwaste/MTHM*(m3/10970kgUO2), 89 BWRs, Carter et al 2012 Table 3-7
MECHANISM_NAME csnf-no-crit
SPACER_MECHANISM_NAME spc_01
/
```

```
WASTE_FORM
REGION wp0_4
EXPOSURE_FACTOR 1.d0
VOLUME 2.10d0 m^3 #89*0.179MTHM*1.44e3kgwaste/MTHM*(m3/10970kgUO2), 89 BWRs, Carter et al 2012 Table 3-7
MECHANISM_NAME csnf-no-crit
SPACER_MECHANISM_NAME spc_01
/
```

```
WASTE_FORM
REGION wp0_5
EXPOSURE_FACTOR 1.d0
VOLUME 2.10d0 m^3 #89*0.179MTHM*1.44e3kgwaste/MTHM*(m3/10970kgUO2), 89 BWRs, Carter et al 2012 Table 3-7
MECHANISM_NAME csnf-no-crit
SPACER_MECHANISM_NAME spc_01
/
```

```
WASTE_FORM
REGION wp0_6
EXPOSURE_FACTOR 1.d0
VOLUME 2.10d0 m^3 #89*0.179MTHM*1.44e3kgwaste/MTHM*(m3/10970kgUO2), 89 BWRs, Carter et al 2012 Table 3-7
MECHANISM_NAME csnf-no-crit
SPACER_MECHANISM_NAME spc_01
/
```

```
WASTE_FORM
REGION wp0_7
EXPOSURE_FACTOR 1.d0
VOLUME 2.10d0 m^3 #89*0.179MTHM*1.44e3kgwaste/MTHM*(m3/10970kgUO2), 89 BWRs, Carter et al 2012 Table 3-7
MECHANISM_NAME csnf-no-crit
SPACER_MECHANISM_NAME spc_01
/
```

```
WASTE_FORM
REGION wp0_8
EXPOSURE_FACTOR 1.d0
VOLUME 2.10d0 m^3 #89*0.179MTHM*1.44e3kgwaste/MTHM*(m3/10970kgUO2), 89 BWRs, Carter et al 2012 Table 3-7
MECHANISM_NAME csnf-no-crit
SPACER_MECHANISM_NAME spc_01
```

# PWRs (drifts 14 - 41)

```

WASTE_FORM
  REGION wp14_0
  EXPOSURE_FACTOR 1.d0
  VOLUME 1.83d0 m^3 #32*.435MTHM*1.44e3kgwaste/MTHM*(m3/10970kgUO2), 32 PWRs, Freeze et al 2013
  MECHANISM_NAME csnf-no-crit
  SPACER_MECHANISM_NAME spc_01
/

WASTE_FORM
  REGION wp14_1
  EXPOSURE_FACTOR 1.d0
  VOLUME 1.83d0 m^3 #32*.435MTHM*1.44e3kgwaste/MTHM*(m3/10970kgUO2), 32 PWRs, Freeze et al 2013
  MECHANISM_NAME csnf-no-crit
  SPACER_MECHANISM_NAME spc_01
/

WASTE_FORM
  REGION wp14_2
  EXPOSURE_FACTOR 1.d0
  VOLUME 1.83d0 m^3 #32*.435MTHM*1.44e3kgwaste/MTHM*(m3/10970kgUO2), 32 PWRs, Freeze et al 2013
  MECHANISM_NAME csnf-no-crit
  SPACER_MECHANISM_NAME spc_01
/

WASTE_FORM
  REGION wp14_3
  EXPOSURE_FACTOR 1.d0
  VOLUME 1.83d0 m^3 #32*.435MTHM*1.44e3kgwaste/MTHM*(m3/10970kgUO2), 32 PWRs, Freeze et al 2013
  MECHANISM_NAME csnf-no-crit
  SPACER_MECHANISM_NAME spc_01
/

WASTE_FORM
  REGION wp14_4
  EXPOSURE_FACTOR 1.d0
  VOLUME 1.83d0 m^3 #32*.435MTHM*1.44e3kgwaste/MTHM*(m3/10970kgUO2), 32 PWRs, Freeze et al 2013
  MECHANISM_NAME csnf-no-crit
  SPACER_MECHANISM_NAME spc_01
/

WASTE_FORM
  REGION wp14_5
  EXPOSURE_FACTOR 1.d0
  VOLUME 1.83d0 m^3 #32*.435MTHM*1.44e3kgwaste/MTHM*(m3/10970kgUO2), 32 PWRs, Freeze et al 2013
  MECHANISM_NAME csnf-no-crit
  SPACER_MECHANISM_NAME spc_01
/

WASTE_FORM
  REGION wp14_6
  EXPOSURE_FACTOR 1.d0
  VOLUME 1.83d0 m^3 #32*.435MTHM*1.44e3kgwaste/MTHM*(m3/10970kgUO2), 32 PWRs, Freeze et al 2013
  MECHANISM_NAME csnf-no-crit
  SPACER_MECHANISM_NAME spc_01
/

WASTE_FORM
  REGION wp14_7
  EXPOSURE_FACTOR 1.d0
  VOLUME 1.83d0 m^3 #32*.435MTHM*1.44e3kgwaste/MTHM*(m3/10970kgUO2), 32 PWRs, Freeze et al 2013
  MECHANISM_NAME csnf-no-crit
  SPACER_MECHANISM_NAME spc_01
/

WASTE_FORM
  REGION wp14_8
  EXPOSURE_FACTOR 1.d0
  VOLUME 1.83d0 m^3 #32*.435MTHM*1.44e3kgwaste/MTHM*(m3/10970kgUO2), 32 PWRs, Freeze et al 2013
  MECHANISM_NAME csnf-no-crit
  SPACER_MECHANISM_NAME spc_01
/

WASTE_FORM
  REGION wp14_9
  EXPOSURE_FACTOR 1.d0
  VOLUME 1.83d0 m^3 #32*.435MTHM*1.44e3kgwaste/MTHM*(m3/10970kgUO2), 32 PWRs, Freeze et al 2013
  MECHANISM_NAME csnf-no-crit
  SPACER_MECHANISM_NAME spc_01
/

```

### A-3. PFLOTRAN Source Sink File (clips)

```
#BWRs (drifts 0 - 13) no criticality event  
#           only decay heat applied  
#           through SOURCE_SINK
```

```
SOURCE_SINK wp0_0  
  FLOW_CONDITION wp_heatsource_BWR  
  TRANSPORT_CONDITION initial  
  REGION wp0_0  
END
```

```
SOURCE_SINK wp0_1  
  FLOW_CONDITION wp_heatsource_BWR  
  TRANSPORT_CONDITION initial  
  REGION wp0_1  
END
```

```
SOURCE_SINK wp0_2  
  FLOW_CONDITION wp_heatsource_BWR  
  TRANSPORT_CONDITION initial  
  REGION wp0_2  
END
```

```
SOURCE_SINK wp0_3  
  FLOW_CONDITION wp_heatsource_BWR  
  TRANSPORT_CONDITION initial  
  REGION wp0_3  
END
```

```
SOURCE_SINK wp0_4  
  FLOW_CONDITION wp_heatsource_BWR  
  TRANSPORT_CONDITION initial  
  REGION wp0_4  
END
```

```
SOURCE_SINK wp0_5  
  FLOW_CONDITION wp_heatsource_BWR  
  TRANSPORT_CONDITION initial  
  REGION wp0_5  
END
```

```
SOURCE_SINK wp0_6  
  FLOW_CONDITION wp_heatsource_BWR  
  TRANSPORT_CONDITION initial  
  REGION wp0_6  
END
```

```
SOURCE_SINK wp0_7  
  FLOW_CONDITION wp_heatsource_BWR  
  TRANSPORT_CONDITION initial  
  REGION wp0_7  
END
```

```
SOURCE_SINK wp0_8  
  FLOW_CONDITION wp_heatsource_BWR  
  TRANSPORT_CONDITION initial  
  REGION wp0_8  
END
```

```
#PWRs (drifts 14 - 41) no criticality event
#           only decay heat applied
#           through SOURCE_SINK
SOURCE_SINK wp14_0
  FLOW_CONDITION wp_heatsource_PWR
  TRANSPORT_CONDITION initial
  REGION wp14_0
END

SOURCE_SINK wp14_1
  FLOW_CONDITION wp_heatsource_PWR
  TRANSPORT_CONDITION initial
  REGION wp14_1
END

SOURCE_SINK wp14_2
  FLOW_CONDITION wp_heatsource_PWR
  TRANSPORT_CONDITION initial
  REGION wp14_2
END

SOURCE_SINK wp14_3
  FLOW_CONDITION wp_heatsource_PWR
  TRANSPORT_CONDITION initial
  REGION wp14_3
END

SOURCE_SINK wp14_4
  FLOW_CONDITION wp_heatsource_PWR
  TRANSPORT_CONDITION initial
  REGION wp14_4
END

SOURCE_SINK wp14_5
  FLOW_CONDITION wp_heatsource_PWR
  TRANSPORT_CONDITION initial
  REGION wp14_5
END

SOURCE_SINK wp14_6
  FLOW_CONDITION wp_heatsource_PWR
  TRANSPORT_CONDITION initial
  REGION wp14_6
END

SOURCE_SINK wp14_7
  FLOW_CONDITION wp_heatsource_PWR
  TRANSPORT_CONDITION initial
  REGION wp14_7
END

skip #
SOURCE_SINK wp14_8
  FLOW_CONDITION wp_heatsource_PWR
  TRANSPORT_CONDITION initial
  REGION wp14_8
END
noskip #

SOURCE_SINK wp14_9
  FLOW_CONDITION wp_heatsource_PWR
  TRANSPORT_CONDITION initial
  REGION wp14_9
END
```

This page is intentionally left blank.

